DOCTOR OF PHILOSOPHY

APPLICATION OF HYBRID OBSERVATION TECHNIQUES FOR FAULT DIAGNOSIS OF ROTATING MACHINES

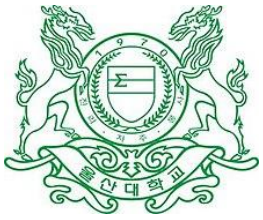

The Graduate School

of the University of Ulsan

Department of Computer Engineering

FARZIN PILTAN

Application of Hybrid Observation Techniques for Fault Diagnosis of Rotating Machines

---

Dissertation

for the Degree of

Doctor of Philosophy

(Computer Engineering)

University of Ulsan

Farzin Piltan

April 2020

Application of Hybrid Observation Techniques for Fault Diagnosis of Rotating Machines

Dissertation

Submitted in partial fulfillment of the requirements

for the degree of

Doctor of Philosophy

(Computer Engineering)

at the

University of Ulsan

by

Farzin Piltan

Under the supervision of

Prof. Jong-Myon Kim

April 2020

Publication No._____

Application of Hybrid Observation Techniques for Fault Diagnosis of Rotating Machines

Approved by supervisory committee:

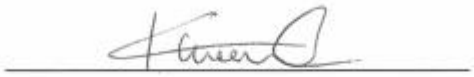

Prof. Kwon, Yung-Keun, Chair

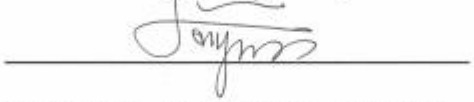

Prof. Kim, Jong-Myon, Advisor

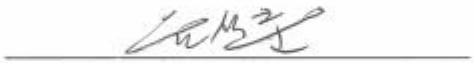

Prof. Yoon, Seok-Hoon, Member

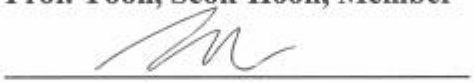

Dr. Kim, Gi-Hong, Member

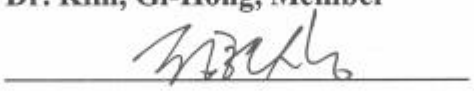

Dr. Chung, Hyun-Sang, Member

Department of Electrical, Electronics and Computer Engineering

University of Ulsan, Korea

May 2020

VITA

Farzin Piltan was born in Shiraz, Iran in 1975. He did his B.Sc. and M.Sc. in Electrical and Electronic Engineering from the Shiraz University of Technology, Shiraz, Iran in 2000, and University Putra Malaysia, Malaysia in 2012, respectively. His interest in Masters was robotics and modern control. Since March 2017, he has been working for his Ph.D. Degree in the Department of Computer Engineering, University of Ulsan, South Korea, under the supervision of Professor Jong-Myon Kim. His Ph.D. dissertation is based on exploring Modern Control and Artificial Intelligence techniques for hybrid-based Diagnostics of rotary machinery. His current research interests include model-based and hybrid-based anomaly estimation, detection, identification, fault tolerant-control, artificial intelligence, and modern control. In 2009, he joined the Department of Mechatronics at the Iranian Advanced Science and Technology (IRAN SSP) research center as a dean, researcher, and educator at the field of control, system modeling, artificial intelligence, and robotics.

DEDICATION

This thesis is dedicated to
many beautiful things that
inspired us

From who we were
to who we are
and whom we will become

We are traveling
on a journey of discovery
full of curiosity

To create
many beautiful things that
inspire others

*This effort is dedicated to the two women who have taught me the most important lessons in my life. To my **wife**, whose love is the greatest gift of my life and whose commitment, support and patience are true models for all; and to my daughter, **Pantea**, who inspires me to grow and who will always be a continual source of pride and enlightenment.*

Thanks, mom and dad for always believing in me and for encouraging me to strive for my dreams.

ACKNOWLEDGMENTS

Indeed, it’s been a long journey of assorted movements. The movements of distresses and soothes, desolation and hope, a sense of accomplishment and at same time endeavoring for progress. Eventually, all the hard work pays off. First of foremost I would like to extend my heartfelt gratitude to my advisor Prof. Jong Myon Kim for his kind supervision and the continuous support for my PhD study and related research work, for his patience, motivation and sharing immense knowledge. Throughout the period of my PhD, he has provided me the kind support both in technical and non-technical matters. Without his help the vision of both this research work and the arc of the research direction would be hazy or to be apt short-sighted. I am indebted to him for all his guidance, trust and generous support in this long journey of my studies. Besides my advisor, I extend my gratitude to my Ph.D. supervisory committee for taking out the time to invest in the improvement of my thesis.

I thank my fellow lab members in the SMART *Health*, *Safety and Environment laboratory (SMART HSE)*, University of Ulsan (UoU) for the thought-provoking discussions, and for all the fun we have had in the last four years. I am thankful, no particular order, Prosvirin Alexander, Dr. Muhammad Sohaib, and Dr. M. M. Manjurul Islam and other lab mates for their valuable feedbacks and recommendations throughout the research seminars and always available when asked for help.

I would also like to thankfully acknowledge the gracious financial support of the BK21 plus program, the Korea Institute of Energy Technology Evaluation and Planning (KETEP), the Ministry of Trade, Industry & Energy (MOTIE) of the Republic of Korea, the ministry of Science, ICT and Future Planning, and the National Research Foundation of Korea (NRF).

I really owe my sincere thanks to my family especially my wife and my daughter for their great help, lovely support in these years and understanding of their time lost during my studies.

I am thankful to my friends here in Korea and back home and spread throughout the world who have been my anchors in the hardest of my times. The beautiful part of my life is the days I have spent with my group of friends in Korea.

Farzin Piltan

University of Ulsan, Ulsan, South Korea

April, 2020

ABSTRACT

Application of Hybrid Observation Techniques for Fault Diagnosis of Rotating Machines

by

Farzin Piltan

Supervisor: Prof. Jong-Myon Kim

Submitted in partial fulfillment of the requirements for the Degree of Doctor of Philosophy (Computer Engineering)

April 2020

The fault diagnosis of industrial facilities is one of the significant and ever-growing fields of research. Fault diagnosis can be applied to a diversity of industrial components such as rotary machines, motors, pipelines, robot manipulators, gearboxes, etc. In this research, hybrid approaches are developed for detection and classification of the rotary machine bearing faults. Rolling element bearing represents a class of nonlinear and multiple-degrees-of-freedom rotating machines that have pronounced coupling effects and can be used in various industries. Uncertain conditions in which a rolling element bearing operates, as well as nonlinearities, represent challenges for fault diagnosis that are addressed through the fault diagnosis techniques. If defects in the rolling element bearing are not identified and diagnosed in time they can lead to the failure of the whole mechanical system. The failure of the rolling element bearing results in unexpected downtimes and great economic losses. Moreover, it can be a threat to the safety of the people working in the facility. The condition monitoring of a rolling element bearing can be achieved through different techniques. This work focuses on vibration and acoustic emission analysis method because these signals are suitable for fault

diagnosis in rolling element bearing. Several methods have been advised for anomaly detection and identification in rolling element bearings. These techniques can be divided into four principal divisions: model-based techniques, signal-based approaches, data-driven algorithms, and hybrid-based procedures. In this dissertation, hybrid-based techniques that uses a combination of the system modeling algorithms, observation techniques, and a machine learning-based classification are introduced for the diagnosis of bearing faults of various severities.

System modeling is the main argument in designing observation-based techniques for fault diagnosis. Numerous procedures have been used to model bearings and can be classified into two main groups: mathematical-based system modeling, and system identification techniques. The mathematical-based bearing modeling such as five-degrees-of-freedom mathematical modeling of vibration signals, and system identification techniques such as ARX-Laguerre and fuzzy ARX-Laguerre bearing vibration and acoustic emission signal modeling are prescribed in this work.

The model-based fault diagnosis techniques are reliable and robust algorithms and have been used in various applications. Observation-based algorithms are the main model-based techniques used for bearing fault diagnosis. Despite the advantages of observation-based approaches, these techniques have some limitations in the presence of uncertain and unknown conditions. Nonlinear-based observation techniques (e.g., sliding mode observer, feedback linearization observer) and linear-based observation algorithms (e.g., proportional-integral (PI) observer) are the main procedures used to develop observation to estimate the signals. The sliding mode observer is a nonlinear and high-gain observer that can improve a system's dynamic and reduce the estimator error infinite time. This technique is robust and reliable, but is prone to chattering phenomenon and limited estimation accuracy. To minimize the chattering phenomenon, the higher-order sliding mode observer is recommended in this work. This technique suffers from a somewhat reduced estimation accuracy. To improve the estimation accuracy, a higher-order super-twisting sliding mode observer was developed.

Sliding mode observer and high-order super twisting (extended-state) sliding mode observer have acceptable state estimation and works in uncertain condition; however,

chattering phenomenon is the main drawback of these techniques in uncertain conditions. To minimize the effect of the chattering phenomenon, a feedback linearization observer was developed. The feedback linearization observer is a powerful technique for signal estimation. The main idea of this approach is to algebraically transform the nonlinear system dynamic parameters into a linearized system so that the feedback observation algorithm can be applied. This observer is based on the dynamics of the system's behavior, thus it works perfectly if all parameters are known. Apart from the stability and reliability of this observation technique, it suffers from a lack of robustness. To address this issue, the variable structure (extended-state) feedback linearization observer is developed in this work.

Despite the advantages of high-order super-twisting sliding mode observer and variable structure feedback linearization observer for fault diagnosis of bearing based on five-degrees-of-freedom mathematical modeling of vibration signals such as reliability and robustness, these techniques have some limitations in the presence of uncertain and unknown conditions. To decrease these limitations, the auto-regressive exogenous input (ARX) technique is advised for bearing system modeling in this work. To improve the stability and robustness of ARX modeling for vibration/acoustic emission signals, an orthonormal function technique based on the ARX-Laguerre method is developed. Moreover, The ARX-Laguerre PI observer is a linear and easy to implement technique for signals estimation but have limited robustness and accuracy. To address these issues, an extended-state technique based on a sliding mode algorithm is applied to the ARX-Laguerre PI observer to perform fault diagnosis and overcome potential problems that may appear when applying a linear observer to a nonlinear signal. Moreover, the simplicity and flexibility of the ARX-Laguerre extended-state PI observation method allow it to be applied in industrial environments for single-type and multiple-type fault diagnosis of bearing.

The ARX-Laguerre technique is robust and stable, but has some limitations when applied to nonlinear and non-stationary signal modeling. To address these problems, a fuzzy ARX-Laguerre technique for vibration and acoustic emission bearing signals is prescribed in this work. Through the high-order super-twisting (extended-state) sliding mode observer increases the robustness and reduces the chattering phenomenon, this scheme, unfortunately, suffers from the small rate chattering phenomenon and signal estimation accuracy in the

presence of uncertainties and unknown conditions. Therefore, in this dissertation, the fuzzy technique is applied to the fuzzy ARX-Laguerre high-order super-twisting (extended-state) sliding mode observer to increases the signal estimation accuracy and design fuzzy ARX-Laguerre fuzzy high-order super-twisting (fuzzy extended-state) sliding mode observer.

Once the rotary machinery bearing is modeled based on a mathematical-based modeling (e.g., five-degrees-of-freedom mathematical modeling of vibration signals) or system identification techniques (e.g., ARX-Laguerre technique, and fuzzy ARX-Laguerre method), and the rotary machinery bearing signals are estimated based on the extended-state observers (e.g., high-order super-twisting sliding mode observer, variable structure feedback linearization observer, and ARX-Laguerre sliding mode PI observer) or fuzzy extended-state observer (e.g., fuzzy ARX-Laguerre fuzzy high-order super-twisting sliding mode observer), the decision regarding the bearing conditions can be made. In this work, machine learning-based classification techniques called a support vector machine (SVM) and decision tree (DT) are employed the decision-making procedure for bearing fault diagnosis to complete the proposed techniques for diagnosis the faults. Specifically, during the experiment the high-order super-twisting sliding mode observer, variable structure feedback linearization observer, ARX-Laguerre sliding mode PI observer, and fuzzy ARX-Laguerre fuzzy high-order super-twisting sliding mode observer an average fault diagnosis accuracy of 95.8%, 96.1%, 94.3%, and 99.2%, respectively.

Contents

List of Figures

List of Tables

List of Algorithms

Nomenclature

PI observer	Proportional-Integral observer
ARX	Auto Regressive eXogenous
SVM	Support vector machine
DT	Decision tree
GHG	Greenhouse gas
CO2	Carbon dioxide
Gt	Gigatonne
EMS	Electric motor system
MCSA	Motor current signature analysis
AE	Acoustic emission
REB	Rolling-element bearing
FDD	Fault detection and diagnosis
PMI	Proportional multiple-integral
SMO	Sliding mode observer
HOSMO	Higher-order sliding mode observer
HOSTSMO	Higher-order super-twisting sliding mode observer
K-NN	k-nearest neighbor
CARTs	Classification and regression trees
ANNs	Artificial neural networks
DOF	Degrees of freedom
FTF	Fundamental train frequency
CWRU	Case Western Reverse University
APIO	ARX-Laguerre proportional integral observer
LMI	Linear matrix inequality
OR	Outer raceway
IR	Inner raceway
FLO	Feedback linearization observer
PFLO	Proposed feedback linearization observer
VSO	Variable structure observer

FDI	Fault detection and identification
hp	horsepower
PIO	Proportional-integral observer
SMALPIO	Sliding mode extended-state ARX-Laguerre PI observer
IR-OR	Inner-Outer raceway
IR-Ball	Inner-Ball raceway
OR-Ball	Outer-Ball raceway
IR-OR-Ball	Inner-Outer-Ball raceway
SHSE Lab	Smart Health, Safety, Environment Lab
NDES	No-drive-end shaft
DES	Drive-end shaft
FEDI	Fault estimation, detection, and identification
OFB	Orthonormal function bases
GOB	Generalized orthonormal bases
FAL	T-S fuzzy ARX-Laguerre
FO	Fuzzy observer
SO	Suboptimal
QC	Quasi-continuous
TW	Twisting method
ASMO	Advanced sliding mode observer
AFSMO	Advanced fuzzy sliding mode observer
AI	Artificial intelligence
ML	Machine learning
DL	Deep learning
NH	Negative high
NM	Negative medium
NL	Negative low
Z	Zero
PL	Positive low
PM	Positive medium
PH	Positive high

1D	One Dimensional
GDI	Gini Diversity Index
ACA	Average classification accuracy
RUL	Remaining useful life

Chapter 1

Introduction

Energy is essential for the survival and strength of modern industrial civilization. Generally, the sources of energy are fossil fuels such as oil and coal. Use of these fuels has significant impacts on the environment, one of the main challenges being greenhouse gas (GHG) emissions, with carbon dioxide (CO2) as their major component [1]. Regularly, 29 Gigatons (Gt) of CO2 are emitted every year, of which about 7 Gt can be absorbed naturally [2]. The remainder enters into the atmosphere, causing issues such as global warming and pollution. In recent years, the rate of industrialization has sharply increased, causing an increase in the rate of GHG emissions. About 50% of the energy produced by various techniques is consumed by heavy industries. The most widely used electro-mechanical equipment, consuming about 80% of the industrial electricity total, is various types of motors. Based on the energy-efficiency trends seen in the energy audits of the various industries, optimization of power consumption, condition monitoring and fault diagnosis, and power quality improvements are important factors in energy efficiency. There is also serious attention on the disturbing effects of systems anomalies on energy efficiency and thus the environment since conservation of the environment's quality and energy efficiency are major challenges in most countries around the world[2, 3]. Most research and industry initiatives over the last decade have resulted in a significant decrease in the share of energy losses due to faulty industrial systems. However, in some fields, such as induction motors, reliable techniques must still be designed.

Induction motors have been used in diverse industries, such as the machine tool and oil industries. The dynamic behavior of an induction motor is entirely nonlinear, which can cause various challenges in control and fault diagnosis. High-temperature environments, heavy-duty cycles, poor installation, overloading, and aging of components cause a diverse range of electrical and mechanical defects in motors. Diverse faults have been defined in induction motors, such as motor failures, air-gap faults, bearing and cage faults, and stator failures. The two main types of induction motor defects are mechanical and electrical failures. Various types of induction motor faults are mostly associated with mechanical defects (79%),

such as bearing defects (69%) and the other types of rotor faults (10%). The other types of induction motor faults are electrical failures (21%), such as open circuits and short circuits in stator windings [4]. Various techniques have been presented recently for rotating machines fault diagnosis and can be divided into two main categories: a) hardware-based techniques that rely on various physical instruments installed on the industrial systems and b) software-based techniques that utilize limited equipment. Recently, software-based techniques for fault diagnosis have been used in various applications. Different techniques have been used for software-based fault diagnosis, such as model-based techniques, signal-based methods, knowledge-based algorithms, and hybrid methods [5, 6].

Based on this introduction the thesis will focus on developing efficient fault diagnosis schemes for bearing of a rotary machine that are used in various industries. The proposed fault diagnosis schemes for this component will be based on hybrid solutions. The focus will be to develop reliable and robust fault diagnoses schemes that can perform satisfactorily under inconsistent working conditions, i.e., variable shaft speed, and multiple crack severities.

This chapter provides concise descript of the motivation behind and objectives of the conducted research work which is presented in the dissertation. The research work described in the dissertation has been published in peer reviewed journals. Moreover, within each chapter necessary motivation, introduction and background study of the given problem is provided. Nonetheless, motivation behind this research work is given in section 1.1, and section 1.2 outlines the dissertation itself.

1.1 Motivation

Nowadays, induction motors are profoundly used in the industries to carry out numerous tasks. These motors consist of two main parts; 1) stator and 2) rotor [4]. The rotor part of the motors contains bearings. Bearings have been extensively used in several industries, such as the automotive, steam and gas turbines, and power generation industries, to improve their efficiency by reducing friction[4, 5]. The complexities of the required tasks, with time-varying and nonlinear parameters in rolling element bearings, make their fault estimation, detection, and identification highly challenging. The fault estimation, detection, and identification are intransitive to prevent the bearing’s destruction. Here, the fault estimation

technique is used to estimate the signal (fault) to obtain the valuable differentiation between various conditions of bearing, the fault detection algorithm is used to detect normal and abnormal conditions, and the fault identification technique is used to identify the specific types of faults in the bearings. Various types of failures have been representing in bearings, which are divided into four foremost groups, i.e., inner race faults, outer race faults, ball or rolling-element faults, and cage faults. To analyze the faults conditions in a bearing, various bearing condition monitoring techniques such as vibration, motor current signature analysis (MCSA), and acoustic emission (AE) measurements have been used [7]. This research exploits the vibration and acoustic emission (AE) measurements since these signals are suitable for fault estimation, detection, and identification in rotating machines.

Different techniques have been used for the diagnosis of faults in bearings, including signal-based fault diagnosis, knowledge-based fault diagnosis, model-based fault diagnosis, and hybrid/active approaches to fault diagnosis. All methods for fault diagnosis have specific advantages and challenges. Signal-based fault diagnosis extracts the main features from output signals. Because of the presence of disturbances, the performance of this method is degraded. Knowledge-based fault diagnosis is highly dependent on the historical data used for training, which incur high computational costs for real-time data. The model-reference method identifies faults using a small dataset, but it requires an accurate system model. Hybrid fault diagnosis techniques use a combination of high-performance methods to design a robust, stable and reliable technology [5, 6].

The core of this thesis is observer-based fault diagnosis. The main challenge in designing the procedure of observation-based fault diagnosis is system modeling. System modeling was divided into two principal techniques: (a) Physical-based (mathematical-based) system modeling and (b) signal-based system identification. In the mathematical-based system modeling, the Lagrange technique can be used for modeling the REBs in this thesis, i.e., chapters 2 and 3 [8, 9]. Apart from the reliability and accuracy of mathematical-based system modeling, this technique has drawbacks in uncertain and noisy conditions. To address this issue, the system identification techniques based on Auto-Regressive with eXogenous input (ARX)-Laguerre technique and fuzzy ARX-Laguerre procedure is used to modeling the vibration and AE bearing signals in this thesis, i.e., chapters 4 and 5 [10, 11].

Various observation-based techniques have been used for fault detection, estimation, and identification, and they are divided into two main groups: (a) linear-based observers and (b) nonlinear-based observers. Proportional integral (PI) observers are linear and have been used in different systems for fault diagnosis, but they are ineffective in the presence of uncertainties and disturbances [11-13]. To improve the robustness, the robust extended-state technique (e.g., sliding mode extended-state observer) was presented in this thesis [11]. Compared to linear observers, nonlinear observers (e.g., sliding mode and feedback linearization) have more edges, such as robustness and reliability. Feedback linearization observers are reliable and stable; however, they are not adequately robust. Due to the lack of robustness in the feedback linearization observers, a robust extended-state (i.e., variable structure extended-state observer) is developed in this dissertation. The variable structure extended-state technique is a robust, stable, and reliable method to improve the robustness in the feedback linearization observer. The next scenario to increase the performance of fault diagnosis technique is sliding mode observer. The sliding mode observer is reliable and robust, but is prone to high-frequency oscillations, especially in faulty conditions. The high-frequency oscillation (chattering phenomenon) is one of the significant disadvantages of sliding mode observer. The main effect of this challenge is the increase of some serious mechanical obstacles such as heats the mechanical components and saturation. These oscillations can be reduced using a high-order sliding mode observer. To modify the performance of high-order sliding mode observers, a super twisting high-order sliding mode observer is recommended. Despite its satisfactory stability, robustness, reliability and high-frequency attenuation, the signal estimation accuracy of these (sliding mode observers and feedback linearization observers) methods must be increased to improve the rate of fault identification. To increase the signal estimation accuracy and fault identification performance, an artificial intelligence (e.g., fuzzy logic) algorithm is recommended in the rotating machines [8-10,14].

To perform fault detection and identification in the presence of uncertainties, machine learning-based techniques i.e., support vector machine (SVM) and decision trees govern the observers to find the exact solution for fault diagnosis under various crack types and motor speed conditions [10, 14]. The block diagram of the main steps for fault diagnosis of the bearing based on the extended-state observation techniques or fuzzy extended-state

observation techniques and machine learning algorithms (further referred to as hybrid) is represented in Figure 1.1.

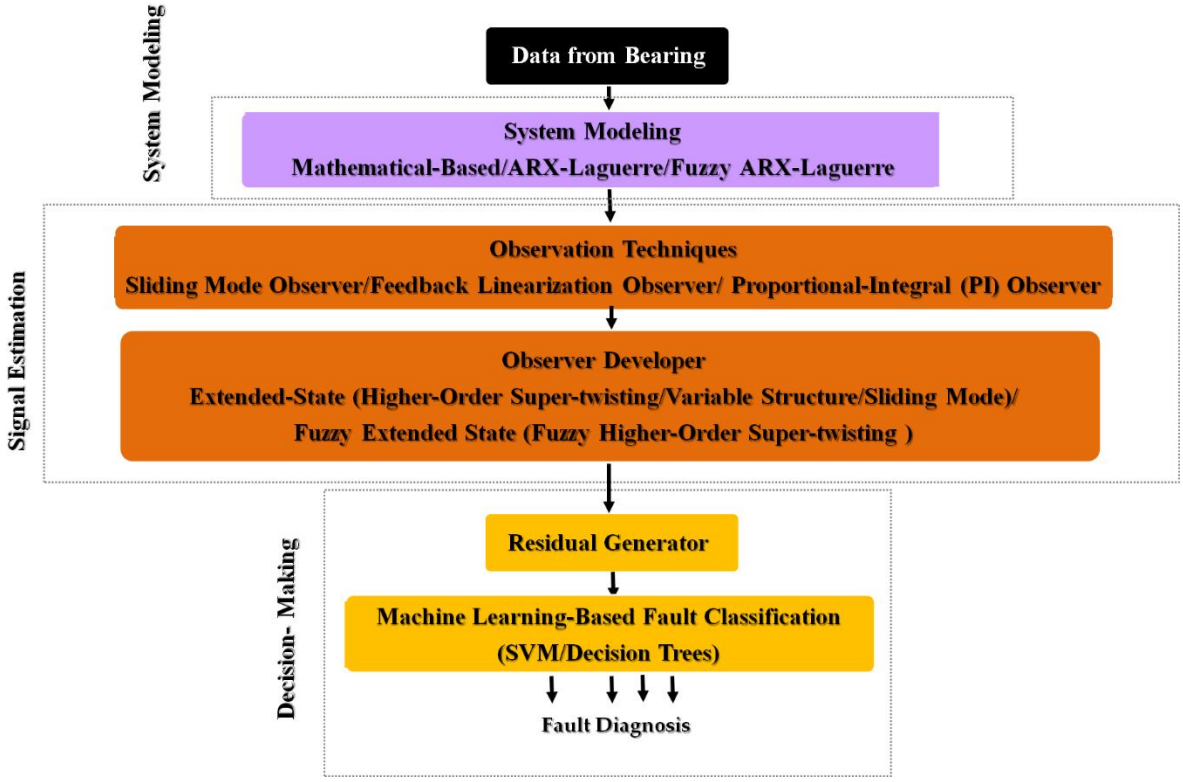

Figure 1.1. Block diagram of the algorithms for fault diagnosis of bearing based on hybrid approach.

The diagram has three parts: (a) modeling the dynamic behavior of the bearing, (b) estimation of the bearing signals based on the extended-state observers or fuzzy extended-state observers, and (c) detection and classification of faults based on the machine learning algorithms. Three different techniques are used to bearing modeling in this research such as mathematical vibration bearing modeling, ARX-Laguerre technique, and fuzzy ARX-Laguerre procedure. Estimating the bearing signals has two principal sub-blocks: (i) designing the classical linear or nonlinear observers such as Proportional-Integral (PI) observer, sliding mode observer, and feedback linearization observer, (ii) implementing an extended-state algorithm (e.g., higher-order super-twisting technique, variable structure algorithm, sliding mode procedure) or fuzzy extended-state technique (e.g., fuzzy high-order super-twisting algorithm) to reduce chattering, improving the robustness and reliability, and evaluating the

estimation accuracy. Detection and identification of faults based on the machine learning algorithms has two main sub-blocks: (i) generation of the residual signal based on the difference between the original and estimated signals, and (ii) the detection and classification of the fault types using the SVM or decision trees techniques.

The objective of this dissertation is to perform fault detection and identification or diagnosis of rotating machine that includes: (i) investigating robust and reliable fault diagnosis under inconsistent (uncertain)working conditions based on extended-state observation techniques, and (ii) investigating robust, reliable, and accurate fault diagnosis under inconsistent (uncertain)working conditions based on fuzzy extended-state observation algorithm.

1.2 Thesis Outline

The dissertation is composed of three parts, excluding Chapter 1. Extended-state observation fault diagnosis of bearings under inconsistent working conditions is presented in Part I, i.e., Chapter 2, 3, and 4. Part II is about the fuzzy extended-state observation fault diagnosis of bearings under inconsistent working conditions, i.e., Chapter 5. Finally, the summary of work, conclusion, and future work is presented in Part III, i.e., Chapter 6.

Chapter 2 discusses the mechanism of robust and reliable fault diagnosis of rotary machine bearings based on sliding mode observation technique. This chapter presents the advantages of sliding mode observer such as stability and robustness in process of bearing fault diagnosis. Apart from advantages of sliding mode observer for fault diagnosis such as stability and robustness but this technique is suffering from chattering phenomenon especially in uncertain conditions. To address this issue the super-twisting higher-order sliding mode observer is presented in this chapter. Once the residual signal is obtained based on the difference between the original signal and estimated signal, this signal can be successfully used to perform the decision making. In addition, the support vector machine (SVM) is used for fault detection and diagnosis. The effectiveness of the proposed technique is evaluated using a vibration dataset provided by Case Western Reserve University (CWRU) dataset. Bearing fault diagnosis is difficult when some fluctuations in working conditions such as shaft

speed are experienced. Therefore, this chapter focuses on the fault diagnosis of bearings under variable load.

In Chapter 3 a nonlinear observation technique for bearing fault diagnosis based on robust extended-state (variable structure) feedback linearization observer is presented. The feedback linearization observer is stable; however, this technique suffers from a lack of robustness. The proposed variable structure technique was used to improve the robustness of the fault estimation while reducing the effect of uncertainties (e.g., load variant) in the feedback linearization observer. Once the residual signal is obtained, the support vector machine (SVM) technique is used for fault detection and diagnosis. The effectiveness of the variable structure feedback linearization observer procedure for the identification of the faults was tested using the Case Western University vibration dataset. In this chapter a solution for the fault diagnosis of the bearings under such conditions is presented.

Chapter 4 is about the identification and detection of bearing defects based on robust observation approach when there are inconsistent working conditions. In previous two chapters, the mathematical bearing modeling was used to develop extended-state observation approaches for fault diagnosis. To address the challenges posed by the complexities and disturbance problems of mathematical-based system modeling, we used a signal-based system identification technique based on the ARX–Laguerre technique. To improve the performance of signal estimation, the ARX-Laguerre proportional integral (PI) observer is developed for vibration and acoustic emission signals in this chapter. To address the challenges of ARX-Laguerre PI observer (e.g., stability and robustness), the sliding mode (extended-state) ARX-Laguerre PI observer technique is developed in this chapter. Finally, a machine learning technique, called a support vector machine (SVM) is used for fault detection and identification in this chapter. The effectiveness of the sliding mode (extended-state) ARX-Laguerre PI observer was evaluated using two different datasets: a) the Case Western Reverse University (CWRU) bearing vibration dataset and b) the Smart HSE (SHSE) Lab bearing AE dataset to validate the single and multiple-types of fault diagnosis, respectively. In this chapter the inconsistent working condition are assumed when there is significant shaft speed variation as well as bearing single and multiple-defects of multiple scales exist at the same time.

In Chapter 5 fuzzy extended-state fault diagnosis of a bearing is developed. The complexity of the system's dynamic behavior and uncertainty result in substantial challenges for fault estimation, detection, and identification in rotating machines. To address the aforementioned challenges, this chapter proposes a novel technique for fault diagnosis of a rolling-element bearing (REB), founded on a fuzzy ARX-Laguerre fuzzy higher-order super-twisting (fuzzy extended-state) sliding mode observer. First, a fuzzy ARX-Laguerre algorithm is implemented to model the bearing in the presence of uncertainty. Next, the sliding mode observer is applied to resolve the problems of signal estimation in a complex system with a high degree of uncertainty, such as rotating machinery. To address the problem of chattering phenomenon that is inherent in the sliding mode observer, the higher-order super-twisting (extended-state) technique is introduced. In addition, the fuzzy method is applied to the higher-order super-twisting (extended-state) technique sliding mode observer to improve the accuracy of fault estimation in uncertain conditions. As a result, the fuzzy higher-order super-twisting (fuzzy extended-state) sliding mode observer adaptively improves the reliability, robustness, and estimation accuracy of rolling-element bearing fault estimation. Finally, a machine learning technique, called a decision tree, adaptively derives the threshold values that are used for problems of fault detection and fault identification in this study. The effectiveness of the fuzzy higher-order super-twisting (extended-state) sliding mode observer was evaluated using two diverse datasets: a) the Case Western Reverse University (CWRU) bearing vibration dataset and b) the Smart HSE (SHSE) Lab bearing AE dataset to validate the single and multiple-types of fault diagnosis, respectively. Therefore, observation technique, artificial intelligence, and machine learning based approached is developed in this chapter to address the fault diagnosis issue in bearing.

Finally, chapter 6 concludes the thesis and presents a brief summary of the contributions and discusses future work.

Part I

Extended-State Observation Fault Diagnosis of Bearings Under Inconsistent Working Conditions

Chapter 2

Bearing Fault Diagnosis by a Robust Higher-Order Super-Twisting Sliding Mode Observer

2.1 Introduction

Rolling element bearings (REBs) are very important components in rotating machines, as they are used to reduce the friction between moving parts for linear and rotational motion [5]. Bearings have been widely used in the rotating machinery in various industries, such as steel mills, paper mills, and wind power generators, to improve their lifespan and efficiency by reducing friction and facilitating motion [15]. Complexities of the tasks and nonlinear parameters in REBs make their fault detection and diagnosis (FDD) very challenging. The detection and diagnosis of faults is necessary to prevent the complete failure of the bearing and hence avoid the impairment of the machinery. Several types of faults have been defined in REBs, which are divided into four main categories, i.e., inner raceway faults, outer raceway faults, ball faults, and cage faults [16].

Different techniques have been introduced for the diagnosis of faults in bearings, including signal-based fault diagnosis [17-22], knowledge-based fault diagnosis [23, 24], model-based fault diagnosis [25-27], and hybrid/active approaches to fault diagnosis [28, 29]. Although signal-based fault diagnosis has several advantages, this method has challenges associated with system reliability in the presence of uncertainty and external disturbances. Knowledge-based fault diagnosis has its own challenges, as it requires massive quantities of data for training the system to make diagnostic decisions. Model-based fault diagnosis identifies the faults by using a small dataset, but it needs to model the system's dynamics [6]. Various model-based methods have been rigorously studied in the field of detection, isolation, and identification for REBs [5, 6]. Model-reference methodologies detect faults by setting a threshold for the residual signal, which is generated from the difference between an actual signal and the system's estimation of that signal [7]. These residuals are highly sensitive to the possible faults in the system, which can affect the diagnostic performance [15, 30]. These

signals are certainly independent of the inputs and outputs under normal conditions. Model-reference based fault diagnosis utilizes output observers, system identification and parameter estimation, and the parity equation [5, 26, 31, 32].

Specifically, the system-observer-based technique is regarded as an important model-reference methodology for FDD [5]. Observation methods are designed using different algorithms, such as the proportional-integral (PI) observation technique [13, 33, 34], the proportional multiple-integral (PMI) observation method [35-37], the descriptor observation technique [38, 39], adaptive observation methods [40-42], and sliding mode observation techniques [27, 43-46]. Sliding mode observer (SMO) is an excellent FDD candidate for systems that operate in uncertain and noisy conditions. In this technique, the output estimation error is forced to zero based on the nonlinear switching term. This method can detect and isolate a fault as it adaptively updates the system parameters, which can significantly improve the diagnostic performance of this method if applied for FDD in bearings. Furthermore, this observer works based on the system's behavior, which tends to work very well when most of the dynamic and physical parameters are adequately known [47-50]. Apart from several advantages, such as stability and reliability, this method of using an SMO suffers from the chattering phenomenon, and requires the relative degree of the outputs concerning the uncertainties or disturbances to be one. In mechanical systems based on the position observation, the estimation of the first and second derivative of position, such as velocity and acceleration, respectively, is necessary. Thus, in the acceleration equation, uncertainties and external disturbances are relative to the second derivative of the measured position [50]. The higher-order sliding mode observer (HOSMO) has been proposed to improve the performance of SMO in the presence of uncertainty and disturbances [51-56]. Since HOSMO employs a discontinuous control algorithm on the higher-order derivatives, chattering can be attenuated by moving the switching to the higher derivatives in HOSMO. The performance of the higher-order sliding mode technique has been improved by using different algorithms, such as the suboptimal algorithm [57], the quasi-continuous technique [58], and the twisting method [59]. Apart from the many advantages of sub-optimal HOSMO, the quasi-continuous HOSMO, and the twisting HOSMO, these methods face a critical challenge related to the first-order derivative of the sliding variable. This issue has been addressed by proposing a higher-order

super-twisting sliding mode technique [48]. For unmeasurable state observers and high-accuracy velocity estimation without filtration, the higher-order super-twisting sliding mode observer (HOSTSMO) was proposed [43, 45, 60, 61]. In this chapter, we propose a robust higher-order super-twisting sliding mode observer for fault detection and isolation in the presence of uncertainty and external disturbances for rolling element bearings (REBs).

In the past decade, different machine learning solutions that utilize statistical feature parameters as attributes to learn how to solve various fault diagnosis problems, have been proposed. The most popular approaches reported in the literature include k-nearest neighbor (k-NN) classification algorithms (fault diagnosis) [62], classification and regression trees (CARTs) (fault diagnosis and prognosis) [63, 64], artificial neural networks (fault diagnosis) [65, 66], and other various types of regression algorithms (fault prognosis) [67]. However, these fault diagnosis methods have some limitations. Specifically, k-NN does not learn any specific mathematical function during its training, so the classification result is completely dependent on the quality and scale of the features used in the training set. Moreover, the value of k and the distance function used in this algorithm must be chosen, and a proper tradeoff between accuracy and the time needed for training must be found. Similarly, CART algorithms are also sensitive to the quality of the features used for training; however, they are insensitive to the scale of the data. Like k-NN, CART methods do not manipulate the input data during training, and in cases of overlapping feature spaces, the classification performance of the decision trees can be poor. During the training stage, artificial neural networks (ANNs) may neglect some data problems while adjusting the weights and hyperparameters. However, ANNs have some limitations, such as gradient pitfalls and longer training times for large data sets that may not allow for an optimal solution.

To avoid these issues and to address the problem of fault diagnosis, the support vector machines (SVMs) [68-71] machine learning algorithm is utilized in this chapter. This algorithm has a strong mathematical background, and better addresses feature dimensionality due to the availability of the different types of kernels that can be used for training. For this chapter, a linear kernel [72] was chosen as the kernel function due to the small number of extracted features and the linear separability of the available data. To extend the capabilities

of SVM and solve the multiclass classification problem, a "one-against-one" [73] strategy was employed for training.

Figure 2.1 shows a block diagram of a hybrid fault diagnosis approach based on the SVM-based robust high-order super-twisting sliding mode observer for fault diagnosis for rolling element bearings. The diagram has three main parts: (a) mathematical modeling the dynamic behavior of the REBs [74], (b) estimation of the normal and abnormal signals based on the robust high-order super-twisting sliding mode observer, and (c) detection and identification of faults based on the machine learning (SVM) algorithm [14]. Estimating normal and abnormal signals based on the robust high-order super-twisting sliding mode observer has two principal sub-blocks: (i) designing the sliding mode observer (SMO), (ii) implementing a high-order SMO to reduce chattering, and evaluating it using the super-twisting method. Detection and identification of faults based on the support vector machine (SVM) algorithm has three main sub-blocks: (i) generation of the residual signal based on the difference between the original and estimated signals, (ii) characterization of windows by the energy feature for residual signals, and (iii) the detection and classification of the fault types using the SVM technique.

The rest of this chapter is organized as follows. Section 2.2 gives the problem statements and fault diagnosis objectives. Section 2.3 presents the detailed mathematical modeling of an REB with 5 degrees of freedom. Section 2.4 shows a comprehensive methodology to design an SVM-based robust higher-order super-twisting sliding mode observation (hybrid) technique for fault detection and diagnosis. Datasets, results, and discussion are presented in Section 2.5. Section 2.6 concludes this chapter.

2.2 Problem Statements and Fault Diagnosis Objectives

The main objective of this chapter is to devise a robust scheme for the detecting and estimating of faults in rolling element bearings (REBs), including inner, outer, and roller faults. The proposed scheme is based on vibration modeling and a higher-order sliding mode observer in the presence of uncertainty and disturbance. The foremost challenge is to model the REB vibration data in terms of the energy. This chapter utilizes vibration data collected

using an experimental testbed, which is illustrated in Figure 2.2 [15]. The corresponding Lagrangian formulation for this system consists of potential energy, kinetic energy, and generalized forces as shown below:

$$\frac{d}{dt}\left(\frac{\partial K}{\partial \dot{q}_i}\right) - \frac{\partial K}{\partial q_i} + \frac{\partial P}{\partial q_i} = Q_i, i = 1,2,3,4, \dots, n_{DOF} \tag{2.1}$$

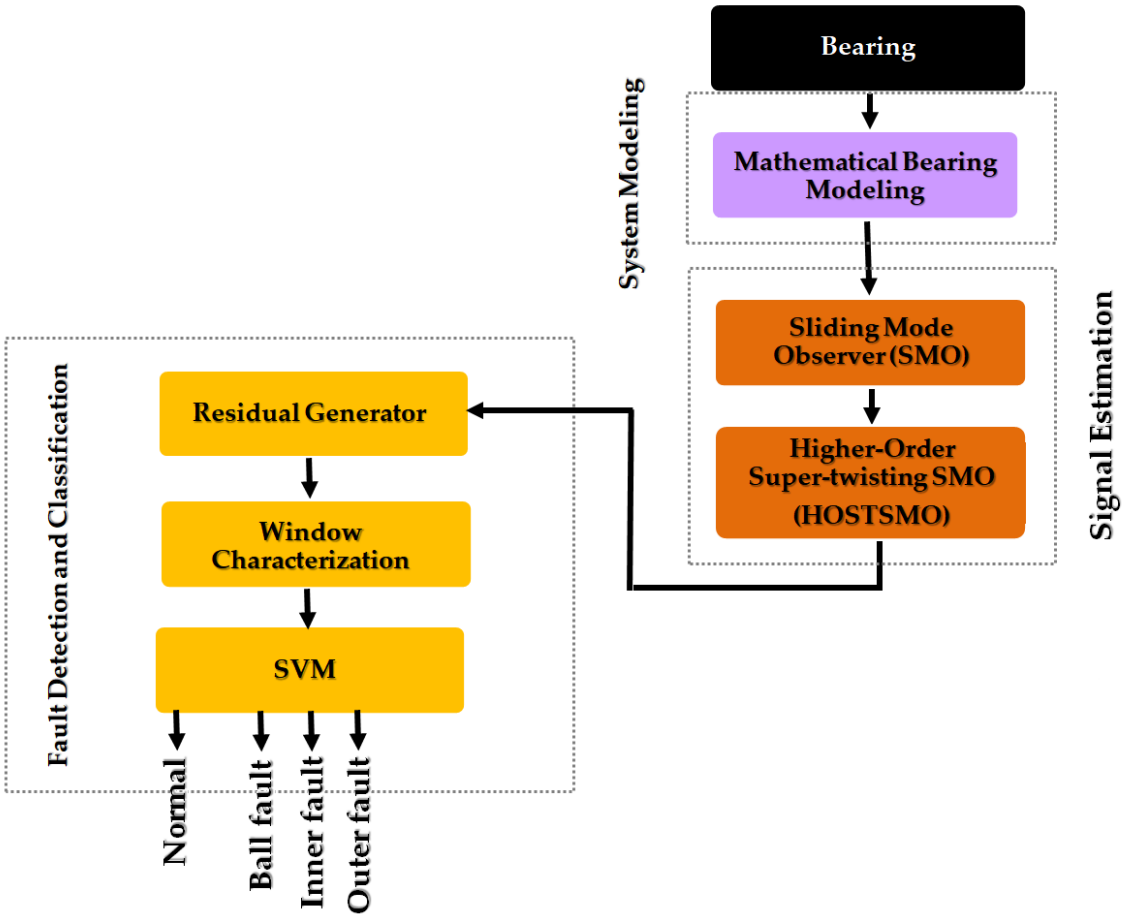

Figure 2.1. Block diagram of the SVM-based robust high-order super-twisting (extended-state) sliding mode observer fault diagnosis of REBs.

where K is the kinetic energy, P represents the potential energy, Q_i represents a generalized force, q_i is the generalized coordinate, and n_{DOF} is the number of degrees of freedom. Each generalized coordinate corresponds to a degree of freedom (DOF) of the system, and each generalized force in the system acts along the corresponding generalized coordinate. The

energy equation is obtained by taking the derivative of Equation (2.1) with respect to each generalized coordinate as follows:

$$F_{(\theta)} = M(\theta)[\ddot{\theta}] + \mathrm{H}(\theta, \dot{\theta}) + \varphi + \Delta + \delta(t - T_f), \tag{2.2}$$

where $F_{(\theta)}, M(\theta), \varphi, \Delta, \delta, \delta(t - T_f)$ and T_f are the force vector, time-variant mass matrix, time-variant nonlinear bearing vector, unknown modeling parameters, faults vector (inner, outer, and ball), time profile of the faults, and time of fault occurrence, respectively. If $\mathrm{H}(\theta, \dot{\theta}) = \mathrm{C}(\theta)[\dot{\theta}] + \mathrm{K}(\theta)[\theta]$ and $\Delta = (\Delta M)(\theta)[\ddot{\theta}] + (\Delta C)(\theta)[\dot{\theta}] + (\Delta K)(\theta)[\theta]$, then the Lagrange dynamic formulation of a bearing can be written as follows:

$$F_{(\theta)} = (M + \Delta M)(\theta)[\ddot{\theta}] + (C + \Delta C)(\theta)[\dot{\theta}] + (K + \Delta K)(\theta)[\theta] + \varphi + \delta(t - T_f), \tag{2.3}$$

where $\mathrm{C}(\theta), \mathrm{K}(\theta)$ and $(\Delta M, \Delta C, \Delta K)$ are the time-variant stiffness matrix, time-variant damping matrix, and unknown modeling parameters for mass, stiffness, and damping matrices, respectively.

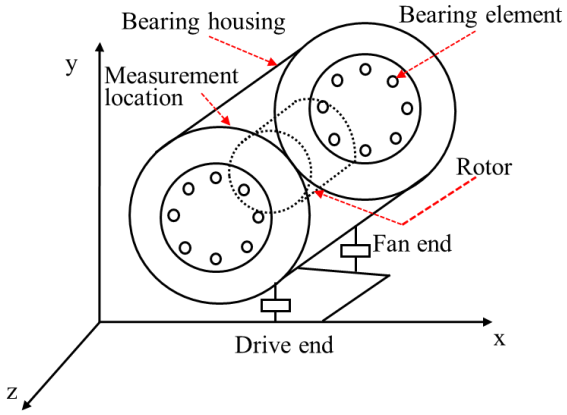

Figure 2.2. The system geometry, measurement location, and configuration of the system.

To simplify the modeling and analysis, ((2.2) and (2.3)) are re-written as follows:

$$[\ddot{\theta}] = M(\theta)^{-1}\{F_{(\theta)} - \Psi(\theta, \dot{\theta})\} - \lambda(\theta, \dot{\theta}, t), \tag{2.4}$$

where $\Psi(\theta,\dot{\theta}) = \mathrm{C}(\theta)[\dot{\theta}] + \mathrm{K}(\theta)[\theta]$ and $\lambda(\theta,\dot{\theta},t) = M(\theta)^{-1}(\Delta + \delta(t-T_f))$ represent the modeling uncertainty and faults of the bearings. For a bearing in healthy condition, it is assumed that the uncertainty is bounded as follows:

$$if\ (t < T_f) \rightarrow \delta(t-T_f) = 0 \rightarrow \|M(\theta)^{-1} \times \Delta\| \leq \Gamma, \tag{2.5}$$

where Γ is a constant. In the faulty condition, (2.5) can be written as follows:

$$if\ (t > T_f) \rightarrow \left\|M(\theta)^{-1} \times M(\theta)^{-1}(\Delta + \delta(t-T_f))\right\| = \lambda(\theta,\dot{\theta},t) > \Gamma, \tag{2.6}$$

Based on the above formulations, we can see that mathematical modeling of REBs is very complicated, and it is not exact. Moreover, the model's behavior may be different from the real system's behavior in both healthy and faulty conditions because the model is usually obtained under various assumptions that may not hold true for a real system. This makes the detection and diagnosis of faults in rolling element bearings more challenging and warrants the development of an algorithm that is robust to modeling uncertainties and disturbances. To solve the challenge of uncertain parameters in system modeling, a higher-order super-twisting sliding mode observer is recommended in this study. This observation technique estimates the faults based on robust model-based nonlinear methods and improves the rate of fault detection and diagnosis. The objectives of fault diagnosis for an REB in the presence of uncertainty is the estimation of inner, outer, and ball faults based on model reference HOSTSMO, which is defined as follows:

$$[\delta_{i_{estimate}}] \rightarrow [\delta_{i_d}], [\delta_{o_{estimate}}] \rightarrow [\delta_{o_d}], [\delta_{b_{estimate}}] \rightarrow [\delta_{b_d}] \tag{2.7}$$

Where $[\delta_{i_{estimate}}], [\delta_{i_d}], [\delta_{o_{estimate}}], [\delta_{o_d}], [\delta_{b_{estimate}}]$ and $[\delta_{b_d}]$ are the estimated inner fault, desired inner fault, estimated outer fault, desired outer fault, estimated ball fault, and desired ball fault, respectively.

2.3 Mathematical Modeling of REBs

As bearing data is inherently nonlinear, we choose the HOSTSMO technique for fault detection and diagnosis. This robust method is highly efficient and can provide excellent

detection and diagnostic performance. The HOSTSMO technique offers a flexible way to find the optimized parameters for a nonlinear data model.

The mathematical model of the REB can be expressed in terms of the angular position of the ball, the fundamental train frequency (FTF), and time, using the following formulations [74-76]:

$$\begin{cases} \theta_j = \dfrac{2\pi(j-1)}{n_b} + \omega_c t + \theta_0 \\ \omega_c = \dfrac{\omega_i}{2}\left(1 - \dfrac{d}{D}\right) \end{cases}, \tag{2.8}$$

where θ_j, n_b, ω_c, ω_i, t, θ_0, d, and D are the angular position of the j-th ball, number of balls, FTF, constant rotor velocity, elapsed time, initial position, ball diameter, and pitch diameter of the bearing, respectively. Figure 2.3 illustrates the 5 degrees of freedom for modeling the REB.

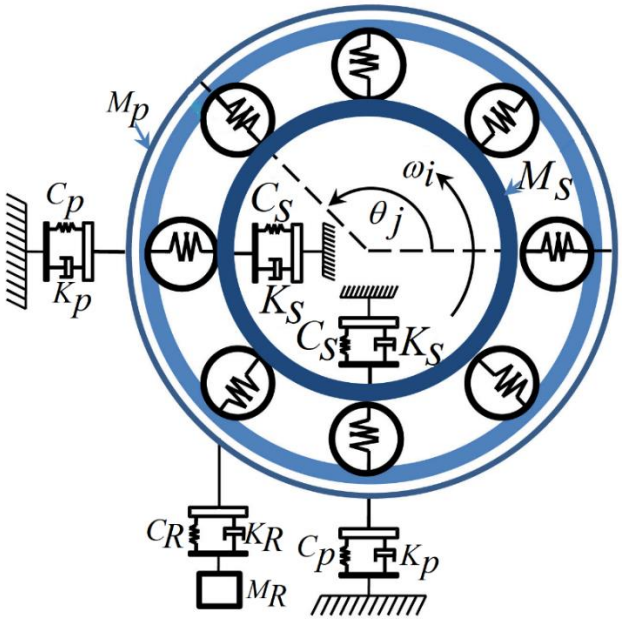

Figure 2.3. Five degrees of freedom of the rolling element bearing (REB) [74].

The contact forces are defined by the following equations [74, 75]:

$$\begin{cases} F_x = \sum_{j=1}^{N_b} C_P \delta_j^{\gamma} \cos(\theta_j) . h(-\delta_j) \\ F_y = \sum_{j=1}^{N_b} C_P \delta_j^{\gamma} \cos(\theta_j) . h(-\delta_j) \end{cases}, \tag{2.9}$$

$$h(x) = \begin{cases} 1 & x \geq 0 \\ 0 & x < 0 \end{cases}. \tag{2.10}$$

The contact deformation is defined as follows:

$$\delta_j = \theta_{xd}\, cos(\theta_j) + \theta_{yd}\, sin(\theta_j - \omega) \tag{2.11}$$

Here, $\delta_j, \theta_j, \gamma, h(x), C_P, \theta_{xd}$, and θ_{yd} are the contact deformation, angular position of the *j*-th REB, force exponent, Heaviside function, stiffness of outer race, and displacements between inner race and ball in the inner, outer, and ball faults in the *x* and *y* directions, respectively. Based on [74, 76], the 5-DOF REB model has three main parts: an outer race, which is modeled by 2-DOF, an inner race, which is modeled by 2-DOF, and the sprung mass, which is modeled by 1-DOF. The equation of the outer race is defined as follows [74]:

$$\begin{aligned} M_P \ddot{\theta}_{x_0} &= F_x - K_P \dot{\theta}_{x_0} - C_P \theta_{x_0} \\ M_P \ddot{\theta}_{y_0} &= F_y - M_P g - (K_P + K_R)\dot{\theta}_{y_0} - (C_P + C_R)\theta_{y_0} + C_R \theta_{y_R} + K_R \dot{\theta}_{y_R} \end{aligned} \tag{2.12}$$

where $M_P, \theta_{x_0}, \theta_{y_0}, K_P, g, K_R, C_R$, and θ_{y_R} are the outer mass, outer center of mass along the *x-axis*, outer center of mass along the *y-axis*, outer damping, gravity, damping of the sprung-mass, stiffness of the sprung-mass, and sprung-mass displacement, respectively. To model the inner race, the equation of the inner race is defined as follows [74]:

$$\begin{aligned} M_S \ddot{\theta}_{x_i} &= -F_x + K_S \dot{\theta}_{x_i} + C_S \theta_{x_i} \\ M_S \ddot{\theta}_{y_i} &= -F_y - M_S g - K_S \dot{\theta}_{y_i} - C_S \theta_{y_i} \end{aligned} \tag{2.13}$$

where $M_S, \theta_{x_i}, \theta_{y_i}, K_S$, and C_S are the mass of the shaft, inner center of mass along the *x-axis*, inner center of mass along the *y-axis*, damping of the shaft, and stiffness of the shaft, respectively. The sprung mass equation (1-DOF) along the *y-axis* is given as follows [74]:

$$M_R \ddot{\theta}_{y_R} = C_R(\theta_{y_0} - \theta_{y_R}) + K_R(\dot{\theta}_{y_0} - \dot{\theta}_{y_R}) - M_R g \tag{2.14}$$

Here, M_R is the mass of the sprung-mass. Based on [74, 76], the localized faults for the outer race, inner race, and ball are given in the following equations. If centers of mass in the *x* and *y* directions are different, then the fault deformation is given by Equations (2.15) and (2.16):

$$\theta_{x_d} = \theta_{x_i} - \theta_{x_o} \qquad \theta_{y_d} = \theta_{y_i} - \theta_{y_o} \tag{2.15}$$

$$\delta_f = \begin{cases} \omega_d & \emptyset_d < \theta_j < \emptyset_d + \Delta_{\emptyset_d} \\ 0 & otherwise \end{cases}. \tag{2.16}$$

whereas the outer contact deformation fault is defined as follows:

$$\delta_o = \max\left(\theta_{x_d}\cos(\theta_j) + \theta_{y_d}\sin(\theta_j) - \omega - \delta_f, 0\right) \tag{2.17}$$

The inner contact deformation fault is defined by Equation (2.20) if the specified angular position $\emptyset_d$ and fault deformation δ_{f_i} are given by Equations (2.18) and (2.19), respectively:

$$\emptyset_d = \omega_i t + \emptyset_0 \tag{2.18}$$

$$\delta_{f_i} = \begin{cases} \omega_d & \emptyset_d < \theta_j < \emptyset_d + \Delta_{\emptyset_d} \\ 0 & otherwise \end{cases} \tag{2.19}$$

$$\delta_i = \max\left(\theta_{x_d}\cos(\theta_j) + \theta_{y_d}\sin(\theta_j) - \omega - \delta_{f_i}, 0\right) \tag{2.20}$$

where $\emptyset_0$ and δ_i are the initial spall location and the inner contact deformation fault, respectively. If the fault deformation is expressed as follows:

$$\delta_f = \begin{cases} \omega_{dr} - \omega_{do} & 0 < \emptyset_S < \emptyset_{bo} \\ \omega_{dr} + \omega_{do} & \pi < \emptyset_S < \pi + \emptyset_{bi} \\ 0 & otherwise \end{cases}, \tag{2.21}$$

where $\emptyset_{bi}$ and $\emptyset_{bo}$ are the angular widths of inner and outer faults, respectively, then ω_{dr} and ω_{do} can be given as follows:

$$\omega_{dr} = \frac{1}{2[d - \sqrt{(d^2 - 4x^2)}]} \tag{2.22}$$

$$\omega_{do} = \frac{1}{2[D_o - \sqrt{(D_o{}^2 - 4x^2)}]} \tag{2.23}$$

Therefore, the ball contact deformation fault is then defined as follows:

$$\delta_b = \max(\theta_{x_d} \cos(\theta_j) + \theta_{y_d} \sin(\theta_j) - \omega - \delta_f, 0) \tag{2.24}$$

Thus, the rolling element bearing model in the presence of uncertainty and faults can be expressed as follows:

$$F_{(\theta_{x,y})} = (M)(\theta)[\ddot{\theta}] + (C)(\theta)[\dot{\theta}] + (K)(\theta)[\theta] + \varphi + F_d(\dot{\theta}) + (\delta_i(t - T_{f_i}) + \delta_o(t - T_{f_o}) + \delta_b(t - T_{f_b})), \tag{2.25}$$

To design a model-reference-based fault diagnosis scheme for bearings, this section uses a 5-DOF mathematical model for an REB system and a benchmark bearing dataset, which was acquired from Case Western Reserve University (CWRU) [77]. The data is collected using vibration acceleration sensors installed on the bearing housings. The bearings used for the collection of this data are 6205-2RS JEM SKF roller bearings, and their parameters for the 5 degrees of freedom model are given in Table 2.1 [78, 79].

Table 2.1. Parameters of REB model.

Parameters	Value
Number of balls	9
Stiffness of ball	$5.96\times10^7(\mathrm{N/m})$
Mass of outer (Kg)	2.7(Kg)
Stiffness of outer	$1.31\times10^5(\mathrm{N/m})$
Mass of shaft (Kg)	1.36(Kg)
Stiffness of Shaft	$23.3\times10^6(\mathrm{N/m})$
Damping	$654(\mathrm{NS/m})$
Ball diameter	7.940(mm)
Pitch diameter	39.04(mm)
Defect size	7(mm)
Defect depth	2(mm)

2.4 Fault Diagnosis: Robust High-Order Super-Twisting Sliding Mode Observer

The vibration signals of an REB have various types of disturbances. Thus, designing a robust approach for fault detection and diagnosis is the principal challenge. In the first step, ARX-Laguerre proportional integral observer (APIO) is briefly discussed. The primary challenge of this technique is robustness. To address this challenge, the proposed higher-order super-twisting sliding mode observer (HOSTSMO) is the second candidate for fault diagnosis in an REB. This technique is designed to ensure fast convergence of the estimated faults to the measured faults in the presence of uncertainties, and to attenuate the chattering.

2.4.1. ARX-Laguerre Proportional-Integral Observer (APIO)

As the rolling element bearing is a nonlinear system, if $X_1 = \theta$ and $X_2 = \dot{\theta}$, the state-space formulation for an REB can be given as follows:

$$\begin{cases} \dot{X}_2 = \alpha(X_1, X_2, u) + \Delta(X_1, X_2, t) + \delta_i(t) + \delta_o(t) + \delta_b(t) \\ Y = (K)^T X_1 \end{cases} \tag{2.26}$$

where $\dot{X}_1 = X_2 = \dot{\theta}, u = F(\theta), \alpha(X_1, X_2, u) = M(\theta)^{-1}\{F_{(\theta)} - \Psi(\theta, \dot{\theta})\}$, $(\dot{X}_1, \dot{X}_2)$ are system states, K is a coefficient, u is the control input, $\delta_i(t)$ is the inner fault, $\delta_o(t)$ is the outer fault, $\delta_b(t)$ is the ball fault, $\Delta(X_1, X_2, t)$ is the system uncertainty, and Y is the measured output**.** The ARX-Laguerre orthonormal technique is given as follows [12]:

$$\begin{aligned} Y(k) = &\sum_{0}^{N_a-1} K_{n,a}\Big(\sum_{j=1}^{\infty} \frac{\sqrt{1-\zeta_a{}^2}}{Z-\zeta_a}\Big(\frac{1-\zeta_a z}{Z-\zeta_a}\Big)^n * y(k)\Big).x_{n,y}(k) + \\ &\sum_{0}^{N_b-1} K_{n,b}\Big(\sum_{j=1}^{\infty} \frac{\sqrt{1-\zeta_b{}^2}}{Z-\zeta_b}\Big(\frac{1-\zeta_b z}{Z-\zeta_b}\Big)^n * u(k)\Big).S_{n,u}(k) \end{aligned} \tag{2.27}$$

where $Y(k), u(k), (K_{n,a} \& K_{n,b}), (N_a, N_b), \Big(\big(\frac{\sqrt{1-\zeta_a{}^2}}{Z-\zeta_a}\frac{1-\zeta_a z}{Z-\zeta_a}\big) \& \big(\frac{\sqrt{1-\zeta_b{}^2}}{Z-\zeta_b}\frac{1-\zeta_b z}{Z-\zeta_b}\big)\Big), (\zeta_a \& \zeta_b), *, x_{n,y}(k)$, and $x_{n,u}(k)$ are the system output, system input, Fourier coefficients, system order, Laguerre-based orthonormal function, Laguerre pole, convolution product, output signal filter, and input

signal filter, respectively. The state space equation for the ARX-Laguerre orthonormal function can be written as follows:

$$\begin{cases} X(k) = [AX(k-1) + b_y y(k-1) + b_u u(k-1)] + \Delta(k-1) + \delta(k-1) \\ Y(k) = (K)^T X(k) \end{cases} \tag{2.28}$$

where $X(k), Y(k), u(k), \Delta(k), \delta(k), (A, b_y, b_u)$ and $(K)^T$ are the input/output filter, measured output, control input, uncertainty and disturbance, faults, coefficient matrices, and the Fourier coefficient, respectively. The matrix A is given as follows:

$$A = \begin{bmatrix} A_y & O_{N_a,N_b} \\ O_{N_b,N_a} & A_u \end{bmatrix}, \tag{2.29}$$

$$A_y = \begin{bmatrix} \zeta_a & 0 & \dots & 0 \\ 1-\zeta_a{}^2 & \zeta_a & \dots & 0 \\ -\zeta_a(1-\zeta_a{}^2) & 1-\zeta_a{}^2 & \dots & 0 \\ \dots & \dots & \dots & 0 \\ \dots & \dots & \dots & 0 \\ (-\zeta_a)^{N_a-1}(1-\zeta_a{}^2) & \dots & \dots & \zeta_a \end{bmatrix} \text{and}$$

$$A_u = \begin{bmatrix} \zeta_b & 0 & \dots & 0 \\ 1-\zeta_b{}^2 & \zeta_a & \dots & 0 \\ -\zeta_b(1-\zeta_b{}^2) & 1-\zeta_b{}^2 & \dots & 0 \\ \dots & \dots & \dots & 0 \\ \dots & \dots & \dots & 0 \\ (-\zeta_b)^{N_b-1}(1-\zeta_b{}^2) & \dots & \dots & \zeta_b \end{bmatrix} \tag{2.30}$$

O_{N_a,N_b} and O_{N_b,N_a} are null matrices of dimensions $N_a \times N_b$ and $N_b \times N_a$, respectively. The vectors b_y and b_u can be defined as follows:

$$b_y = \sqrt{1-\zeta_a^2} \begin{bmatrix} 1 \\ -\zeta_a \\ (-\zeta_a)^2 \\ \cdot\cdot \\ \cdot\cdot \\ (-\zeta_a)^{N_a-1} \end{bmatrix} \tag{2.31}$$

$$b_u = \sqrt{1-\zeta_b^2}\begin{bmatrix} 1 \\ -\zeta_b \\ (-\zeta_b)^2 \\ \vdots \\ (-\zeta_b)^{N_b-1} \end{bmatrix} \tag{2.32}$$

The ARX-Laguerre PI observer for a faulty system is given as follows:

$$\begin{cases} \hat{X}_{PIO}(k) = [A\hat{X}_{PIO}(k-1) + b_y\hat{Y}_{PIO}(k-1) + b_u u(k-1)] + \hat{\Delta}(k-1) \\ +\hat{\delta}_i(k-1) + \hat{\delta}_o(k-1) + \hat{\delta}_b(k-1) + K_p[Y(k-1) - \hat{Y}_{PIO}(k-1)]] \\ \hat{Y}_{PIO}(k) = (K_\alpha)^T \hat{X}(k) \\ \hat{\delta}_{i-PIO}(k) = \hat{\delta}_i(k-1) + K_{ii}[Y(k-1) - \hat{Y}_{PIO}(k-1)] \\ \hat{\delta}_{o-PIO}(k) = \hat{\delta}_o(k-1) + K_{io}[Y(k-1) - \hat{Y}_{PIO}(k-1)] \\ \hat{\delta}_{b-PIO}(k) = \hat{\delta}_b(k-1) + K_{ib}[Y(k-1) - \hat{Y}_{PIO}(k-1)] \end{cases} \tag{2.33}$$

where $\hat{X}_{PIO}(k), \hat{Y}_{PIO}(k), u(k), \hat{\Delta}(k), \hat{\delta}_{i-PIO}(k), \hat{\delta}_{o-PIO}(k), \hat{\delta}_{b-PIO}(k)$ and $(K_\alpha, K_p, K_{ii}, K_{io}, K_{ib})$ are the estimated system state based on APIO, estimated measured output based on APIO, control input, estimated uncertainty and disturbance, estimated inner fault, estimated outer fault and estimated ball fault, and gains, respectively. Gains are optimized based on the Linear Matrix Inequality (LMI) optimization method as follows:

$$\begin{cases} \\ \\ (1-2\gamma)P - (A_\gamma^T P - K_\gamma^T)P^{-1}(PA_\gamma - K_\gamma) > 0 \\ \gamma \in [0, 0.5] \\ K_\varepsilon = \begin{bmatrix} K_P \\ K_{i*} \end{bmatrix}, * = i, o, b \\ K_\gamma = \begin{bmatrix} K^T & 0 \end{bmatrix} \\ A_\gamma = \begin{bmatrix} A + b_y C^T & b_u \\ 0_{1,M} & 1 \end{bmatrix} \end{cases} \tag{2.34}$$

where γ is the decay rate that is used to quantify the convergence rate of the estimation error and P is the Lyapunov symmetric and positive definite matrix. When the accuracy of the signal estimation increases, the estimated output $(\hat{Y}_{PIO})$ converges to the measured output Y. This means that the difference between these two signals converges to zero. Thus, the residual signal based on APIO can be calculated as follows:

$$r_{PIO}(k) = Y(k) - \hat{Y}_{PIO}(k) . \tag{2.35}$$

Though useful in many cases, this method is not robust in detecting and isolating faults in the presence of uncertainties and disturbances. To improve its robustness, a sliding mode observer is used.

2.4.2. Proposed High-Order Super-Twisting Sliding Mode Observer (HOSTSMO)

Based on Figure 2.1, the robust high-order super twisting sliding mode observer fault diagnosis for REBs is presented in this chapter. The fault diagnosis of the REB based on the proposed algorithm has two main steps. To increase the fault detection and classification, the signal estimation accuracy of the normal and abnormal signals based on the robust high-order super twisting sliding mode observer is presented in the first step. The sliding mode observer is a robust technique that can be used for signal estimation. A high-order super twisting technique is used to mitigate the issue of chattering in sliding mode observer. The second step for fault diagnosis is fault detection and classification. To increase the fault detection and identification accuracy, SVM is considered in this chapter. The sliding mode observer is defined as follows [50]:

$$\begin{cases} \hat{\dot{X}}_{1-SMO} = \hat{X}_{2-SMO} + \lambda_a sgn(e_{1-SMO}) + \hat{\delta}_{SMO}, \ (e_{1-SMO} = X_1 - \hat{X}_{1-SMO}) \\ \hat{\dot{X}}_{2-SMO} = \alpha(X_1, \hat{X}_{2-SMO}, u) + \lambda_b sgn(e_{2-SMO}), \ \left(e_{2-SMO} = \hat{\dot{X}}_{1-SMO} - \hat{X}_{2-SMO}\right), \\ \hat{Y}_{SMO} = (K_\beta)^T \hat{X}_{1-SMO} \end{cases} \tag{2.36}$$

In addition, the equation to define fault estimation based on the SMO is:

$$\hat{\delta}_{SMO}(k+1) = \hat{\delta}_{SMO}(k) + \lambda_a(e_{1-SMO}) + \lambda_b sgn(e_{2-SMO}). \tag{2.37}$$

where$u = F(\theta), \alpha(X_1, X_2, u) = M(\theta)^{-1}\{F_{(\theta)} - \Psi(\theta, \dot{\theta})\}$, $(\widehat{X}_{1-SMO}, \widehat{X}_{2-SMO})$ are estimated system states based on sliding mode observer, $(K_\beta, \lambda_a, \lambda_b)$ are coefficients, u is the control input, $\hat{\delta}_{SMO}$ is fault estimation based on the sliding mode observer, and $\hat{Y}_{SMO}$ is the estimated measured output based on sliding mode observer. The SMO is stable and robust; however, it suffers from the chattering phenomenon. The new part is defined as follows:

$$H = \lambda \|e_i\|^{0.5} sgn(e_i),\ \lambda > 0 \tag{2.38}$$

where H and λ are an observation function and coefficient, respectively. If the uncertainties are estimated, the sliding dynamics can converge to zero in finite time.

$$\begin{cases} H = \lambda \|e_i\|^{0.5} sgn(e_i) - \hat{\chi} \\ \dot{\hat{\chi}} = -\lambda_0 \times sgn(e_i) \end{cases}, \tag{2.39}$$

where $\dot{\hat{\chi}}$ and λ_0 are the super-twisting variable and coefficient, respectively. The compensate sliding variable dynamic is defined as follows:

$$\begin{cases} \lambda \|e_i\|^{0.5} sgn(e_i) - \hat{\chi} = \hat{\lambda}(X_1, X_2, t) \\ \dot{\hat{\chi}} = -\lambda_0 \times sgn(e_i) \end{cases}, \tag{2.40}$$

where $\lambda(\theta, \dot{\theta}, t) = M(\theta)^{-1}\{\Delta + \delta(t - T_f)\}$ represents the modeling uncertainty and estimated bearing faults. Based on (2.39) and (2.40), the challenge of uncertainties and unknown inputs (faults) estimation can be solved in finite time. Equation (2.40) is called the super-twisting algorithm. Based on (2.39), the formulation of HOSTSMO can be given as follows:

$$\begin{cases} \dot{\hat{X}}_{1-HOSTSMO} = \hat{X}_{2-HOSTSMO} + \lambda_1 |e_1|^{\frac{2}{3}} sgn(e_1) + \hat{\delta}_{SMO}, \quad \left(e_1 = X_1 - \hat{X}_{1-HOSTSMO}\right) \\ \dot{\hat{X}}_{2-HOSTSMO} = \alpha\left(X_1, \hat{X}_{2-HOSTSMO}, u\right) + \lambda_2 |e_2|^{0.5} sgn(e_2) + \hat{\chi}, \\ \hat{Y}_{HOSTSMO} = \left(K_\beta\right)^T \hat{X}_{1-HOSTSMO}, \left(e_{2-HOSTSMO} = \hat{X}_{1-HOSTSMO} - \hat{X}_{2-HOSTSMO}\right) \end{cases} \tag{2.41}$$

when $\dot{\hat{\chi}} = \lambda_0 \times sgn(e_1)$. In addition, the equation to define fault estimation based on the HOSTSMO is:

$$\begin{cases} \hat{\delta}_{SMO}(k+1) = \hat{\delta}_{SMO}(k) + \lambda_a(e_{1-SMO}) + \lambda_b sgn(e_{2-SMO}) + \lambda_2 |e_2|^{0.5} sgn(e_2) - \hat{\chi} \\ \dot{\hat{\chi}} = \lambda_0 \times sgn(e_1) \end{cases} \tag{2.42}$$

According to Equations (2.26) and (2.41), the estimation error performance of model reference HOSTSMO in REBs can be given as follows:

$$\begin{cases} \tilde{\dot{X}}_{1-HOSTSMO} = \dot{X}_1 - \hat{\dot{X}}_{1-HOSTSMO}, \\ \tilde{\dot{X}}_{2-HOSTSMO} = \dot{X}_2 - \hat{\dot{X}}_{2-HOSTSMO}, \\ \tilde{\dot{X}}_{1-HOSTSMO} = \tilde{X}_{2-HOSTSMO} - \lambda_1 |e_1|^{\frac{2}{3}} sgn(e_1), \\ \tilde{\dot{X}}_{2-HOSTSMO} = \mathrm{X}\left(X_1, \hat{X}_{2-HOSTSMO}, \tilde{X}_{2-HOSTSMO}, u\right) - \lambda_2 |e_2|^{0.5} sgn(e_2) - \hat{\chi}, \\ \mathrm{X}\left(X_1, \hat{X}_{2-HOSTSMO}, \tilde{X}_{2-HOSTSMO}, u\right) = \alpha(X_1, X_2, u) - \alpha\left(X_1, \hat{X}_{2-HOSTSMO}, u\right) + \Delta(X_1, X_2) + \delta, \\ \tilde{Y}_{HOSTSMO} = (K)^T X_1 - \left(K_\beta\right)^T \hat{X}_{1-HOSTSMO} \end{cases}, \quad (2.43)$$

If the system states are bounded as $\left|\mathrm{X}\left(X_1, \hat{X}_{2-HOSTSMO}, \tilde{X}_{2-HOSTSMO}, F\right)\right| < H^+$, then the sliding gains $(\lambda_0, \lambda_1, \lambda_2)$ can be calculated as follows to guarantee stability and convergence:

$$\begin{cases} \lambda_0 = 1.1 \times H^+ \\ \lambda_1 = 1.9 \times \sqrt[3]{H^+}. \\ \lambda_2 = 1.5 \times \sqrt{H^+} \end{cases} \quad (2.44)$$

When the accuracy of the signal estimation increases, the estimated output $\left(\hat{Y}_{HOSTSMO}\right)$ converges to the measured output Y. This means that the difference between these two signals converges to zero. Thus, the residual signal based on HOSTSMO can be calculated as follows:

$$r_{HOSTSMO}(k) = Y(k) - \hat{Y}_{HOSTSMO}(k). \quad (2.45)$$

2.4.3. Fault Diagnosis Using Support Vector Machine

Based on Figure 2.1, after estimating the normal and abnormal signals using the HOSTSMO technique and finding the residual signals, the decision-making ability can be introduced using a support vector machine (SVM) technique. This part has two main steps: a) residual signal characterization, and b) SVM-based fault detection and identification. The residual signals obtained for normal and abnormal conditions are utilized for the fault diagnosis of the REBs. First, numerical attributes such as feature parameters are used for fault diagnosis. Various types of features can be used. In this chapter, the energy of residual signals was selected. The value of the energy attribute can be computed as follows:

$$E = \sum_{i=1}^{M} r_{xi}^2 \tag{2.46}$$

where E, M and r_{xi} are the energy of the residual signals in different conditions, the total number of instances, and the residual signal, respectively. After extracting the feature (e.g., energy) from the residual signals in normal and abnormal conditions, the SVM technique is used for fault diagnosis [14]. The outline realization of the proposed high-order super-twisting sliding mode observer method for the fault diagnosis of the bearing is summarized in Algorithm 2.1.

Algorithm 2.1. Proposed high-order super-twisting sliding mode observer for fault diagnosis of the bearing.

1: Bearing mathematical modelling (2.25)
2: Run the sliding mode observer (2.36), (2.37)
3: Reduce the chattering and improve the accuracy in sliding mode observer based on high-order super-twisting algorithm (2.41), (2.42)
4: Run the residual signal characterization by energy (2.45), (2.46)
5: Apply the SVM classification technique for fault detection and identification [14].

2.5 Datasets, Results, and Analysis

2.5.1. Dataset

To validate the effectiveness of the proposed algorithm, this section uses the 5-DOF mathematical formulation in [15, 74] for REB system modeling and a benchmark bearing dataset that was acquired from Case Western Reserve University (CWRU) [77]. The apparatus employed in the experiment included a 2-hp motor, a torque transducer, a load motor, and a dynamometer. Figure 2.4 illustrates the detailed location of each component [15]. In this system, the vibration sensor is used for data collection from roller bearings 6205-2RS JEM SKF for the diagnosis of bearing faults. Single-point faults with three different crack sizes (i.e., severity levels) of 0.007, 0.014, and 0.021 inches in diameter were seeded on the drive-end bearings at different bearing locations as the outer raceway fault (OR), inner raceway fault (IR), and the ball fault (Ball), respectively. Data was collected for the three fault conditions and bearings in normal healthy state. The data was recorded at a 48 kHz sampling rate under four different motor loads from 0 to 3 hp. The description of the data is given in Table 2.2.

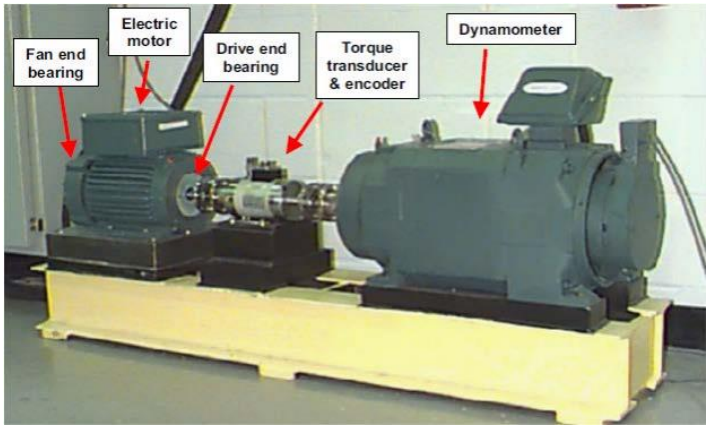

Figure 2.4. The seeded roller bearing test rig for recording fault data.

Table 2.2. Case Western Reverse University (CWRU) dataset.

Dataset f = 48 kHz	Fault Types	Motor Load (hp)	Motor Speed (rpm)	Fault Crack Size (in)
Dataset 1	Normal states	0	1797	0.007, 0.014, and 0.021
	IR fault states	0	1797	
	OR fault states	0	1797	
	Ball fault states	0	1797	
Dataset 2	Normal states	1	1772	0.007, 0.014, and 0.021
	IR fault states	1	1772	
	OR fault states	1	1772	
	Ball fault states	1	1772	
Dataset 3	Normal states	2	1750	0.007, 0.014, and 0.021
	IR fault states	2	1750	
	OR fault states	2	1750	
	Ball fault states	2	1750	
Dataset 4	Normal states	3	1730	0.007, 0.014, and 0.021
	IR fault states	3	1730	
	OR fault states	3	1730	
	Ball fault states	3	1730	

IR = inner raceway fault; OR = outer raceway fault; Ball = ball fault.

2.5.2. Training and Testing Subset Configuration

For analyzing the fault detection and fault identification capabilities of the proposed methodology, the dataset consisting of 1600 samples (400 data instances per class) was randomly split into training and testing subsets. Specifically, 1200 samples (75 instances per class) were used for training SVM classification algorithms, whereas the remaining previously unobserved 400 samples (100 instances per class) were utilized for the testing process. The

similar dataset perturbations were applied to the residual signals obtained by the referenced APIO and SMO methods in order to perform the comparison between them and the proposed technique (HOSTSMO) used in conjunction with the SVM classification algorithm.

2.5.3. Fault Detection and Fault Identification

To validate the efficacy of the proposed HOSTSMO, APIO, and SMO methods for fault detection and diagnosis method, we test it with benchmark bearing datasets as described in Table 2.2. Figure 2.5 shows the residual signals for the normal, inner fault, outer fault, and ball fault conditions based on proposed HOSTSMO. Based on this figure, the difference between various states of signals in the HOSTSMO is clear for fault detection and identification.

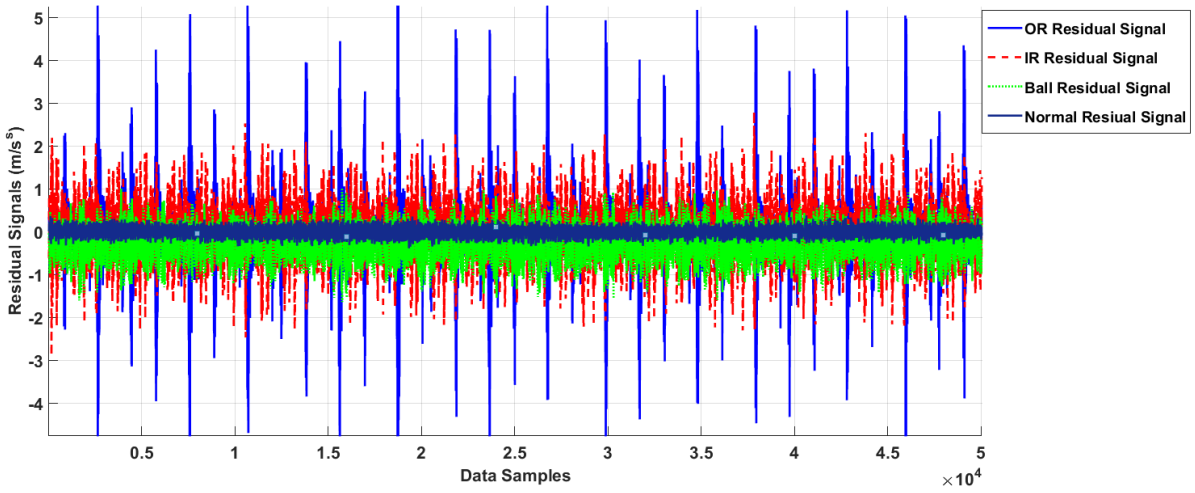

Figure 2.5. Residual of acceleration for normal, inner, outer, and ball faults.

To provide a comprehensive performance evaluation, the two case-studies are considered in this result sections: evaluating fault diagnosis accuracies on crack-variant datasets provided by CWRU and the created custom load-variant datasets. In the first step, we investigate the fault identification capabilities of the proposed HOSTSMO, SMO, and the state-of-the-art APIO technique [12] on four crack-variant datasets, where the torque load remained fixed. The fault diagnosis results obtained for the REB datasets with various crack diameters under fixed load conditions are tabulated in Tables 2.3–2.6. The diagnostic performance is reported as the percentage of correct detections in all data.

Table 2.3. Fault diagnosis results when the torque load is 0 hp.

Algorithms	HOSTSMO (Proposed Method)			SMO			APIO		
Crack Diameters (in)	0.007	0.014	0.021	0.007	0.014	0.021	0.007	0.014	0.021
Normal	100%	100%	100%	100%	100%	100%	88%	88%	88%
Ball Fault	100%	97%	100%	89%	91%	92%	88%	78%	78%
OR Fault	95%	96%	96%	81%	89%	92%	75%	81%	78%
IR Fault	96%	93%	95%	88%	90%	94%	70%	70%	71%
Average	97.75%	96.5%	97.75%	89.5%	92.5%	94.5%	80.25%	79.25%	78.75%

Tables 2.3-2.6 demonstrates that HOSTSMO and SMO methods show high fault detection accuracies (i.e., differentiating between normal and abnormal states). Regarding the fault identification (i.e., differentiating between types of faults), it can be seen that the proposed method resulted in the highest accuracy in comparison with the SMO and APIO methods. The results shown in Tables 2.3-2.6 indicate that the HOSTSMO method outperforms the SMO and APIO techniques in terms of average accuracy with a value of 96.19%, 94.88%, and 96.44% for three fault severity levels characterized by crack sizes of 0.007, 0.014, and 0.021 inches, respectively.

Table 2.4. Fault diagnosis results when the torque load is 1 hp.

Algorithms	HOSTSMO (Proposed Method)			SMO			APIO		
Crack Diameters (in)	0.007	0.014	0.021	0.007	0.014	0.021	0.007	0.014	0.021
Normal	100%	100%	100%	98%	98%	98%	88%	88%	88%
Ball Fault	98%	92%	96%	89%	90%	92%	80%	81%	85%
OR Fault	95%	96%	95%	90%	89%	92%	78%	80%	81%
IR Fault	98%	98%	97%	88%	92%	90%	70%	74%	75%
Average	97.75%	96.5%	97%	91.25%	92.25%	93%	79%	80.75%	82.25%

Table 2.5. Fault diagnosis results when the torque load is 2 hp.

Algorithms	HOSTSMO (Proposed Method)			SMO			APIO		
Crack Diameters (in)	0.007	0.014	0.021	0.007	0.014	0.021	0.007	0.014	0.021
Normal	100%	100%	100%	100%	100%	100%	85%	85%	85%
Ball Fault	91%	89%	93%	89%	90%	88%	79%	81%	84%
OR Fault	93%	88%	94%	88%	84%	85%	79%	75%	80%
IR Fault	97%	95%	100%	89%	90%	92%	75%	76%	79%
Average	95.25%	93%	96.75%	91.5%	91%	91.25%	79.5%	79.25%	82%

Table 2.6. Fault diagnosis results when the torque load is 3 hp.

Algorithms	HOSTSMO (Proposed Method)			SMO			APIO		
Crack Diameters (in)	0.007	0.014	0.021	0.007	0.014	0.021	0.007	0.014	0.021
Normal	100%	100%	100%	100%	100%	100%	90%	90%	90%
Ball Fault	93%	89%	90%	86%	85%	86%	79%	79%	80%
OR Fault	89%	90%	90%	82%	86%	88%	76%	78%	80%
IR Fault	94%	95%	97%	87%	94%	89%	75%	77%	79%
Average	94%	93.5%	94.25%	88.75%	91.25%	90.75%	80%	81%	82.25%

As shown in these tables, the proposed method for bearing fault diagnosis outperforms the state-of-the-art SMO method yielding average performance improvements of 5.94%, 3.13%, and 4.065% , and outperforms the state-of-the-art APIO method yielding average performance improvements of 16.49%, 14.78%, and 15.13% for three fault severity levels characterized by crack sizes of 0.007, 0.014, and 0.021 inches, respectively.

The fault diagnosis results obtained for the REB datasets with load-variant conditions is tabulated in Table 2.7. Based on Table 2.2 we re-configured the available CWRU dataset and created three custom load-variant datasets to validate the robustness of the proposed fault identification technique under changing load conditions.

Table 2.7. The accuracy of the fault diagnosis for the load-variant datasets.

Algorithms	HOSTSMO (Proposed Method)			SMO			APIO		
Crack Diameters (in)	0.007	0.014	0.021	0.007	0.014	0.021	0.007	0.014	0.021
Normal	100%	100%	99%	97%	98%	98%	91%	91%	88%
Ball fault	94%	94%	95%	86%	89%	91%	80%	81%	83%
OR Fault	91%	92%	91%	78%	80%	85%	73%	75%	79%
IR Fault	93%	92%	94%	89%	90%	93%	80%	84%	84%
Average	94.5%	94.5%	94.75%	87.5%	89.25%	91.75%	81%	82.75%	83.5%

The results presented in this table allow us to conclude that the HOSTSMO method is highly robust to the changing experimental conditions, such as torque loads and rotating speeds. The proposed technique outperformed its counterparts with the lowest average classification accuracy of 94.5%, achieved for the crack with diameters of 0.007 and 0.014 inches under different load level conditions in this case study.

2.6 Conclusions

In this chapter, a hybrid approach using the SVM-based higher-order super-twisting sliding mode observation method is developed for detection and classification of REB faults.

The bearing fault signal is highly nonlinear and composed of uncertain dynamic parameters. To design a robust model-reference observation technique, bearing was modeled using a 5-degree-of-freedom nonlinear system. To increase the signal estimation accuracy and reduce the chattering phenomenon, a high-order super-twisting sliding mode observer is developed. Once the residual signal is obtained based on the difference between the original signal and estimated signal, these signals are characterized by energy and can be successfully used to perform the decision making. In addition, the support vector machine (SVM) is used for fault detection and diagnosis. The effectiveness of the proposed observation technique was tested with a benchmark dataset that was provided by Case Western Reserve University. As a result, the proposed method improved the average fault identification performance by about 5.94%, 3.13%, and 4.065% compared with the state-of-the-art SMO for the crack sizes of 0.007, 0.014, and 0.021 inches, respectively. In addition, the proposed algorithm improved the average performance of fault identification by about 16.49%, 14.78%, and 15.13% compared with the state-of-the-art APIO for the crack sizes of 0.007, 0.014, and 0.021 inches, respectively. Moreover, the proposed algorithm demonstrated its robustness while performing the tasks of REB fault detection and identification under changing operating conditions, such as variable load levels and variable rotating speeds. In addition, the use of the HOSTSMO improved the average fault identification performance for under changing operating conditions by about 5.1% and 12.2% compared with the SMO and APIO, respectively. Based on the results we can conclude that the proposed methodology is highly efficient in diagnosing bearing faults.

Chapter 3

Bearing Fault Diagnosis Using an Extended Variable Structure Feedback Linearization Observer

3.1 Introduction

The most common method to decrease the friction in rotating machinery is the use of rolling element bearings (REBs) [5]. REBs have been used in many diverse applications, such as industrial meters, aerospace, and engines [15]. Across industries, the reliability and lifespan of the rotating machine are two critical factors for its safe and continued operation. However, various parameters can reduce the bearing lifespan; such as improper installation, the presence of contaminants, and incorrect handling [80]. Thus, the design and application of stable and reliable techniques for fault detection and diagnosis (FDD) are critical for identifying various faults prior to complete machine failure.

The four main types of bearing failure are the inner, outer, ball, and cage faults [16]. When a crack or spall exists in any of these raceways, the bearing will generate impulses, depending on its dynamics. To analyze the bearing condition, different condition monitoring techniques based on acoustic emissions, stator current, shaft voltage, bearing circuit analysis, vibration, and bearing current have been studied [81]. Among these, the vibration and acoustic emission measurement techniques have been the most widely used [81-86]. Various signature analysis methods of vibration measurements have been explored to improve the performance and reliability of the condition monitoring techniques [83-85]. Moreover, fault detection and diagnosis can be divided into four major categories: (a) Signal-based [83, 87-91], knowledge-based [92-97], model-based [25-27], and hybrid-based fault diagnosis [29, 87, 98]. The main challenge of signal-based FDD is the reliability of the diagnosis in the presence of uncertainties and external disturbances [5, 6]. To address this issue, statistical features extracted from the signals and machine learning algorithms, such as support vector machine (SVM) and proximal support vector machine [93], have been used in the literature. Recently,

several deep learning techniques such as deep autoencoders [97], artificial neural networks (ANNs), and hierarchical convolution networks have been introduced by various researchers for signal-based FDD [92, 94-96]. Meanwhile, the diagnosis decision in the knowledge-based approach is fully dependent on the data and on proper tuning, using the various hyper-parameters [99]. The model-based method, on the other hand, is relatively simple and can be easily applied if the appropriate dynamics of the target system are available.

In this chapter, therefore, a model-reference fault detection and diagnosis technique for the rolling element bearing is proposed [5, 32, 96, 100]. Various researchers have used observational techniques, based on different algorithms. Examples include the proportional-integral (PI) technique [12, 101], proportional multiple-integral (PMI) method [37, 102, 103], descriptor technique [104, 105], adaptive methods [42, 106, 107], sliding mode techniques [45, 46, 108, 109], and feedback linearization techniques [110, 111]. Linear observer methods (e.g., PI and PMI) have been used in various applications for FDD, but these techniques have challenges in the presence of uncertainties [8, 112]. To solve the challenge of linear observers, nonlinear observer techniques have been recommended [46, 110, 111]. One of the well-known nonlinear observation techniques for FDD is the sliding mode observer [45, 46, 108, 109]. Apart from the numerous positive attributes of the sliding mode observer, such as stability and reliability, this technique has the challenge of a chattering phenomenon [8]. To avoid chattering, a proposed feedback linearization observer is recommended in this research. Feedback linearization is a procedure for system linearization, but it is ultimately a nonlinear control theory technique. This observer works based on the system behavior, and thus the output performance can be excellent if the system's dynamics are adequately known. The traditional feedback linearization observer is stable; however, this technique suffers in its robustness. The variable structure technique was used to improve the robustness with respect to fault estimation and the uncertainties in the feedback linearization observer. The support vector machine (SVM) algorithm is used for fault identification in this chapter. The efficacy of the proposed feedback linearization observer (PFLO) approach was validated using data collected from Case Western Reverse University (CWRU) rolling element bearing tests [113].

Figure 3.1 shows a block diagram of the hybrid technique based on the SVM-based variable structure feedback linearization fault diagnosis for rolling element bearings. This block diagram has three main parts: (a) mathematical modeling the dynamic behavior of the REBs [74], (b) estimation of the normal and abnormal signals based on the robust feedback linearization observer, and (c) detection and identification of faults based on the machine learning (SVM) algorithm [14]. Estimating normal and abnormal signals based on the robust feedback linearization observer has two principal sub-blocks: (i) designing the feedback linearization observer (FLO), (ii) improving the robustness of the feedback linearization observer based on the variable structure algorithm. Detection and identification of faults based on the support vector machine (SVM) algorithm has three main sub-blocks: (i) generation of the residual signal based on the difference between the original and estimated signals, (ii) characterization of windows by the energy feature for residual signals, and (iii) the detection and classification of the fault types using the SVM technique.

The remainder of this chapter is organized as follows. The mathematical formulation of rolling bearing element (REB) is described in Section 3.2. The proposed feedback linearization observer is presented in Section 3.3. Bearing dataset, results, and discussion are provided in Section 3.4. In Section 3.5, conclusions are presented.

3.2 Rolling Element Bearing Mathematical Formulation

Based on [8, 74], the bearing model is presented as a five-degree-of-freedom nonlinear and time-varying system. The energy formulation for REB is defined as in the following equation [74].

$$F_{(q)} = (I + \Delta I)(q)[\ddot{q}] + (C + \Delta C)(q)[\dot{q}] + (g + \Delta g)(q)[q] + N + \psi, \qquad (3.1)$$

where $F_{(q)}, I(q), C(q), g(q), N, \psi$, and $(\Delta I, \Delta C, \Delta g)$ are the force vector, mass vector, time-variant stiffness matrix, time-variant damping matrix, nonlinear bearing parameter vector, various types of fault, and unknown modeling parameters for mass, stiffness, and damping matrix, respectively. The uncertainty is defined as in the following equation.

$$\Delta_d = (\Delta I)(q)[\ddot{q}] + (\Delta C)(q)[\dot{q}] + (\Delta g)(q)[q], \tag{3.2}$$

where Δ_d is uncertain and unknown parameters.

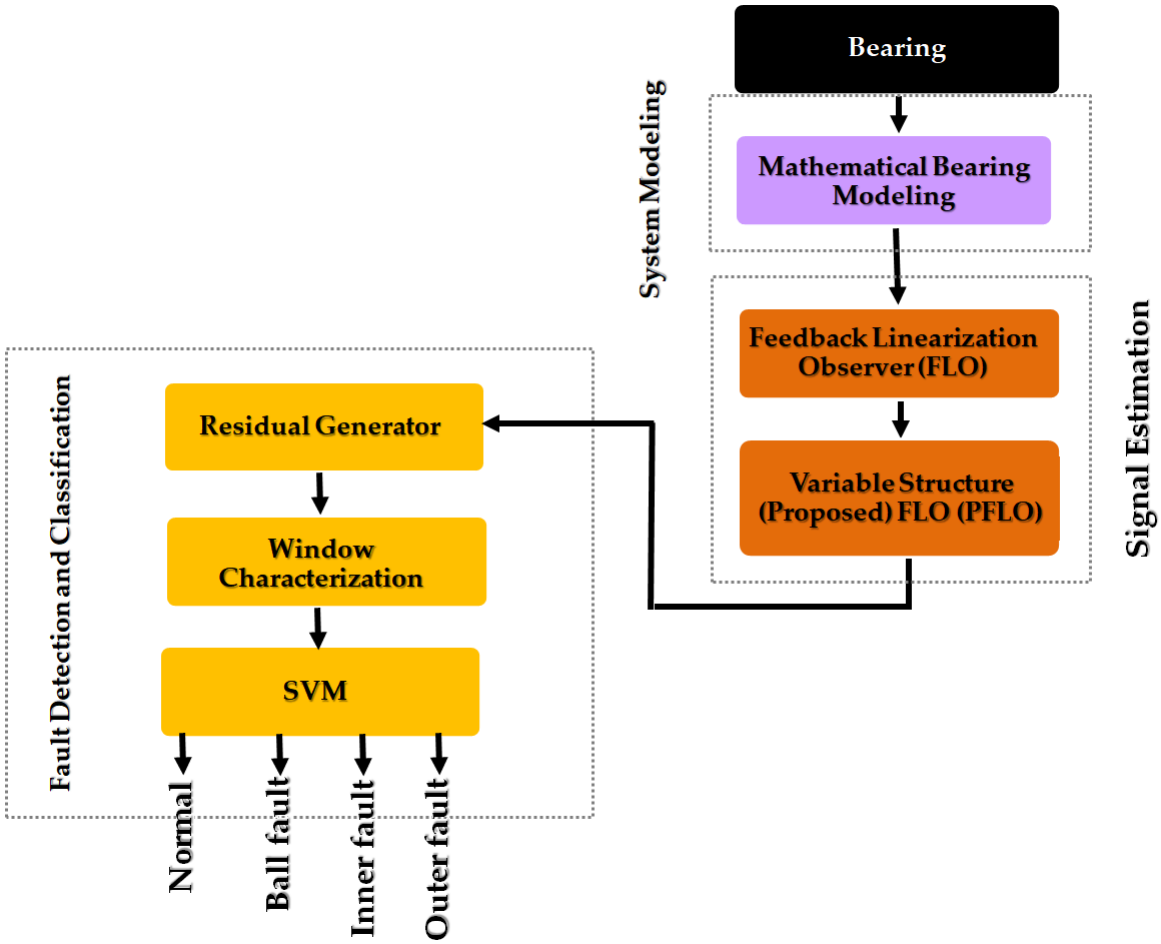

Figure 3.1. Block diagram of the SVM-based variable structure feedback linearization observer fault diagnosis of REBs.

Based on Equations (3.1) and (3.2), the dynamic equation of the bearing is represented as follows:

$$F_{(q)} = I(q)[\ddot{q}] + C(q)[\dot{q}] + g(q)[q] + \Delta_d + N + \psi, \tag{3.3}$$

To model the above system equation, we have:

$$[\ddot{q}] = I(q)^{-1}\{F_{(q)} - C(q)[\dot{q}] - g(q)[q] - \Delta_d - N - \psi\}. \quad (3.4)$$

If $\Omega(q,\dot{q}) = C(q)[\dot{q}] + g(q)[q] + N$, and $\Gamma(q,\dot{q}) = I^{-1}(q)(\Delta_d + \psi)$, then Equation (3.4) is re-written as follows:

$$[\ddot{q}] = I(q)^{-1}\{F_{(q)} - \Omega(q,\dot{q})\} - \Gamma(q,\dot{q}). \quad (3.5)$$

In a healthy condition, the bounded uncertainty is defined as follows:

$$if\ \psi = 0 \rightarrow \|I(q)^{-1} \times \Delta_d\| \leq \sigma_n \quad (3.6)$$

In a faulty condition, Equation (3.6) can be re-written as follows:

$$if\ \psi \neq 0 \rightarrow \|I(q)^{-1} \times (\psi + \Delta_d)\| > \sigma_n \quad (3.7)$$

Here σ_n is a normal threshold value. Based on Equation (3.5), the mathematical modeling of the REBs includes uncertainties and unknown conditions. To address this drawback, and to increase the accuracy of the signal estimation, the proposed feedback linearization observer (PFLO) can as described in the following section.

3.3 Fault Diagnosis: Proposed Feedback Linearization Observer

Based on Figure 3.1, the proposed feedback linearization observer (PFLO) fault diagnosis for a REBs is presented in this chapter. The fault diagnosis of the REB based on the PFLO has two main parts. To have a robust and reliable fault detection and identification, the signal estimation accuracy of the normal and abnormal signals based on the PFLO is presented in the first step. The FLO is a nonlinear observer that can be used for signal estimation. In addition to effectively estimate the signal, robustness is the other challenge that needs to be addressed. To increase the signal estimation robustness, a variable structure technique is introduced. After estimate the signal, to increase the fault detection and identification accuracy, SVM is considered in this chapter.

Based on references [8, 74], the Case Western Reserve University (CWRU) bearing is modelled as a 5-DOF (degrees of freedom) system. Let us consider $Z_1 = q \; and \; Z_2 = \dot{q}$. The Lagrange formulation of the bearing in Equation (3.3) can be written in state space form as:

$$\begin{cases} \dot{Z}_1 = Z_2 = \dot{q} \\ \dot{Z}_2 = \ddot{q} = f(Z_1, Z_2, u) + \Delta_d(Z_1, Z_2, t) + \psi, \\ W = (C)^T Z_1 \end{cases} \tag{3.8}$$

where $f(Z_1, Z_2, u) = I(q)^{-1}\{F_{(q)} - \Omega(q, \dot{q})\}$. Here, $(\dot{Z}_1, \dot{Z}_2), u = F_{(q)}, W$, and $(C)^T$ are the state of bearing, system's input, system's output, and output coefficient, respectively. To validate the proposed method, we will compare this method with a state-of-the-art ARX-Laguerre proportional-integral observation (APIO) technique [8, 12], and the feedback linearization observer (FLO) in Equation (3.9). Therefore, the APIO is represented in the following section.

3.3.1. ARX-Laguerre Proportional-Integral Observer (APIO)

In the first step, the ARX-Laguerre proportional-integral observer (APIO) is recommended for the FDD of the bearing. This technique is linear and models the fault based on the integral term. The formulation of the APIO technique for FDD in the bearing is defined as follows [12]:

$$\begin{cases} \hat{Z}(k) = \left[\alpha \hat{Z}(k-1) + \beta_w \widehat{W}(k-1) + \beta_u u(k-1)\right] + \hat{\Delta}_d(k-1) + \hat{\psi}(k-1) + \\ \qquad K_P\left[W(k-1) - \widehat{W}(k-1)\right], \\ \widehat{W}(k) = (C_\alpha)^T \hat{Z}(k) \end{cases}, \tag{3.9}$$

Based on the APIO technique, the fault is modeled based on the linear integral theorem, as follows:

$$\hat{\psi}(k) = \hat{\psi}(k-1) + K_i\left[W(k-1) - \widehat{W}(k-1)\right]. \tag{3.10}$$

where $\hat{Z}(k), \widehat{W}(k), \hat{\psi}(k), K_P, K_i, (C_\alpha)^T$ and $(\alpha, \beta_w, \beta_u)$ are the system state estimation, measured output estimation, faults (error) estimation, proportional coefficient, integral coefficient, output coefficient, and coefficients, respectively. Based on reference [12], the coefficients $\alpha, \beta_w,$ and β_u are calculated as follows:

$$\alpha = \begin{bmatrix} \alpha_w & O_{N_a,N_b} \\ O_{N_b,N_a} & \alpha_u \end{bmatrix}, \tag{3.11}$$

The α_w and α_u coefficients can be written as [8, 12]

$$\alpha_w = \begin{bmatrix} \zeta_a & 0 & \dots & 0 \\ 1-{\zeta_a}^2 & \zeta_a & \dots & 0 \\ -\zeta_a(1-{\zeta_a}^2) & 1-{\zeta_a}^2 & \dots & 0 \\ \cdots & \dots & \dots & 0 \\ \dots & \dots & \dots & 0 \\ (-\zeta_a)^{N_a-1}(1-{\zeta_a}^2) & \dots & \dots & \zeta_a \end{bmatrix} \text{and}$$

$$\alpha_u = \begin{bmatrix} \zeta_b & 0 & \dots & 0 \\ 1-{\zeta_b}^2 & \zeta_a & \dots & 0 \\ -\zeta_b(1-{\zeta_b}^2) & 1-{\zeta_b}^2 & \dots & 0 \\ \cdots & \dots & \dots & 0 \\ \dots & \dots & \dots & 0 \\ (-\zeta_b)^{N_b-1}(1-{\zeta_b}^2) & \dots & \dots & \zeta_b \end{bmatrix} \tag{3.12}$$

where (ζ_a, ζ_b) and $(O_{N_b,N_a}, O_{N_a,N_b})$ are Laguerre poles, and null matrices, respectively. Based on the recursive nature of Equation (3.10) when inserted into Equation (3.9), it is clear that this technique is prone to large fluctuations in uncertain and highly nonlinear conditions. To address this issue, the proposed feedback linearization observer is recommended.

3.3.2. Variable Structure Feedback Linearization Observer (PFLO)

Based on Figure 3.1, the variable structure feedback linearization observer (PFLO) can be designed to estimate signals in the presence of uncertainties. The feedback linearization observer (FLO) offers a nonlinear approach to find an optimized estimation of the system and fault. This technique is stable, but it has some issues in the presence of uncertainties. To evaluate the feedback linearization observer, a variable structure observer is recommended. This technique is one of the highly robust fault detectors for uncertain and faulty systems. The FLO model adaptively improves the linearized model. The state space feedback linearization observer is defined in the following formulation:

$$\begin{cases} \dot{\hat{Z}}_1 = \hat{Z}_2 + K_{p_1} e_1, (e_1 = Z_1 - \hat{Z}_1) \\ \dot{\hat{Z}}_2 = f(Z_1, \hat{Z}_2, u) + I^{-1} \times (K_{p_2} e_2) + \hat{\psi} + \hat{\Delta}_d(Z_1, Z_2, t), (e_2 = \dot{\hat{Z}}_1 - \hat{Z}_2) \\ \widehat{W} = (C_\alpha)^T \hat{Z}_1 \end{cases} \quad (3.13)$$

The fault is modelled based on the following definition:

$$\hat{\psi}(k) = I^{-1}\{\hat{\psi}(k-1) + K_{i_1}[W(k-1) - \widehat{W}(k-1)]\}. \quad (3.14)$$

where $(K_{p_1}, K_{p_2}, (C_\alpha)^T, K_{i_1})$ are coefficients. The feedback linearization observer is stable; however, this technique suffers from a lack of robustness. A variable structure observer (VSO) is one of the nonlinear and robust fault detectors for uncertain and faulty systems. The state space formulation for the VSO is defined follows [8]:

$$\begin{cases} \dot{\hat{Z}}_1 = \hat{Z}_2 + \gamma_a \, sgn(e_1), (e_1 = Z_1 - \hat{Z}_1) \\ \dot{\hat{Z}}_2 = f(Z_1, \hat{Z}_2, u) + \gamma_b \, sgn(e_2) \quad , (e_2 = \dot{\hat{Z}}_1 - \hat{Z}_2) \\ \widehat{W} = (C_\alpha)^T \hat{Z}_1 \end{cases} \quad (3.15)$$

According to [8], the VSO suffers from a chattering phenomenon. To address the issues of the variable structure observer and feedback linearization observer, the robust variable structure technique was applied to the feedback linearization observer. The fault estimate based on the robust variable structure technique is defined as follows:

$$\begin{cases} K_z \left\| W(k-1) - \widehat{W}(k-1) \right\|^{0.5} sgn\left(W(k-1) - \widehat{W}(k-1)\right) - \hat{\chi} = \hat{\Delta}_d(Z_1, \hat{Z}_2, t) + \hat{\psi} \\ \dot{\hat{\chi}} = K_{z_0} \times sgn\left(W(k-1) - \widehat{W}(k-1)\right) \end{cases} \quad (3.16)$$

where $(\gamma_a, \gamma_b, K_z)$ and $\dot{\hat{\chi}}$ are coefficients and the variable for the super-twisting technique, respectively. Based on Equations (3.15) and (3.16), the proposed variable structure extended feedback linearization observer is defined as follows:

$$\begin{cases} \dot{\hat{Z}}_1 = \hat{Z}_2 + K_{p_1} e_1, (e_1 = Z_1 - \hat{Z}_1) \\ \dot{\hat{Z}}_2 = f(Z_1, \hat{Z}_2, u) I^{-1} \times (K_{p_2} e_2) + \hat{\Delta}_d(Z_1, Z_2, t) + \hat{\psi}, (e_2 = \dot{\hat{Z}}_1 - \hat{Z}_2) \\ \widehat{W} = (C_\alpha)^T \hat{Z}_1 \end{cases} \quad (3.17)$$

The fault estimation formulation is defined as follows:

$$\begin{cases} \hat{\psi} = \hat{\psi}(k-1) + K_{i_1}\left[W(k-1) - \widehat{W}(k-1)\right] + K_z\left\|W(k-1) - \widehat{W}(k-1)\right\|^{0.5} \times \\ sgn\left(W(k-1) - \widehat{W}(k-1)\right) - \hat{\chi}, \\ \dot{\hat{\chi}} = K_{z_0} \times sgn\left(W(k-1) - \widehat{W}(k-1)\right) \end{cases} . \quad (3.18)$$

Based on Equations (3.8) and (3.17), the residual signal $(r(k))$ is defined as follows:

$$r(k) = W(k) - \widehat{W}(k) \quad (3.19)$$

where $\widehat{W}(k)$ is calculated in Equation (3.17), respectively. After obtaining the stability, the state space estimation of $\hat{Z}_1, \hat{Z}_2$ converges to Z_1, Z_2, and the estimation error converges to zero and $K_z\left\|W(k-1) - \widehat{W}(k-1)\right\|^{0.5} sgn\left(W(k-1) - \widehat{W}(k-1)\right) = 0$. More specifically, the convergence conditions are specified by the following criteria:

$$\begin{gathered} \widehat{\Delta}_d\left(Z_1, \hat{Z}_2, t\right) + \hat{\psi} - K_z\left\|W(k-1) - \widehat{W}(k-1)\right\|^{0.5} sgn\left(W(k-1) - \widehat{W}(k-1)\right) - \hat{\chi} = 0 \rightarrow \\ K_z\left\|W(k-1) - \widehat{W}(k-1)\right\|^{0.5} sgn\left(W(k-1) - \widehat{W}(k-1)\right) \rightarrow \\ \widehat{\Delta}_d\left(Z_1, \hat{Z}_2, t\right) + \hat{\psi} > \sigma_n. \end{gathered} \quad (3.20)$$

where σ_n is a normal threshold value. When the variable structure observer is applied to the feedback linearization observer, as in Equation (3.18), the challenge of uncertainties and fault estimation can be solved in finite time. If the states of the system are bounded as $f\left(Z_1, \hat{Z}_2, u\right) < J^+$, to guarantee the stability and convergence, the variable structure fault estimator gains $K_{z_0}$and K_z is calculated as follows:

$$\begin{cases} K_z = 1.5\sqrt{J^+} \\ K_{z_0} = 1.1J^+ \end{cases}, \quad (3.21)$$

where J^+ is a positive constant. Based on the Lyapunov theorem, the Lyapunov function $(V(x))$of the proposed observer is defined by the following equation.

$$\mathrm{V(x)} = 2\mathrm{K}\left|W(k-1) - \widehat{W}(k-1)\right| + \frac{1}{2}\hat{\chi}^2 + \frac{1}{2}(\mathrm{K_Z}\left|W(k-1) - \widehat{W}(k-1)\right|^{0.5} \times sgn\left(W(k-1) - \widehat{W}(k-1)\right) - \hat{\chi} \tag{3.22}$$

Based on Equation (3.22), the Lyapunov derivative function is proposed in Equation (3.23).

$$\dot{\mathrm{V}}(\mathrm{x}) = \frac{\left[\left(W(k-1) - \widehat{W}(k-1)\right)^{0.5} sgn\left(W(k-1) - \widehat{W}(k-1)\right) \quad \hat{\chi}\right]}{\left|W(k-1) - \widehat{W}(k-1)\right|^{0.5}} \times \frac{\mathrm{K_Z}}{2}\begin{bmatrix}\mathrm{K_Z}^2 & -\mathrm{K_Z}\\ -\mathrm{K_Z} & 1\end{bmatrix}\begin{bmatrix}\left(W(k-1) - \widehat{W}(k-1)\right)^{0.5} sgn\left(W(k-1) - \widehat{W}(k-1)\right)\\ \hat{\chi}\end{bmatrix} + \frac{\Delta_d(Z_1, Z_2, t) - \hat{\Delta}_d(Z_1, \hat{Z}_2, t)}{\left|W(k-1) - \widehat{W}(k-1)\right|^{0.5}}\begin{bmatrix}\frac{\mathrm{K_Z}^2}{2} & \frac{-\mathrm{K_Z}}{2}\end{bmatrix} \times \begin{bmatrix}\left(W(k-1) - \widehat{W}(k-1)\right)^{0.5} sgn\left(W(k-1) - \widehat{W}(k-1)\right)\\ \hat{\chi}\end{bmatrix} \tag{3.22}$$

The uncertainty estimation accuracy band is defined by the following

$$\left|\Delta_d(Z_1, Z_2, t) - \hat{\Delta}_d(Z_1, \hat{Z}_2, t)\right| \leq \varphi\left|\left(W(k-1) - \widehat{W}(k-1)\right)^{0.5}\right| \tag{3.24}$$

Here, φ is a positive constant. Based on Equation (3.24) the Lyapunov derivative function is applied to Equation (3.24) and rewritten in Equation (3.25).

$$\dot{\mathrm{V}}(\mathrm{x}) \leq \frac{-\left[\left(W(k-1) - \widehat{W}(k-1)\right)^{0.5} sgn\left(W(k-1) - \widehat{W}(k-1)\right) \quad \hat{\chi}\right]}{\left|W(k-1) - \widehat{W}(k-1)\right|^{0.5}} \times \frac{\mathrm{K_Z}}{2}\begin{bmatrix}\mathrm{K_Z}^2 - (\mathrm{K_Z})\Delta_d(X_1, X_2, t) - \hat{\Delta}_d(X_1, X_2, t) & -\mathrm{K_Z}\\ -(\mathrm{K_Z} + 2\left(\Delta_d(X_1, X_2, t) - \hat{\Delta}_d(X_1, X_2, t)\right) & 1\end{bmatrix} \times \begin{bmatrix}\left(W(k-1) - \widehat{W}(k-1)\right)^{0.5} sgn\left(W(k-1) - \widehat{W}(k-1)\right)\\ \hat{\chi}\end{bmatrix} \tag{3.25}$$

Based on [114], if $\frac{\mathrm{K_Z}}{2}\begin{bmatrix}\mathrm{K_Z}^2 - (\mathrm{K_Z})\Delta_d(X_1, X_2, t) - \hat{\Delta}_d(X_1, X_2, t) & -\mathrm{K_Z}\\ -(\mathrm{K_Z} + 2\left(\Delta_d(X_1, X_2, t) - \hat{\Delta}_d(X_1, X_2, t)\right) & 1\end{bmatrix} > 0$ thus, $\dot{\mathrm{V}}(\mathrm{x}) < 0$.

Thus, it can converge to zero in finite time.

3.3.3. Fault Detection and Fault Identification Using Support Vector Machine

Based on Figure 3.1, after estimating the normal and abnormal signals using the proposed feedback linearization observer (PFLO) and finding the residual signal based on equation (3.19), the decision-making ability can be introduced using a support vector machine (SVM) algorithm. This section has two main parts: a) residual signal characterization, and b) SVM-based fault detection and identification (FDI). The residual signals obtained for normal and abnormal conditions are utilized for the FDI of the REBs. First, the energy of residual signals was selected. The value of the energy attribute can be computed as follows:

$$E = \sum_{i=1}^{M} r_{xi}^2 \tag{3.26}$$

where E, M and r_{xi} are the energy of the residual signals in different conditions, the total number of instances, and the residual signal, respectively. After extracting the feature (e.g., energy) from the residual signals in normal and abnormal conditions, the SVM technique is used for fault diagnosis. The outline realization of the extended variable structure feedback linearization observer method for the fault diagnosis of the bearing is summarized in Algorithm 3.1.

Algorithm 3.1. SVM-based variable structure (extended-state) feedback linearization observer for fault diagnosis of the bearing.

1: Bearing mathematical modelling (3.8)
2: Run the feedback linearization observer (3.13), (3.14)
3: Improve the robustness in feedback linearization observer based on variable structure algorithm (3.17), (3.18)
4: Run the residual signal characterization by energy (3.19,3.26)
5: Apply the SVM classification technique for fault detection and identification [14].

3.4 Dataset, Results and Analysis

The effectiveness of the proposed feedback linearization observer (PFLO), APIO and FLO for fault detection and identification was evaluated using the Case Western Reverse

University (CWRU) bearing dataset. According to [8, 74], the bearing was modeled using mathematical technique, and the parameters for this modeling are given in Table 2.1.

3.4.1. Bearing Data

The vibration data were collected from a 6205-2RS JEM SKF roller bearing installed in a rotary motor. Based on Figure 3.2, a 2-horsepower (hp), three phase induction motor was connected to a torque transducer and a dynamometer to apply different loads, ranging from 0 hp to 3 hp [15, 77]. The vibration sensor (accelerometers) was attached to the roller bearing for data collection. The vibration signals were collected for normal and faulty conditions with a 48 kHz sampling rate. The rotation velocities of the induction motor also varied from 1730 rpm to 1790 rpm. Table 2.2 presents the details of the Case Western Reverse University (CWRU) bearing dataset. Based on the work in reference [113], which is outlined in Table 2.2, three different crack sizes, four different motor loads, and four different motor speeds were seeded at different positions of the bearing.

3.4.2. Training and Testing Configuration

For analyzing the fault detection and fault identification capabilities of the proposed feedback linearization observer, the dataset consisting of 1600 samples (400 data instances per class) was randomly split into training and testing subsets. Specifically, 1200 samples (75 instances per class) were used for training SVM classification algorithms, whereas the remaining previously unobserved 400 samples (100 instances per class) were utilized for the testing process. The similar dataset perturbations were applied to the residual signals obtained by the referenced APIO and FLO methods in order to perform the comparison between them and the proposed technique (PFLO) used in conjunction with the SVM classification algorithm.

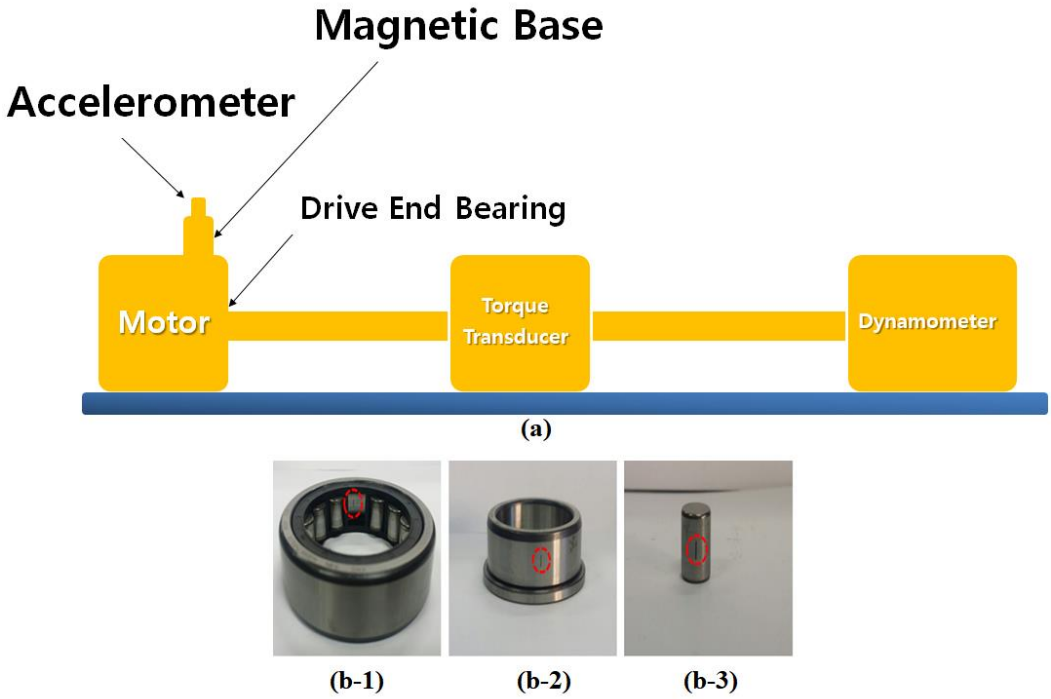

Figure 3.2. An overview of the experimental setup and bearing faults: (a) schematic, (b-1) inner fault, (b-2) outer fault, and (b-3) ball fault.

3.4.3. Fault Detection and Fault Identification

To validate the efficacy of the proposed feedback linearization observer (PFLO), ARX-Laguerre proportional integral observer (APIO), and feedback linearization observer (FLO) methods for fault detection and diagnosis, we test it with benchmark Case Western Reverse University (CWRU) bearing datasets as described in Table 2.2. Figure 3.3 illustrates the residual signals for the normal, inner fault, outer fault, and ball fault conditions based on PFLO. From this figure, it can be observed that the residual signals are well differentiable in normal conditions, which means that they can be used for fault detection (i.e., differentiation between normal and abnormal conditions); and this technique is suitable for identification of the faults. To provide a comprehensive performance of fault diagnosis accuracy, the two case-studies are considered in this result parts: a) crack-variant datasets and b) load-variant datasets provided by CWRU. In the first step, we investigate the fault identification capabilities of the

proposed method (PFLO), FLO, and APIO [12] for four crack-variant datasets, where the torque load remained fixed.

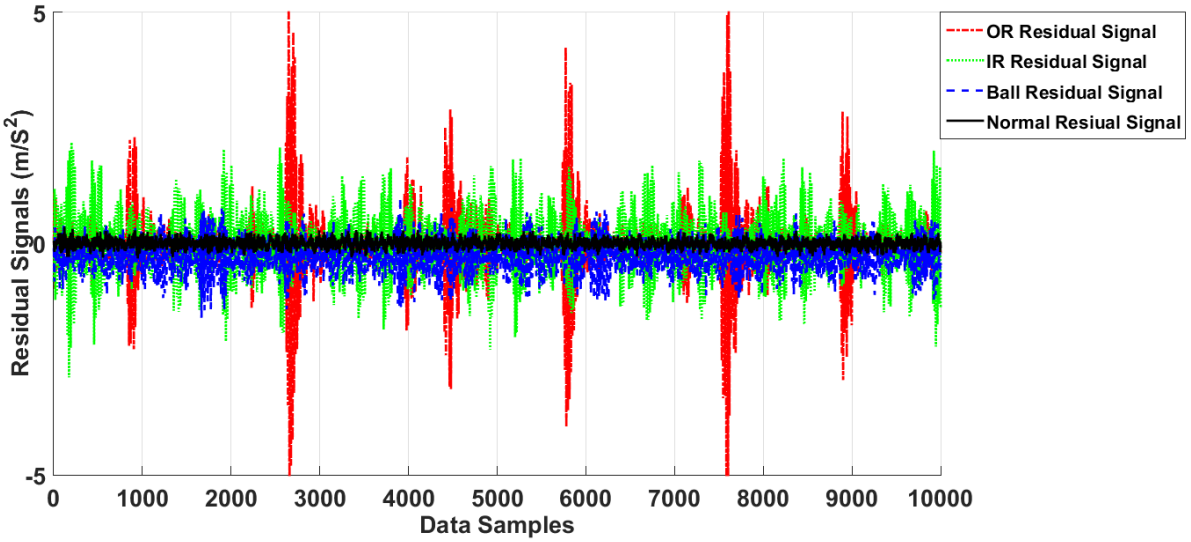

Figure 3.3. Residual of acceleration for normal, inner, outer, and ball faults based on the PFLO.

The fault diagnosis results obtained for the REB datasets with various crack diameters (e.g., 0.007, 0.014, and 0.021 inches) under fixed load conditions are tabulated in Tables 3.1–3.4. Based on these tables the average of the fault detection accuracy (i.e., differentiating between normal and abnormal states) for proposed method (PFLO), FLO, and APIO are 100%, 92.8%, and 87.8%, respectively. Therefore, these tables demonstrate that PFLO show high fault detection accuracies.

Table 3.1. Fault diagnosis results to test the crack-variant dataset when the torque load is 0 hp.

Algorithms	**PFLO (Proposed Method)**			**FLO**			**APIO**		
Crack Diameters (in)	0.007	0.014	0.021	0.007	0.014	0.021	0.007	0.014	0.021
Normal	100%	100%	100%	92%	92%	92%	88%	88%	88%
Ball Fault	100%	100%	100%	89%	92%	90%	88%	78%	78%
OR Fault	95%	95%	96%	87%	90%	92%	75%	81%	78%
IR Fault	95%	93%	94%	89%	88%	89%	70%	70%	71%
Average	97.5%	97%	97.5%	89.25%	90.5%	90.75%	80.25%	79.25%	78.75%

Regarding the fault identification (i.e., differentiating between types of faults), it can be seen that the proposed method (PFLO) resulted in the highest accuracy in comparison with the FLO and APIO methods. Based on Tables 3.1-3.4 the proposed method (PFLO)

outperforms the FLO and APIO techniques in terms of average accuracy with a value of 96%, 95.7%, and 96.7% for three fault severity levels characterized by crack sizes of 0.007, 0.014, and 0.021 inches, respectively.

Table 3.2. Fault diagnosis results to test the crack-variant dataset when the torque load is 1 hp.

Algorithms	**PFLO (Proposed Method)**			**FLO**			**APIO**		
Crack Diameters (in)	0.007	0.014	0.021	0.007	0.014	0.021	0.007	0.014	0.021
Normal	100%	100%	100%	93%	93%	93%	88%	88%	88%
Ball Fault	97%	93%	97%	86%	92%	90%	80%	81%	85%
OR Fault	94%	96%	96%	88%	88%	90%	78%	80%	81%
IR Fault	95%	96%	96%	81%	85%	88%	70%	74%	75%
Average	96.5%	96.25%	97.25%	87%	89.5%	90.25%	79%	80.75%	82.25%

Table 3.3. Fault diagnosis results to test the crack-variant dataset when the torque load is 2 hp.

Algorithms	**PFLO (Proposed Method)**			**FLO**			**APIO**		
Crack Diameters (in)	0.007	0.014	0.021	0.007	0.014	0.021	0.007	0.014	0.021
Normal	100%	100%	100%	90%	90%	90%	85%	85%	85%
Ball Fault	95%	93%	97%	87%	87%	88%	79%	81%	84%
OR Fault	95%	90%	91%	89%	88%	89%	79%	75%	80%
IR Fault	95%	96%	96%	85%	87%	88%	75%	76%	79%
Average	96.25%	94.75%	96%	87.75%	88%	87.75%	79.5%	79.25%	82%

Table 3.4. Fault diagnosis results to test the crack-variant dataset when the torque load is 3 hp.

Algorithms	**PFLO (Proposed Method)**			**FLO**			**APIO**		
Crack Diameters (in)	0.007	0.014	0.021	0.007	0.014	0.021	0.007	0.014	0.021
Normal	100%	100%	100%	96%	96%	96%	90%	90%	90%
Ball Fault	93%	90%	93%	86%	86%	87%	79%	79%	80%
OR Fault	93%	96%	97%	86%	84%	84%	76%	78%	80%
IR Fault	90%	93%	94%	82%	82%	85%	75%	77%	79%
Average	94%	94.75%	96%	87.5%	87%	88%	80%	81%	82.25%

Regarding these tables, the proposed method (PFLO) for bearing fault detection and identification outperforms the FLO technique yielding average performance improvements of 8.1%, 6.95%, and 7.5% for three fault severity levels characterized by crack sizes of 0.007, 0.014, and 0.021 inches, respectively. In addition, the proposed method (PFLO) for bearing fault diagnosis outperforms the APIO technique yielding average performance improvements of 16.7%, 15.8%, and 15.5% for three fault severity levels characterized by crack sizes of 0.007, 0.014, and 0.021 inches, respectively. The fault diagnosis results obtained for the REB datasets with load-variant conditions is tabulated in Table 3.5. Based on Table 2.2 we re-

configured the available CWRU dataset and created three custom load-variant datasets to validate the robustness of the proposed fault identification technique under changing load/motor speed conditions.

Table 3.5. Fault diagnosis results to test the load-variant datasets.

Algorithms	PFLO (Proposed Method)			FLO			APIO		
Crack Diameters (in)	0.007	0.014	0.021	0.007	0.014	0.021	0.007	0.014	0.021
Normal	100%	100%	100%	92%	92%	93%	91%	91%	88%
Ball fault	91%	93%	95%	82%	88%	88%	80%	81%	83%
OR Fault	90%	90%	91%	80%	81%	83%	73%	75%	79%
IR Fault	92%	92%	94%	86%	87%	90%	80%	84%	84%
Average	93.25%	93.75%	95%	85%	87%	88.5%	81%	82.75%	83.5%

Based on Table 3.5 the proposed method (PFLO) is highly robust to the changing experimental conditions, such as torque loads and rotating speeds. Regarding this table, the proposed method (PFLO) for bearing fault diagnosis for the load-variant dataset outperforms the FLO technique yielding performance improvements of 8.25%, 6.75%, and 6.5% for three fault severity levels characterized by crack sizes of 0.007, 0.014, and 0.021 inches, respectively. Moreover, the proposed method (PFLO) for bearing fault diagnosis for the load-variant dataset outperforms the APIO technique yielding performance improvements of 12.25%, 11%, and 11.5% for three fault severity levels characterized by crack sizes of 0.007, 0.014, and 0.021 inches, respectively.

3.5 Conclusions

In this chapter, a hybrid approach using the SVM-based variable structure feedback linearization observer is developed for detection and classification of REB faults. To modeling the vibration bearing signals, the mathematical technique is implemented. Next, signal estimation is developed in two main steps. Firstly, the feedback linearization observer is developed for vibration signals. Secondly, the variable structure technique is recommended to decrease the problems usually encountered with varying motor speeds. Moreover, an SVM is used to detect and classify REB faults. The power of the proposed technique to diagnose REB faults was demonstrated using the Case Western University vibration dataset. As a result, the average performance improvements to test the crack-variant dataset for the recommended

procedure (PFLO) were 7.5% and 16%, compared with the FLO and APIO techniques, respectively. In addition, the average performance improvements to test the load-variant dataset for the proposed method (PFLO) were 7.2% and 11.59%, compared with the FLO and APIO procedures, respectively. In the future, a robust hybrid technique based on the fuzzy robust feedback linearization observation method will be designed to enhance the performance of fault diagnosis. The hybrid extended state observer will be combined with a system estimation technique, and an intelligent extended state robust feedback linearization observer to improve the performance of fault diagnosis in a faulty system.

Chapter 4

Nonlinear Extended-state ARX-Laguerre PI Observer Fault Diagnosis of Bearings

4.1 Introduction

Induction motors have been used in diverse industries, such as the machine tool and oil industries. The dynamic behavior of an induction motor is entirely nonlinear, which can cause various challenges in control and fault diagnosis. High-temperature environments, heavy-duty cycles, poor installation, overloading, and aging of components cause a diverse range of electrical and mechanical defects in motors. Diverse faults have been defined in induction motors, such as motor failures, air-gap faults, bearing and cage faults, and stator failures. The two main types of induction motor defects are mechanical and electrical failures. Various types of induction motor faults are mostly associated with mechanical defects (79%), such as bearing defects (69%) and rotor faults (10%). The other types of induction motor faults are electrical failures (21%), such as open circuits and short circuits in stator windings [4].

The most common defect in induction motors are mechanical failures. These faults are classified as bearing faults and rotor faults. Across industries, bearing defects are the most common critical effect increasing failure in induction motors [4]. The four main types of bearing defects are inner raceway faults, outer raceway faults, ball failures, and cage faults [115, 116]. To analyze the condition of bearings, different types of condition monitoring techniques, such as acoustic emission (AE), stator current, shaft voltage, bearing circuit, and vibration analysis, have been reported in the literature [81]. Vibration and AE measurement techniques are the most widely used for monitoring the bearing conditions [81]. Since AE signals are strongly correlated with actual faults, this research utilizes acoustic emission sensors for data collection.

Two main fault detection and diagnosis methods are hardware-based fault detection and diagnosis (FDD) and functional-based FDD [15]. Fault detection and identification based on the hardware method is a stable, reliable, and preventive maintenance technique, but it is also expensive. To address this issue, functional-based FDD has been presented. The four foremost types of functional-based fault detection and diagnosis are signal-based FDD [83, 87-91], knowledge-based FDD [92-97], model-based FDD [25-27], and hybrid-based FDD [29, 87, 98]. Several signal-based techniques, such as motor current signature analysis (MCSA), vibration analysis, the noise monitoring technique, and torque monitoring analysis, have been introduced. A common signal-based technique for FDD in the induction motor is the MCSA technique. This technique is more common for broken rotor bar (BRB) faults, air-gap eccentricity faults, and stator electric current faults. To diagnose faults in the mechanical parts of an induction motor, such as a bearing, vibration and acoustic emission analysis are more common [7]. The main drawbacks of signal-based FDD are reliability and robustness. Knowledge-based FDD has various advantages, but this technique needs massive quantities of data for training. Model-based FDD has been considered a robust and reliable FDD technique.

The main concept of model-based FDD is system modeling, which has been acknowledged by several researchers in the field [5]. System modeling was divided into two principal techniques: (a) Physical-based system modeling, which uses a mathematical formulation for system modeling, and (b) signal-based system identification, which uses various identification techniques. To address the challenges posed by the complexities and disturbance problems of physical-based system modeling, we used a signal-based system identification technique based on the autoregressive exogenous input (ARX)–Laguerre technique [12].

The main techniques for model-reference FDD use output observers, system identification and parameter estimation, and the parity equation [32, 117]. Various researchers have used observational methods for FDD, such as a proportional integral (PI) observer [12, 101], proportional multiple integral (PMI) observer [37, 102, 103], and sliding mode observer

(SMO) [45, 46, 108, 109]. The fault diagnosis in noisy conditions and state-estimation in the highly nonlinear systems are the main drawbacks in the PI and PMI observers. The sliding mode observer has been considered to solve the linear observer's drawback [109]. Apart from several advantages of the sliding mode observer, chattering phenomenon is the main drawback. The higher order sliding mode observer (HOSMO) was presented to solve the chattering phenomenon in the sliding mode observer [118]. This observer works based on the system's dynamic behavior, and thus the observer performance can be significant if most system dynamic parameters are known. To address the challenges of proportional integral observer (PIO) and SMO, the sliding mode extended-state ARX-Laguerre PI observer technique is introduced in this chapter. The support vector machine (SVM) algorithm is used for fault detection and identification in this chapter. The efficacy of the proposed sliding mode extended-state ARX-Laguerre PI observer (SMALPIO) approach was validated using two different scenarios to analyze the single and multiple-crack detection.

As shown in Figure 4.1, the sliding mode extended-state ARX-Laguerre PI observer technique consists of three main steps: (a) System modeling, (b) the advanced observation technique, and (c) decision part for fault diagnosis. The ARX–Laguerre technique is used for system modeling. The extended- observation algorithm is divided into two main steps: (a) The ARX–Laguerre PI observer, and (b) sliding mode extended-state ARX–Laguerre PI observer. The ARX–Laguerre PI observer is used for signal estimation based on the PI observation technique. While the ARX–Laguerre PI observer is easy to implement, the main drawback of this technique is robustness. To address the robustness issue, a sliding mode extended algorithm is introduced. The decision part based on the support vector machine (SVM) has three main sub-blocks: (a) generation of the residual signal based on the difference between the original and estimated signals, (b) characterization of windows by the energy feature for residual signals, and (c) the detection and classification of the fault types using the SVM technique. The main contributions of this chapter can be summarized as follows:

(1) Modeling the vibration signals based on ARX-Laguerre technique.

(2) Improved estimation accuracy of normal and abnormal signals based on the sliding mode extended-state ARX–Laguerre PI observer.

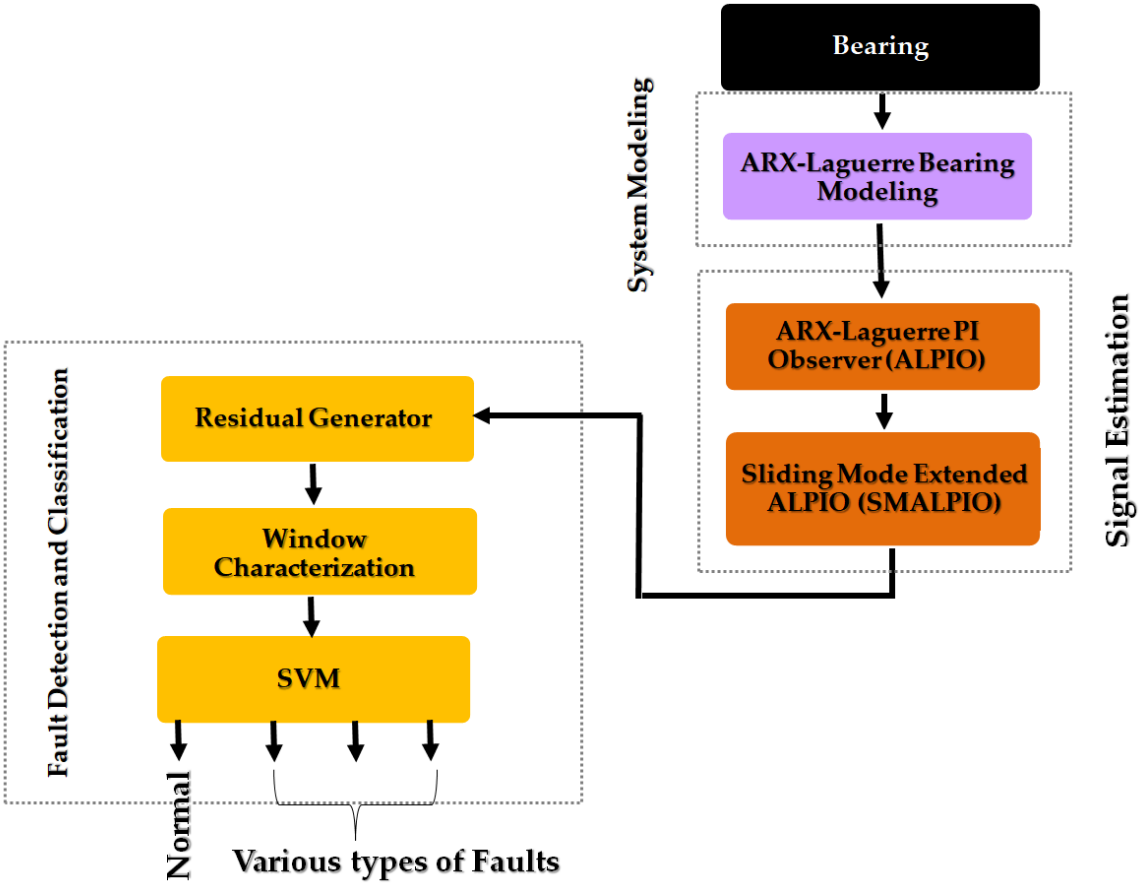

Figure 4.1. Block diagram of the SVM-based sliding mode (extended-state) ARX-Laguerre PI observer for fault diagnosis in the REBs.

The rest of this chapter is organized as follows. In Section 4.2, the rolling element bearing (REB) is modeled using the ARX–Laguerre procedure. The proposed sliding mode extended-state ARX–Laguerre PI observer for bearing fault detection, estimation, and identification is presented in Section 4.3. In the first step of that process, a PI observer is built using the ARX–Laguerre technique; in the second step, the extended-state sliding mode algorithm is added to the ARX–Laguerre PI observer to improve its reliability and robustness. In Section 4.4, two types of datasets are introduced. Results and discussion are presented in Section 4.5. Conclusions are provided in Section 4.6.

4.2 Rolling Element Bearing Modeling

The principal target of this chapter is to detect and estimate an induction motor's mechanical faults based on the sliding mode extended-state ARX-Laguerre PI observer. The foremost issue of the induction motor is mathematical modeling in the presence of uncertainties and faults. Thus, this chapter utilizes a state-of-the-art induction motor experiment for modeling based on system identification. The three-phase space vector of induction motor formulation based on the stator and rotor voltage, current, and flux are presented below [4]:

$$\begin{cases}[V_{stator}] = [Z_{stator}] \times [i_{stator}] + [\dot{\varphi}_{stator}] \\ [V_{rotor}] = [Z_{rotor}] \times [i_{rotor}] + [\dot{\varphi}_{rotor}] \end{cases} \tag{4.1}$$

where $V_{stator}, V_{rotor}, [Z_{stator}], [Z_{rotor}], i_{stator}, i_{rotor}, \dot{\varphi}_{stator}$ and $\dot{\varphi}_{rotor}$ are the three phase stator voltage, three phase rotor voltage, stator impedance, rotor impedance, three phase stator current, three phase rotor current, change of stator flux, and change of rotor flux, respectively. The flux linkage can be written as follows:

$$\begin{cases}[\varphi_{stator}] = [L_{stator}] \times [i_{stator}] + [M_{stator.rotor}] \times [i_{rotor}] \\ [\varphi_{rotor}] = [L_{rotor}] \times [i_{rotor}] + [M_{stator.rotor}] \times [i_{stator}] \end{cases} \tag{4.2}$$

Here, $\varphi_{stator}, \varphi_{rotor}, L_{stator}, L_{rotor}$ and $M_{stator.rotor}$ are the stator flux, rotor flux, stator inductance matrix, rotor inductance matrix, and stator-rotor mutual inductance, respectively. Based on (4.1) and (4.2), the stator and rotor currents are calculated as follows:

$$\begin{aligned} &\frac{d}{dt}\begin{bmatrix} i_{stator} \\ i_{rotor} \end{bmatrix} = \begin{bmatrix} L_{stator} & M_{stator.rotor} \\ M_{stator.rotor} & L_{rotor} \end{bmatrix}^{-1} \times \\ &\left(\begin{bmatrix} V_{stator} \\ V_{rotor} \end{bmatrix} - \begin{bmatrix} Z_{stator} & \omega_r \frac{d}{dt} M_{stator.rotor} \\ \omega_r \frac{d}{dt} M_{stator.rotor}{}^T & Z_{rotor} \end{bmatrix} \begin{bmatrix} i_{stator} \\ i_{rotor} \end{bmatrix} \right) \end{aligned} \tag{4.3}$$

where ω_r is rotor rectangular velocity. Based on the dynamic formulation of an induction motor, mathematical modeling of the induction motors is incredibly complicated and

uncertain, and thus, the task of modeling is significantly important. To address this issue, this chapter utilizes an ARX-Laguerre system estimation technique for system modeling. This technique reduces the complexity and improves the robustness [12, 119]. The ARX-Laguerre orthonormal technique for modeling an REB is presented based on the system input and output, Fourier coefficients, and Laguerre-based orthonormal function as follows [12, 119]:

$$O(k) = \sum_{0}^{N_\alpha - 1} K_{n,\alpha} \left(\sum_{j=1}^{\infty} \frac{\sqrt{1-\zeta_\alpha{}^2}}{Z-\zeta_\alpha} \left(\frac{1-\zeta_\alpha, z}{Z-\zeta_\alpha} \right)^n * O(k) \right). S_{n,O}(k) + \sum_{0}^{N_\beta - 1} K_{n,\beta} \left(\sum_{j=1}^{\infty} \frac{\sqrt{1-\zeta_\beta{}^2}}{Z-\zeta_\beta} \left(\frac{1-\zeta_\beta, z}{Z-\zeta_\beta} \right)^n * I(k) \right). S_{n,I}(k) \tag{4.4}$$

where $O(k), (K_{n,a} \& K_{n,b}), (N_a, N_b), \left(\left(\frac{\sqrt{1-\zeta_\alpha{}^2}}{Z-\zeta_\alpha} \frac{1-\zeta_\alpha, z}{Z-\zeta_\alpha} \right) \& \left(\frac{\sqrt{1-\zeta_\beta{}^2}}{Z-\zeta_\beta} \frac{1-\zeta_\beta, z}{Z-\zeta_\beta} \right) \right), (\zeta_\alpha \& \zeta_\beta), *, I(k), S_{n,O}(k)$, and $S_{n,I}(k)$ are the system output, coefficients of Fourier, order of system, functions of the Laguerre-based orthonormal, Laguerre poles, convolution product, system input, output signal filtered, and filtered input signal, respectively. To calculate the state-space equation, the following variables are defined in Equations (4.5) and (4.6).

$$\begin{cases} L_n^\alpha = \dfrac{\sqrt{1-\zeta_\alpha{}^2}}{Z-\zeta_\alpha} \left(\dfrac{1-\zeta_\alpha, z}{Z-\zeta_\alpha} \right)^n \\ L_n^\beta = \dfrac{\sqrt{1-\zeta_\beta{}^2}}{Z-\zeta_\beta} \left(\dfrac{1-\zeta_\beta, z}{Z-\zeta_\beta} \right)^n \end{cases} \tag{4.5}$$

$$\begin{cases} \chi_{n,o}(k, \zeta_\alpha) = \sum L_n^\alpha * O(k) \\ \chi_{n,I}(k, \zeta_\beta) = \sum L_n^\beta * I(k) \end{cases} \tag{4.6}$$

Based on Equations (4.4), (4.5), and (4.6) the ARX-Laguerre technique is represented as

$$O(k) = \sum_{0}^{N_\alpha - 1} K_{n,\alpha} \chi_{n,O}(k)\, S_{n,O}(k) + \sum_{0}^{N_\beta - 1} K_{n,\beta}\, \chi_{n,I}(k) S_{n,I}(k) = A(z^{-1}) S_{n,O}(z) + B(z^{-1}) S_{n,I}(z) \tag{4.7}$$

Here, $A(z^{-1})$ and $B(z^{-1})$ are two polynomials with degrees N_α and N_β, respectively. Based on Equation (4.7) the transfer function is represented as follows:

$$H(z) = \frac{S_{n,O}}{S_{n,I}} = \frac{B(z^{-1})}{1 - A(z^{-1})} \tag{4.8}$$

The identification between Equations (4.6) and (4.7) provides (4.9).

$$A(z^{-1}) = \sum_{0}^{N_\alpha - 1} K_{n,\alpha}\chi_{n,O}(k), \quad B(z^{-1}) = \sum_{0}^{N_\beta - 1} K_{n,\beta}\,\chi_{n,I}(k) \tag{4.9}$$

Based on Equations (4.5), (4.6), (4.7), and (4.9) the optimization problem is defined as follows [119]:

$$\min_{\zeta_\alpha} \left\| A(z^{-1}) - \sum_{0}^{N_\alpha - 1} K_{n,\alpha}\chi_{n,O}(k) \right\|^2, \quad \min_{\zeta_\beta} \left\| B(z^{-1}) - \sum_{0}^{N_\beta - 1} K_{n,\beta}\,\chi_{n,I}(k) \right\|^2 \tag{4.10}$$

From the relations Equations (4.5), (4.6), and (4.9), the minimization technique Equation (4.10) is used to decompose the polynomials $A(z^{-1})$ and $B(z^{-1})$ on the Laguerre orthonormal bases, and the $\zeta_\alpha$and $\zeta_\beta$are optimized. A block diagram of the ARX-Laguerre technique is illustrated in Figure 4.2. The ARX-Laguerre state-space equation is written as follows:

$$\begin{cases} X(k+1) = [AX(k) + b_y y(k) + b_u u(k)] + F_d(k) + \delta(k) \\ Y(k+1) = (K)^T X(k+1) \end{cases} \tag{4.11}$$

where $X(k), (A, b_y, b_u), Y(k), u(k), F_d(k), \delta(k)$ and $(K)^T$ are the system state, coefficient matrices, measured output, control input, uncertainty and disturbance, faults, and the Fourier coefficient, respectively. $A, b_y,$ and $b_u,$ are presented in Equations (4.12), (4.13), (4.14), (4.15) and (4.16), respectively.

$$A = \begin{bmatrix} A_o & O_{N_a,N_b} \\ O_{N_b,N_a} & A_i \end{bmatrix}, \tag{4.12}$$

Here, A_0 and A_i are defined in Equations (4.13) and (4.14), respectively.

$$A_o = \begin{bmatrix} \zeta_\alpha & 0 & \dots & 0 \\ 1-\zeta_\alpha{}^2 & \zeta_\alpha & \dots & 0 \\ -\zeta_\alpha(1-\zeta_\alpha{}^2) & 1-\zeta_\alpha{}^2 & \dots & 0 \\ \dots & \dots & \dots & 0 \\ \dots & \dots & \dots & 0 \\ (-\zeta_\alpha)^{N_a-1}(1-\zeta_\alpha{}^2) & \dots & \dots & \zeta_\alpha \end{bmatrix} \text{and} \tag{4.13}$$

$$A_i = \begin{bmatrix} \zeta_\beta & 0 & \dots & 0 \\ 1-\zeta_\beta{}^2 & \zeta_a & \dots & 0 \\ -\zeta_\beta(1-\zeta_\beta{}^2) & 1-\zeta_b{}^2 & \dots & 0 \\ \dots & \dots & \dots & 0 \\ \dots & \dots & \dots & 0 \\ (-\zeta_\beta)^{N_b-1}(1-\zeta_\beta{}^2) & \dots & \dots & \zeta_\beta \end{bmatrix} \tag{4.14}$$

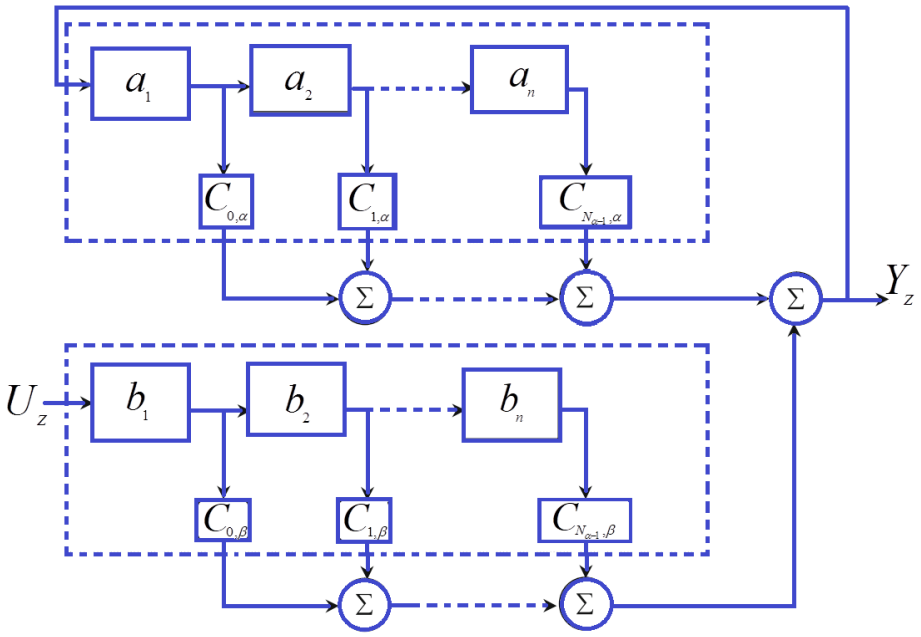

Figure 4.2. ARX-Laguerre Orthonormal Filter Technique.

Here, $a_1 = \frac{\sqrt{1-\zeta_a}}{z-\zeta_a}$, $a_2 = \frac{1-\zeta_a,z}{z-\zeta_a}$, $a_n = \frac{1-\zeta_a,z}{z-\zeta_a}$, $b_1 = \frac{\sqrt{1-\zeta_b}}{z-\zeta_b}$, $b_2 = \frac{1-\zeta_b,z}{z-\zeta_b}$, $b_2 = \frac{1-\zeta_b,z}{z-\zeta_b}$, and $K = [C_{0,\alpha}, \dots, C_{N_\alpha-1,\alpha}, C_{0,\beta}, \dots, C_{N_\beta-1,\beta}]$.

where O_{N_a,N_b} and O_{N_b,N_a} are null matrices of the dimensions $N_a \times N_b$ and $N_b \times N_a$. $b_y$and$b_u$are defined as follows:

$$(b_y = \sqrt{1-\zeta_\alpha^2}\begin{bmatrix} 1 \\ -\zeta_\alpha \\ (-\zeta_\alpha)^2 \\ \vdots \\ (-\zeta_\alpha)^{N_\alpha-1} \end{bmatrix}), \text{and } (b_u = \sqrt{1-\zeta_\beta^2}\begin{bmatrix} 1 \\ -\zeta_\beta \\ (-\zeta_\beta)^2 \\ \vdots \\ (-\zeta_\beta)^{N_\beta-1} \end{bmatrix}) \quad (4.15)$$

Figures 4.3 and 4.4 illustrate the estimation accuracy for the healthy and faulty conditions using the ARX-Laguerre method. For the healthy state in Figure 4.3, the sensitivity of the torque estimation is exceptionally high, and the rate of error is close to zero. In the faulty condition, the error rate increases. Figure 4.4 illustrates the power of the estimated signal and error rate in the faulty condition.

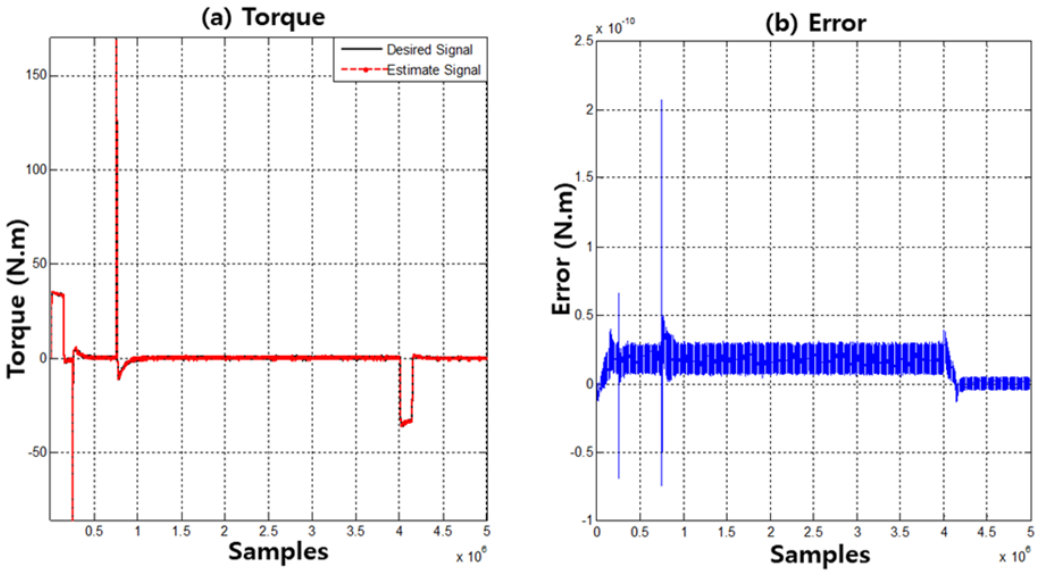

Figure 4.3. ARX-Laguerre orthonormal method for system identification/estimation in the normal condition: (a) desired and estimation torque and (b) error.

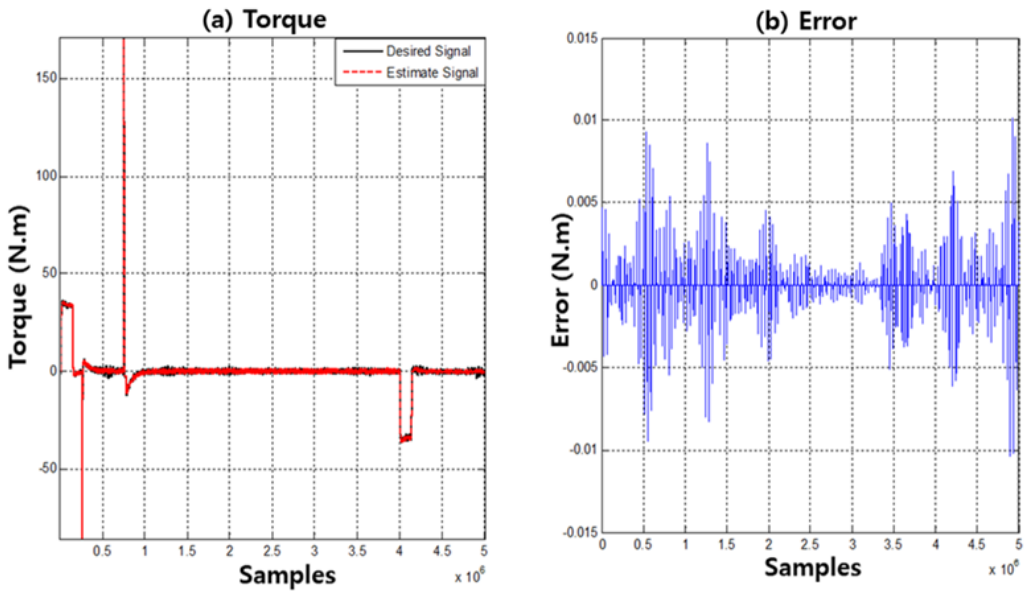

Figure 4.4. ARX-Laguerre orthonormal method for system identification/estimation in the faulty condition: (a) desired and estimated torque and (b) error.

4.3 Fault Diagnosis: Sliding Mode Extended-State ARX-Laguerre PI Observer

An induction motor is a significant system in various industries. Reliable induction motor fault detection and diagnosis is significant for maintaining machine operations in safety conditions. To address the issue of fault diagnosis, the sliding mode extended-state ARX-Laguerre PI observer is proposed in the following section.

4.3.1. Sliding Mode Extended-State ARX-Laguerre PI Observer

The proposed methodology comprises of six major parts, as shown in Figure 4.1: (a) system modeling using the ARX-Laguerre technique, (b) ARX-Laguerre proportional-integral (API) observer, (c) observer evaluator based on the sliding mode extended-state ARX-Laguerre PI observer , (d) residual generator, (e) windows characterization, and (f) decision making based on SVM. The classical ARX-Laguerre PI observer offers a linear approach to find an optimized estimation of the system and fault. This technique is stable, but it has an

issue regarding accurate fault estimation and robustness. To evaluate the ARX-Laguerre PI observer, a sliding mode extended-state observer is considered. This technique improves the robustness and precision of fault estimation. Using ARX-Laguerre state space system modeling, the ARX-Laguerre PI observer method is defined to estimate the system modeling. Therefore, the ARX-Laguerre PI observer is defined as the following equation.

$$\begin{cases} \hat{X}(k+1) = A\hat{X}(k) + b_y\hat{Y}(k) + b_u u(k) + F_d(k) + \hat{\delta}_{ALPIO}(k) + K_p(Y(k) - \hat{Y}(k)) \\ \hat{Y}(k+1) = (K)^T\hat{X}(k+1) \end{cases} \quad (4.16)$$

where $\hat{X}(k), \hat{Y}(k), \hat{\delta}_{ALPIO}(k)$ and K_p are the state estimated, output estimated, faults estimated based on ALPIO technique, and the proportional coefficient, respectively. For fault estimation using the ARX-Laguerre PIO technique, the integral term is used to reduce the fault estimation error. The integral term of fault estimation in the ARX-Laguerre PI observer is given in Equation (4.17).

$$\hat{\delta}_{ALPIO}(k+1) = \hat{\delta}_{ALPIO}(k) + K_I(Y(k) - \hat{Y}(k)) \quad (4.17)$$

Here, $K_I$is the integral term coefficient. This technique has been used in several applications [119], but it has a drawback in the presence of uncertain and noisy conditions. To address this issue, an observer evaluator is considered, as shown in Figure 4.1. The sliding mode extended-state ARX-Laguerre PI observer is designed to improve the performance of faults estimation. Therefore, a sliding mode extended-state algorithm is used to modify the fault estimation, reliability, and robustness of the ARX–Laguerre PI observer, as represented in the following equations:

$$\begin{cases} \hat{X}(k+1) = A\hat{X}(k) + b_y\hat{Y}(k) + b_u u(k) + F_d(k) + \hat{\delta}_{SMALPIO}(k) + K_p(Y(k) - \hat{Y}(k)) \\ \hat{Y}(k+1) = (K)^T\hat{X}(k+1) \end{cases} \quad (4.18)$$

$$\begin{cases} \hat{\delta}_{SMALPIO}(k+1) = \hat{\delta}_{ALPIO}(k) + K_I\left(Y(k) - \hat{Y}(k)\right) + \\ K_{S_1}\left\|Y(k) - \hat{Y}(k)\right\|^{0.5}\text{sgn}\left(Y(k) - \hat{Y}(k)\right) - \gamma \\ \dot{\hat{\gamma}} = K_{S_2}\text{sgn}\left(Y(k) - \hat{Y}(k)\right) \end{cases} \quad (4.19)$$

Here, $\hat{\delta}_{SMALPIO}(k)$ and (K_{S_1}, K_{S_1}) are the faults estimated based on SMALPIO technique and extended-state coefficients. According to Equations (4.18) and (4.19), the system's output and faults are estimated using the sliding mode extended-state ARX-Laguerre PI observer. This technique is more accurate and robust than the ARX-Laguerre PI observer technique. The stability and convergence are proven in below [120]. If the sliding mode extended-state PI observer is defined by the following Equation:

$$\mathrm{U_{hgo}} = \mathrm{K_{c-new}}(\hat{\delta}_{\mathrm{PIO}}(\mathrm{k}+1) + |\mathrm{S}_{\partial}|^{\kappa}\hat{\delta}_{\mathrm{PIO}}(\mathrm{k}+1)) \quad , \mathrm{K_{c-new}} > 0, \tag{4.20}$$

$$\mathrm{S}_{\partial} = \hat{\delta}(\mathrm{k}) + \mathrm{K}(\mathrm{Y}(\mathrm{k}) - \hat{\mathrm{Y}}(\mathrm{k})) \tag{4.21}$$

In the normal condition ($\delta(k) = 0$), the convergence reaching time is calculated based on (4.21).

$$T_{conv} = \frac{2}{K_{c-new}}(S_{\ell} + |S_{\ell}|^{\kappa+1}), 1 < \kappa < 2 \qquad S_{\ell} = K(Y(k) - \hat{Y}(k)) \tag{4.22}$$

Based on [120], in the first step, we defined the convergence time in the normal condition, Equation (4.22). Based on Equation (4.22), the residual signal is converged to zero in a finite time. In the abnormal condition, the compensate variable is defined by

$$\dot{\mathrm{U}}_{\mathrm{hgo}} = \delta_{\mathrm{PIO}}(\mathrm{k}+1) - (\mathrm{K_{c-new}}(\hat{\delta}_{\mathrm{PIO}}(\mathrm{k}+1) + |\mathrm{S}_{\partial}|^{\kappa}\hat{\delta}_{\mathrm{PIO}}(\mathrm{k}+1))) \quad , \mathrm{S}_{\partial}(0) = \mathrm{S}_{\partial_0}, \tag{4.23}$$

Based on [120], to have stability and finite time convergence, the coefficient is bounded as follows:

$$\mathrm{K_{c-new}} > 2 \times (\delta_{\mathrm{PIO}}(\mathrm{k}+1)) - \hat{\delta}_{\mathrm{PIO}}(\mathrm{k}+1)) \tag{4.24}$$

Based on the Lyapunov theorem, the Lyapunov of the proposed observer is defined by the following Equation:

$$\mathrm{V_{proposed}}(\mathrm{x}) = 2\mathrm{K_{c-new}}|\mathrm{S}_{\partial}| + \frac{1}{2}\hat{\delta}_{\mathrm{PIO}}(\mathrm{k}+1)^2 + \frac{1}{2}(\mathrm{K_{c-new}}|\mathrm{S}|^{\kappa} - \hat{\delta}_{\mathrm{PIO}}(\mathrm{k}+1))^2 \tag{4.25}$$

The derivative of the Lyapunov function is defined by Equation (4.25).

$$\dot{V}_{\text{proposed}}(x) \tag{4.26}$$
$$= \frac{1}{|S_\partial|^\kappa}[S_\partial{}^\kappa \quad \hat{\delta}_{\text{PIO}}(k+1)]\frac{K_{c-new}}{2}\begin{bmatrix} K_{c-new}{}^2 & -K_{c-new} \\ -K_{c-new} & 1 \end{bmatrix}\begin{bmatrix} S_\partial{}^\kappa \\ \hat{\delta}_{\text{PIO}}(k+1) \end{bmatrix}$$
$$+ \frac{\delta_{\text{PIO}}(k+1) - \hat{\delta}_{\text{PIO}}(k+1)}{|S_\partial|^\kappa}\begin{bmatrix} \frac{K_{c-new}{}^2}{2} & \frac{-K_{c-new}}{2} \end{bmatrix}\begin{bmatrix} S_\partial{}^\kappa \\ \hat{\delta}_{\text{PIO}}(k+1) \end{bmatrix}$$

The band of the fault estimation based on the proposed method is defined by the following assumption:

$$\left|\delta_{\text{PIO}}(k+1) - \hat{\delta}_{\text{PIO}}(k+1)\right| \le \omega|S_\partial|^\kappa \tag{4.27}$$

Based on Equation (4.26) and Equation (4.27),

$$\dot{V}_{\text{proposed}}(x) = \frac{-1}{|S_\partial|^\kappa}[S_\partial{}^\kappa \quad \hat{\delta}_{\text{PIO}}(k+1)]\frac{K_{c-new}}{2} \times \tag{4.28}$$
$$\begin{bmatrix} K_{c-new}{}^2 - (\frac{1}{K_{c-new}} + K_{c-new})(\delta_{PIO}(k+1) - \hat{\delta}_{PIO}(k+1)) & -K_{c-new} \\ -(K_{c-new} + 2(\delta_{PIO}(k+1) - \hat{\delta}_{PIO}(k+1)) & 1 \end{bmatrix} \times$$
$$\begin{bmatrix} S_\partial{}^\kappa \\ \hat{\delta}_{\text{PIO}}(k+1) \end{bmatrix}$$

$$\dot{V}_{proposed}(x) \le \frac{-1}{|S_\partial|^\kappa}\left[S_\partial{}^\kappa \quad \hat{\delta}_{PIO}(k+1)\right]\frac{K_{c-new}}{2} \tag{4.29}$$
$$\begin{bmatrix} K_{c-new}{}^2 - (\frac{1}{K_{c-new}} + K_{c-new})(\delta_{PIO}(k+1) - \hat{\delta}_{PIO}(k+1)) & -K_{c-new} \\ -(K_{c-new} + 2(\delta_{PIO}(k+1) - \hat{\delta}_{PIO}(k+1)) & 1 \end{bmatrix}\begin{bmatrix} S_\partial{}^\kappa \\ \hat{\delta}_{PIO}(k+1) \end{bmatrix}$$

So, if $\begin{bmatrix} K_{c-new}{}^2 - (\frac{1}{K_{c-new}} + K_{c-new})(\delta_{PIO}(k+1) - \hat{\delta}_{PIO}(k+1)) & -K_{c-new} \\ -(K_{c-new} + 2(\delta_{PIO}(k+1) - \hat{\delta}_{PIO}(k+1)) & 1 \end{bmatrix} > 0,$

$\dot{V}_{proposed}(x) < 0$. Based on [120], when $\dot{V}_{proposed}(x) < 0$, the residual signals converge to zero in a finite time.

After designing the proposed sliding mode extended-state ARX-Laguerre PI observer method, the residual signal can be calculated as follows.

$$\begin{cases} e(k) = X(k) - \hat{X}(k) \\ r(k) = Y(k) - \hat{Y}(k) \end{cases} \tag{4.30}$$

Here, $e(k)$ and $r(k)$ are the signal's error and residual signal, respectively.

4.3.2. Fault Detection and Fault Identification Using Support Vector Machine

Based on Figure 4.1, after estimating the normal and abnormal signals using the proposed sliding mode extended-state ARX-Laguerre PI observer (SMALPIO) and finding the residual signal based on equation (4.30), the decision-making ability can be introduced using a support vector machine (SVM) algorithm. This section has two main parts: a) residual signal characterization, and b) SVM-based fault detection and identification. The residual signals obtained for normal and abnormal conditions are utilized for the fault detection and identification of the REBs. First, the energy of residual signals was selected. The value of the energy attribute can be computed as follows:

$$E = \sum_{i=1}^{M} r_{xi}^2 \tag{4.31}$$

where E, M and r_{xi} are the energy of the residual signals in different conditions, the total number of instances, and the residual signal, respectively. After extracting the feature (e.g., energy) from the residual signals in normal and abnormal conditions, the SVM technique is used for fault detection and identification. Algorithm 4.1 illustrates the sliding mode extended-state ARX-Laguerre PI observer for fault diagnosis of the bearing.

Algorithm 4.1. SVM-based sliding mode (extended-state) ARX-Laguerre PI (hybrid) observer for fault diagnosis of a bearing.

1: Perform system modeling based on the ARX-Laguerre technique (4.4,4.11)
2: Run the ARX-Laguerre PI observer (4.16,4.17)
3: Improve the robustness in ARX-Laguerre PI observer based on sliding mode algorithm (4.18,4.19)
4: Run the residual signal characterization by energy (4.30,4.31)
5: Apply the SVM classification technique for fault detection and identification [14]

4.4 Datasets

The effectiveness of the proposed sliding mode extended-state ARX-Laguerre PI observer (SMALPIO) and ARX-Laguerre PI observer (APIO) for fault detection and identification was evaluated using two different datasets: a) the Case Western Reverse University (CWRU) bearing dataset to test the single type fault and b) the Smart HSE Lab bearing data set to test the multiple types of fault.

4.4.1. Case Western Reverse University (CWRU) Bearing Data

The vibration data were collected from a 6205-2RS JEM SKF roller bearing installed in a rotary motor. Based on Figure 3.2, a 2-horsepower (hp), three phase induction motor was connected to a torque transducer and a dynamometer to apply different loads, ranging from 0 hp to 3 hp [15]. The vibration sensor (accelerometers) was attached to the roller bearing for data collection. The vibration signals were collected for normal and faulty conditions with a 48 kHz sampling rate. The rotation velocities of the induction motor also varied from 1730 rpm to 1790 rpm. Table 2.2 presents the details of the Case Western Reverse University (CWRU) bearing dataset. Based on [113], which is outlined in Table 2.2, three different crack sizes, four different motor loads, and four different motor speeds were seeded at different positions of the bearing.

4.4.2. Smart HSE Lab Bearing Data

Figure 4.5 demonstrates an experimental system for the fault simulator of bearings. To transfer the torque to the no-drive-end shaft (NDES) through the gearbox, the three-phase induction motor is connected to the drive-end shaft (DES) [121]. Figure 4.6 illustrates the

experimental data acquisition system to extract the normal and faulty signals. Faults with crack sizes of 3 mm and 6 mm in diameter are seeded on the drive-end bearings as the outer raceway fault (OR), inner raceway fault (IR), ball raceway fault (Ball), inner-outer raceway fault (IR-OR), inner-ball raceway fault (IR-Ball), outer-ball raceway fault (OR-Ball), and inner-outer-ball raceway fault (IR-OR-Ball) (see Figure 4.7). The data are recorded at 250 kHz sampling rate and the rotational speeds are 300, 400, 450, and 500 RPM. The details of the data are given in Table 4.1. In addition, the raw signal for different faulty conditions is illustrated in Figure 4.8.

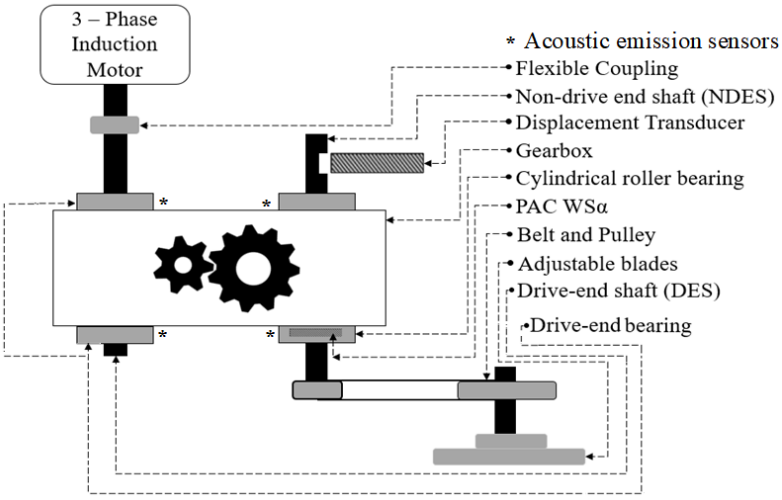

Figure 4.5. Block diagram of the fault simulator.

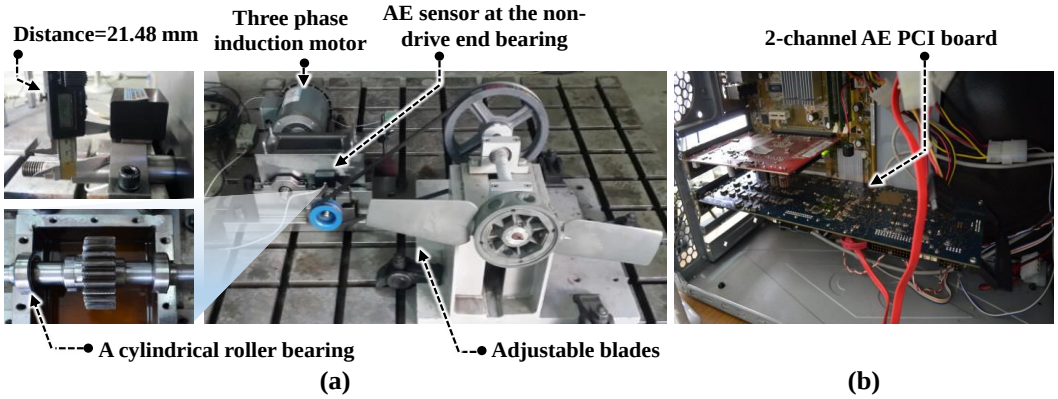

Figure 4.6. (a) Experimental setup to record fault data and (b) PCI-2 AE data acquisition

(**a**) (**b**) (**c**) (**d**) (**e**) (**f**) (**g**)

Figure 4.7. Different fault conditions in a bearing: (a) OR, (b) IR, (c) Ball, (d) IR-OR, (e) IR-Ball, (f) OR-Ball, and (g) IR-OR-Ball.

Table 4.1. Detailed information of the datasets.

Dataset	Fault Types	Rotational Speed (RPM)	Fault Crack Size (mm)
Dataset 1	**Normal States**	300	**3 and 6**
	IR Fault	300	
	OR Fault	300	
	Ball Fault	300	
	Inner-Outer Fault	300	
	Inner-Ball Fault	300	
	Outer-Ball Fault	300	
	Inner-Outer-Ball Fault	300	
Dataset 2	**Normal States**	400	**3 and 6**
	IR Fault	400	
	OR Fault	400	
	Ball Fault	400	
	Inner-Outer Fault	400	
	Inner-Ball Fault	400	
	Outer-Ball Fault	400	
	Inner-Outer-Ball Fault	400	
Dataset 3	**Normal States**	450	**3 and 6**
	IR Fault	450	
	OR Fault	450	
	Ball Fault	450	
	Inner-Outer Fault	450	
	Inner-Ball Fault	450	
	Outer-Ball Fault	450	
	Inner-Outer-Ball Fault	450	
Dataset 4	**Normal States**	500	**3 and 6**
	IR Fault	500	
	OR Fault	500	
	Ball Fault	500	
	Inner-Outer Fault	500	
	Inner-Ball Fault	500	
	Outer-Ball Fault	500	
	Inner-Outer-Ball Fault	500	

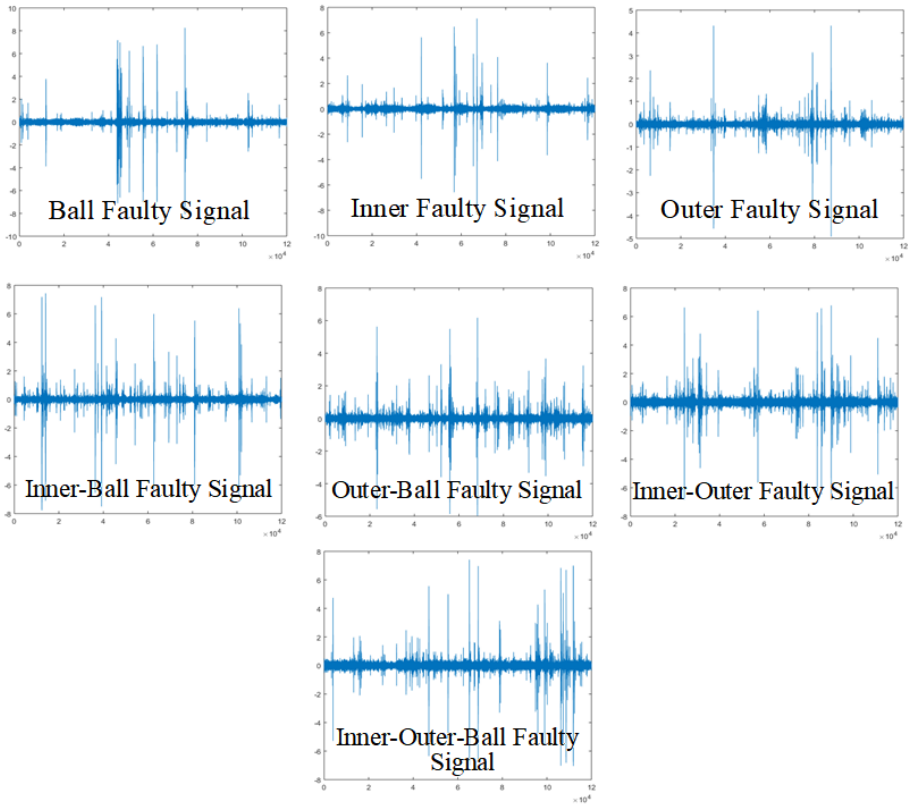

Figure 4.8. Original raw signals for various faulty conditions.

4.5 Results and Analysis

The effectiveness of the proposed sliding mode extended-state ARX-Laguerre PI observer (SMALPIO) for the identification of various conditions (e.g., single type of fault and multiple type of faults) is compared to the ARX-Laguerre PI observer (APIO).

4.5.1. Training and Testing Configuration

For analyzing the single type fault detection and fault identification capabilities of the proposed sliding mode extended-state ARX-Laguerre PI observer, the CWRU dataset consisting of 1600 samples (400 data instances per class) was randomly split into training and testing subsets. Specifically, 1200 samples (75 instances per class) were used for training SVM classification algorithms, whereas the remaining previously unobserved 400 samples

(25 instances per class) were utilized for the testing process. The similar dataset perturbations were applied to the residual signals obtained by the referenced APIO method in order to perform the comparison between that and the proposed technique (SMALPIO) used in conjunction with the SVM classification algorithm.

In addition, for analyzing the multiple types of fault detection and fault identification capabilities of the proposed sliding mode extended-state ARX-Laguerre PI observer, the Smart (Health, Safety, Environment) SHSE Lab bearing datasets (e.g., normal, outer raceway fault (OR), inner raceway fault (IR), ball raceway fault, inner-outer raceway fault (IR-OR), inner-ball raceway fault (IR-Ball), outer-ball raceway fault (OR-Ball), and inner-outer-ball raceway fault (IR-OR-Ball)) consisting of 3200 samples (400 data instances per class) was randomly split into training and testing subsets. Specifically, 2400 samples (75 instances per class) were used for training SVM classification algorithms, whereas the remaining previously unobserved 800 samples (25 instances per class) were utilized for the testing process. The similar dataset perturbations were applied to the residual signals obtained by the referenced APIO method in order to perform the comparison between that and the proposed technique (SMALPIO) used in conjunction with the SVM classification algorithm.

4.5.2. Single Type Fault Detection and Identification

To validate the efficacy of the proposed sliding mode extended-state ARX-Laguerre PI observer (SMALPIO) and ARX-Laguerre PI observer (APIO) methods for single type fault diagnosis, we test it with benchmark Case Western Reverse University (CWRU) bearing datasets as described in Table 2.2. Figure 4.9 shows the residual signals for the normal, inner fault, outer fault, and ball fault conditions based on SMALPIO.

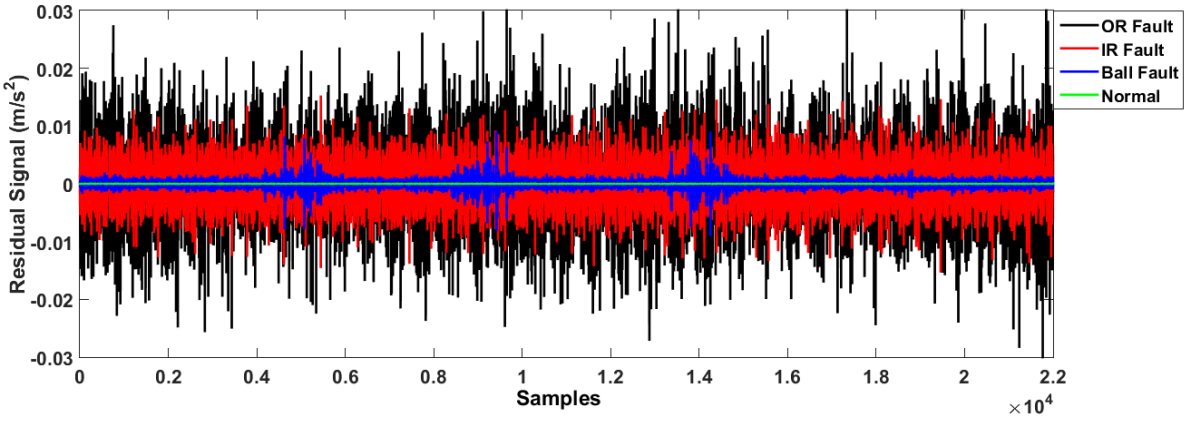

Figure 4.9. Residual signals for normal, inner, outer, and ball faults based on the SMALPIO.

Regarding this figure, the residual signals are well differentiable for fault detection and fault identification. To provide a comprehensive performance of fault diagnosis accuracy, the two case-studies are considered in this result parts: a) crack-variant datasets and b) load-variant datasets provided by CWRU. Firstly, we investigate the fault identification capabilities of the proposed sliding mode extended-state ARX-Laguerre PI observer (SMALPIO) and ARX-Laguerre PI observer (APIO) [12] for four crack-variant datasets, where the torque load remained fixed. The fault diagnosis results obtained for the REB datasets with various crack sizes (e.g., 0.007, 0.014, and 0.021 inches) under fixed load conditions are presented in Tables 4.2–4.5. Based on these tables the average of the fault detection accuracy for proposed method (SMALPIO) and APIO are 100% and 87.8%, respectively.

Table 4.2. Single type fault diagnosis results to test the crack-variant dataset (torque load is 0 hp).

Algorithms	**SMALPIO (Proposed Method)**			**APIO**		
Crack Diameters (in)	0.007	0.014	0.021	0.007	0.014	0.021
Normal	100%	100%	100%	88%	88%	88%
Ball Fault	93%	93%	94%	88%	78%	78%
OR Fault	80%	93%	96%	75%	81%	78%
IR Fault	95%	93%	93%	70%	70%	71%
Average	92%	94.75%	95.75%	80.25%	79.25%	78.75%

Table 4.3. Single type fault diagnosis results to test the crack-variant dataset (torque load is 1 hp).

Algorithms	SMALPIO (Proposed Method)			APIO		
Crack Diameters (in)	0.007	0.014	0.021	0.007	0.014	0.021
Normal	100%	100%	100%	88%	88%	88%
Ball Fault	95%	93%	95%	80%	81%	85%
OR Fault	91%	91%	93%	78%	80%	81%
IR Fault	91%	93%	96%	70%	74%	75%
Average	94.25%	94.25%	96%	79%	80.75%	82.25%

Table 4.4. Single type fault diagnosis results to test the crack-variant dataset (torque load is 2 hp).

Algorithms	SMALPIO (Proposed Method)			APIO		
Crack Diameters (in)	0.007	0.014	0.021	0.007	0.014	0.021
Normal	100%	100%	100%	85%	85%	85%
Ball Fault	93%	93%	96%	79%	81%	84%
OR Fault	95%	90%	90%	79%	75%	80%
IR Fault	95%	94%	94%	75%	76%	79%
Average	95.75%	94.25%	95%	79.5%	79.25%	82%

Table 4.5. Single type fault diagnosis results to test the crack-variant dataset (torque load is 3 hp).

Algorithms	SMALPIO (Proposed Method)			APIO		
Crack Diameters (in)	0.007	0.014	0.021	0.007	0.014	0.021
Normal	100%	100%	100%	90%	90%	90%
Ball Fault	91%	90%	91%	79%	79%	80%
OR Fault	90%	90%	94%	76%	78%	80%
IR Fault	90%	91%	91%	75%	77%	79%
Average	92.75%	92.75%	94%	80%	81%	82.25%

These tables indicate that the average of fault diagnosis accuracy for the proposed technique (SMALPIO) are, yielding 93.7%, 94%, and 95.2% for three levels of crack severity of 0.007, 0.014, and 0.021 inches, respectively. In addition, the proposed method (SMALPIO) outperforms the APIO technique yielding average performance improvements of 14%, 13.9%, and 13.9% for three fault severity levels characterized by crack sizes of 0.007, 0.014, and 0.021 inches, respectively. Moreover, the fault diagnosis results for the REB datasets with load-variant conditions is represented in Table 4.6. Based on Table 2.2 we re-configured the available CWRU dataset and created three custom load-variant datasets to validate the robustness of the proposed fault identification technique under changing load/motor speed conditions. Regarding this table, the proposed method (SMALPIO) in the presence of the

load-variant dataset outperforms the APIO technique yielding performance improvements of 11%, 10.25%, and 9.75% for three fault severity levels characterized by crack sizes of 0.007, 0.014, and 0.021 inches, respectively.

Table 4.6. Single type fault diagnosis results to test the torque/motor speed-variant dataset.

Algorithms	SMALPIO (Proposed Method)			APIO		
Crack Diameters (in)	0.007	0.014	0.021	0.007	0.014	0.021
Normal	100%	100%	100%	91%	91%	88%
Ball fault	91%	90%	91%	80%	81%	83%
OR Fault	87%	90%	90%	73%	75%	79%
IR Fault	90%	92%	92%	80%	84%	84%
Average	92%	93%	93.25%	81%	82.75%	83.5%

4.5.3. Multiple Types Fault Detection and Identification

To validate the efficacy of the proposed method (SMALPIO) and APIO approaches for multiple types fault diagnosis, we test it with benchmark Smart HSE Lab (SHSE) bearing datasets as described in Section 4.4.2. Figure 4.10 demonstrations the residual signals for the normal, ball fault, inner (IR) fault, outer (OR) fault, inner-ball fault, outer-ball (OR-Ball) fault, inner-outer (IR-OR) fault, and inner-outer-ball (IR-OR-Ball) fault conditions for dataset 4 based on proposed technique (SMALPIO).

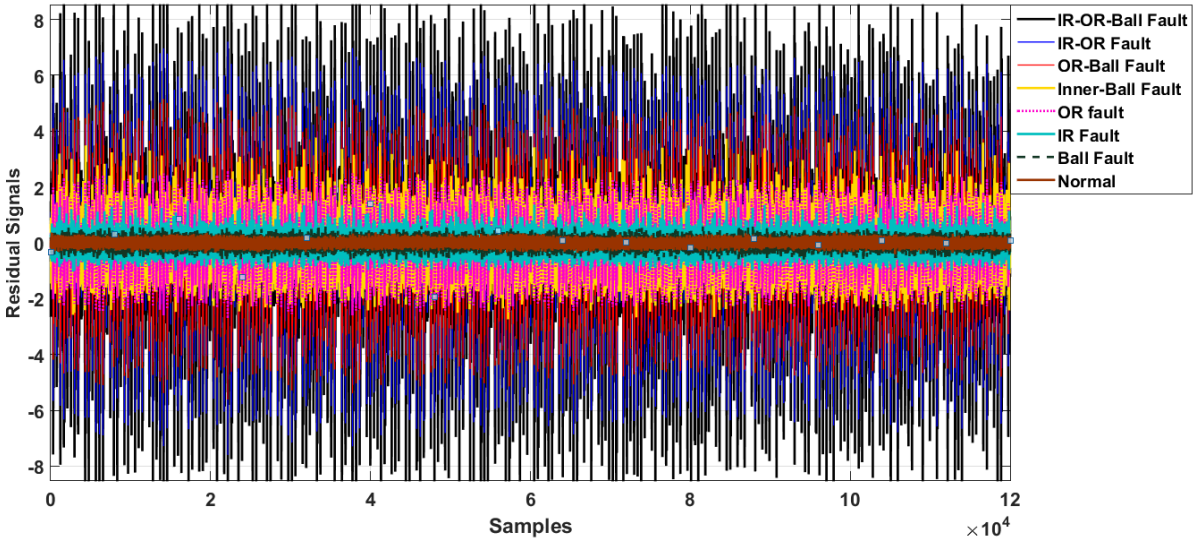

Figure 4.10. Residual signals for normal, inner, outer, ball, inner-ball, outer-ball, inner-outer, and inner-outer-ball faults based on the SMALPIO.

Tables 4.7–4.10 illustrate the accuracy of fault diagnosis using the proposed sliding mode extended-state ARX-Laguerre PI observer (SMALPIO) and ARX-Laguerre PI observer (APIO) for the normal condition, faulty ball state, inner fault, outer fault, inner-outer fault, inner-ball fault, outer-ball fault, and inner-outer-ball fault. The diagnostic accuracy is reported as a percentage of correct fault identification in all data.

Table 4.7. Multiple types of fault diagnosis results to test the crack-variant dataset (torque speed is 300 RPM).

Algorithms	Proposed Method		APIO	
Crack Diameters (mm)	3	6	3	6
Normal Stat	100%	100%	83%	83%
IR Fault	93%	94%	69%	73%
OR Fault	95%	95%	71%	75%
Ball Fault	94%	94%	78%	77%
IR-Ball Fault	93%	96%	79%	81%
OR-Ball Fault	95%	97%	80%	80%
IR-OR Fault	94%	94%	78%	82%
IR-OR-Ball Fault	95%	96%	78%	80%
Average%	94.88	95.75	77	77.88

Table 4.8. Multiple types of fault diagnosis results to test the crack-variant dataset (torque speed is 400 RPM).

Algorithms	Proposed Method		APIO	
Crack Diameters (mm)	3	6	3	6
Normal Stat	100%	100%	86%	86%
IR Fault	94%	96%	73%	73%
OR Fault	93%	93%	71%	78%
Ball Fault	95%	94%	76%	77%
IR-Ball Fault	95%	96%	80%	83%
OR-Ball Fault	94%	95%	83%	84%
IR-OR Fault	98%	96%	78%	80%
IR-OR-Ball Fault	95%	95%	78%	79%
Average%	95.5	95.63	78.13	80

As shown in Tables 4.7–4.10, the average rate of failure identification is 95.5% for the proposed sliding mode extended-state ARX-Laguerre PI observer and 79.7% for the ARX-Laguerre PI observer. The proposed extended-state ARX-Laguerre PI observer fault diagnosis method outperforms the state-of-the-art ARX-Laguerre PI observer (APIO) method, yielding an average performance improvement of 16.16%, and 15.49% for 3 mm and 6 mm cracks,

respectively. Overall, the proposed extended-state ARX-Laguerre PI observer fault diagnosis method efficiently identifies single and composite faults in the bearing.

Table 4.9. Multiple types of fault diagnosis results to test the crack-variant dataset (torque speed is 450 RPM).

Algorithms	Proposed Method		APIO	
Crack Diameters (mm)	3	6	3	6
Normal Stat	100%	100%	88%	88%
IR Fault	94%	94%	74%	74%
OR Fault	95%	94%	76%	78%
Ball Fault	94%	95%	80%	80%
IR-Ball Fault	93%	95%	80%	81%
OR-Ball Fault	94%	94%	79%	78%
IR-OR Fault	96%	97%	80%	81%
IR-OR-Ball Fault	95%	96%	80%	80%
Average%	95.13	95.63	79.63	80

Table 4.10. Multiple types of fault diagnosis results to test the crack-variant dataset (torque speed is 500 RPM).

Algorithms	Proposed Method		APIO	
Crack Diameters (mm)	3	6	3	6
Normal Stat	100%	100%	88%	88%
IR Fault	95%	95%	80%	80%
OR Fault	96%	94%	78%	80%
Ball Fault	97%	96%	81%	83%
IR-Ball Fault	94%	94%	82%	84%
OR-Ball Fault	95%	95%	85%	84%
IR-OR Fault	94%	96%	80%	82%
IR-OR-Ball Fault	95%	95%	81%	81%
Average%	95.75	95.63	81.88	82.8

In this experiment, the bearing data are collected under four different motor speeds, as shown in Table 4.1. The proposed method (SMALPIO) is robust even if the motor speed changes. When the motor speed changes, the system model is changed, and the proposed observer detects the model change. This technique is robust, and the speed variation is defined as an uncertainty condition. Table 4.11 presents the fault diagnosis accuracy for variable motor speeds (e.g., 300 RPM, 400 RPM, 450 RPM, and 500 RPM) in different crack sizes (e.g., 3 mm and 6 mm), various conditions (normal, ball fault, inner fault, outer fault, inner-outer fault, inner-ball fault, outer-ball fault, and inner-outer-ball fault) of the proposed method

(SMALPIO) and APIO. Regarding this table, the proposed method (SMALPIO) in the presence of the motor speed-variant dataset outperforms the APIO technique yielding performance improvements of 13.25% and 13.2% for two fault severity levels characterized by crack sizes of 3 and 6 mm, respectively.

Table 4.11. Multiple types of fault diagnosis results to test the motor speed-variant dataset.

Algorithms	Proposed Method		APIO	
Crack Diameters (mm)	3	6	3	6
Normal Stat	100%	100%	87%	87%
IR Fault	95%	95%	82%	81%
OR Fault	94%	94%	76%	79%
Ball Fault	94%	95%	80%	81%
IR-Ball Fault	93%	94%	82%	82%
OR-Ball Fault	96%	96%	83%	84%
IR-OR Fault	93%	94%	82%	81%
IR-OR-Ball Fault	93%	94%	80%	81%
Average%	94.75	95.25	81.5	82

4.6 Conclusions

In this chapter, a hybrid approach using the SVM-based sliding mode extended-state ARX-Laguerre PI observation technique was evaluated to detect, estimate, and classify several single and multiple-faults in a bearing including ball, inner, outer, inner-ball, outer-ball, inner-outer, and inner-outer-ball faults. To modeling the vibration and AE bearing signals, the ARX-Laguerre technique is proposed. Next, signal estimation is developed in two main steps. Firstly, the ARX-Laguerre PI observer is developed for vibration and AE signals. Secondly, the sliding mode extended-state technique is recommended to increase the robustness, which this problem usually encountered with varying motor speeds. After generating the residual signals, a support vector machine (SVM) is developed for the detection and classification of the bearing fault conditions. The effectiveness of the proposed procedure is validated using two different datasets for single-type fault diagnosis based on the Case Western Reverse University (CWRU) vibration dataset and multi-type fault diagnosis of bearing using the Smart Health Safety Environment (SHSE) Lab acoustic emission dataset. Experimental results showed that average performance improvements for the crack-variant CWRU dataset using the proposed method are 14%, 13.9%, and 13.9%, as compared with the

ARX-Laguerre PI observer technique for three fault severity levels characterized by crack sizes of 0.007, 0.014, and 0.021 inches, respectively. In addition, the proposed method (SMALPIO) in the presence of the load-variant CWRU dataset outperforms the APIO technique yielding performance improvements of 11%, 10.25%, and 9.75% for three fault severity levels characterized by crack sizes of 0.007, 0.014, and 0.021 inches, respectively. Based on the second scenario (e.g., multiple-fault), the proposed fault diagnosis method outperforms the ALPIO method, yielding an average performance improvement of 16.16%, and 15.49% for Smart HSE dataset for 3 mm and 6 mm cracks, respectively. Moreover, the proposed method in the presence of the motor speed-variant SHSE dataset outperforms the APIO technique yielding performance improvements of 13.25% and 13.2% for two fault severity levels characterized by crack sizes of 3 and 6 mm, respectively. Overall, the proposed extended-state ARX-Laguerre PI observer fault diagnosis method efficiently identifies single and composite faults in the bearing.

Part II

Fuzzy Extended-State Observation Fault Diagnosis of Bearings Under Inconsistent Working Conditions

Chapter 5

Rolling-Element Bearing Fault Diagnosis Using Advanced Machine Learning-Based Observer

5.1 Introduction

Rolling element bearings (REBs) have been extensively used in several industries, such as the automotive, steam and gas turbines, and power generation industries, to improve their efficiency by reducing friction [5, 15]. The complexities of the required tasks, with time-varying and nonlinear parameters in rolling bearings, make their fault estimation, detection, and identification highly challenging. The fault estimation, detection, and identification (further referred to as FEDI) are intransitive to prevent the bearing's destruction. Here, the fault estimation technique is used to estimate the signal (fault) to obtain the valuable differentiation between various conditions of bearing, the fault detection algorithm is used to detect normal and abnormal conditions, and the fault identification technique is used to identify the specific types of faults in the REBs. Various types of failures have been representing in bearings, which are divided into four foremost groups, i.e., inner race faults, outer race faults, ball or rolling-element faults, and cage faults that in this research called IR, OR, Ball, and Cage, respectively. To analyze the faults conditions in a bearing, various REB condition monitoring techniques such as vibration, motor current signature analysis (MCSA), and acoustic emission (AE) measurements have been reported [7]. This research exploits the vibration measurements since these signals are suitable for FEDI.

Numerous procedures have been recently presented for FEDI in various systems, which can be divided into four groups: (a) model-based techniques, (b) signal-based approaches, (c) knowledge-based procedures, and (d) hybrid methods [5, 6]. Some recently published representative examples of model-based techniques have been reported in [5, 8, 9, 14, 122]. Model-based techniques for fault diagnosis identify the faults by modeling the system's dynamics using mathematical modeling or system identification techniques using a small dataset. Apart from the various advantages of the model-based method such as reliability and robustness, accuracy is the main drawback of this technique [5]. Signal-based fault

diagnosis approaches extract fault features and differentiate the health conditions of the system by applying various signal processing techniques to the acquired signals. Some recently published representative examples of signal-based approaches can be found in [123-132]. When using the traditional fault diagnosis frameworks (i.e., knowledge-based methods), it is crucial to select an appropriate signal processing technique that is useful for extracting the representative fault features that are used as inputs to the decision-making approaches. Recently, various types of advanced signal processing approaches were applied for rotating machinery fault diagnosis. These techniques include the conventional wavelet transform [123], wavelet-based kurtogram [124], empirical mode decomposition [128], ensemble empirical mode decomposition [130] and their modifications [125, 127, 129], as well as relatively new methods for detecting and extracting the repetitive transients caused by mechanical faults, such as spectral Gini index [131] and spectral l2/l1 norm [132]. These methods are essential for feature engineering; however, in the proposed methodology, the signal processing step is replaced by the observation technique (advanced fuzzy sliding mode observer) which is used to provide new insights and demonstrate the applicability of the control theory field for solving the problems of mechanical fault diagnosis. Knowledge-based approaches were based on the ideas of transferring the industrial knowledge and expertise in fault diagnosis from humans to the machine by creating algorithms that performed fault identification using decision tables and rules. However, recently the trend in knowledge-based approaches has been shifted toward artificial intelligence techniques that are used for automatically extracting valuable features and making decisions about the fault conditions of the system [93, 126, 133]. To address the issues of model-based approaches and knowledge-based techniques, hybrid fault diagnosis can be introduced for bearing fault diagnosis. In the hybrid approach, various algorithms from different groups can be used in parallel to improve the performance of the fault diagnosis method. In this research, a robust hybrid fault diagnosis algorithm is presented using a machine learning-based advanced fuzzy sliding mode observer for the REB.

The main challenge in designing the procedure of sliding mode observer is system modeling. The mathematical-based system modeling and system identification are the main frameworks for modeling the complex (e.g., bearing) systems [8, 122]. In the mathematical-

based system modeling, the Lagrange technique can be used for modeling the REBs [8]. Apart from the reliability and accuracy of physical system modeling, this technique has drawbacks in uncertain and noisy conditions. To address this issue, the system identification techniques are widely applied as indicated in [12, 119, 122]. To estimate the system using system identification technique, various orthonormal procedures such as Auto Regressive with eXogenous input (ARX), orthonormal function bases (OFB), and generalized orthonormal bases (GOB) methods have been used [12, 119]. Apart from several advantages of orthonormal techniques compared to the classical algorithms, these techniques have two important drawbacks. The first one is related to the challenge of finding the optimal orthonormal values and the second problem is related to the restrictions in decoupled systems [8, 9, 12, 119]. To address these issues, ensure an efficient complexity reduction and reduce the system's estimation order, the ARX-Laguerre technique has been applied in [12, 119]. Apart from the advantage of complexity reduction in ARX-Laguerre, it has a challenge related to estimation accuracy in nonlinear systems. To increase the accuracy in the ARX-Laguerre technique, the T-S fuzzy ARX-Laguerre (FAL) technique is presented in the literature [122]. In our work, this technique is used to estimate the vibration signals of REBs.

One of the main model-based techniques that can be used for FEDI is the observation technique [5]. The observation techniques can be categorized into two main groups: (a) The linear observers (e.g., proportional-integral (PI) and proportional multi integral (PMI)) and (b) nonlinear observers (e.g., feedback linearization observer (FLO), sliding mode observer (SMO), and fuzzy observer (FO)). Robustness and reliability in uncertain conditions are the main drawbacks of linear observers [12, 119]. Regarding the nonlinear observers, they can be designed based on driving the dynamic system's behavior in parallel with the linear observer to increase the robustness and reliability of the linear observer for fault estimation [8, 9]. In this chapter nonlinear observer is used for FEDI. Despite the improvement of the accuracy obtained from using the FLO, robustness is the main issue of this technique [9]. The extended-state FLO and SMO have been presented by researchers to improve the robustness of observers [8, 9, 122]. The SMO is a robust technique for FEDI for nonlinear and complex systems (e.g., rolling bearings) which operate in uncertain and noisy conditions. The nonlinear switching function in the SMO is defined to converge the output estimation error toward zero.

This technique can perform FEDI according to adaptive updates of the observer parameters, which can significantly improve the performance of FEDI in nonlinear systems [134, 135]. Though the SMO increases the robustness, this scheme unfortunately suffers from the chattering phenomenon and reduced fault estimation accuracy in the presence of uncertainties and unknown conditions. The chattering phenomenon (high-frequency oscillation) is one of the significant disadvantages of SMO. The main effect of this challenge is the increase of some serious mechanical obstacles such as heats the mechanical components and saturation. To decrease the chattering, the higher-order SMO (HOSMO) is presented and reported in [55, 136]. To increase the performance of the HOSMO, different techniques, such as the suboptimal (SO) method [57], quasi-continuous (QC) algorithm [58], and twisting technique (TW) [59], have been introduced. The main challenge of the QC-HOSMO, SO-HOSMO, and TW-HOSMO approaches is the first-order derivative of the sliding variable. To address this issue, a higher-order super-twisting (advanced) SMO (ASMO) for measurable and unmeasurable state observer has been reported [8]. Apart from the stability, robustness, and chattering attenuation in the ASMO, this method suffers from a somewhat reduced fault estimation accuracy. Therefore, in this chapter, the fuzzy technique is applied to the ASMO to increase the estimation accuracy and design AFSMO.

Once the observer is designed, the decision regarding the REB condition should be made. There are various conventional techniques that can be applied for the decision-making, such as decision tables, rule-based reasoning, and case-based reasoning [137]; however, recently the solutions provided by artificial intelligence (AI) are frequently applied to resolve the problems of fault diagnosis. Machine learning (ML) is one of the fields of AI that introduces some of the most popular techniques for decision-making, such as support vector machines (SVMs) [138] and artificial neural networks (ANNs) [66, 139]. To make a decision on the particular faulty condition, the SVM first attempts to find an optimal hyperplane that best separates the feature parameters corresponding to data instances of different classes. Then, when the new data sample appears, the SVM determines on which side of the hyperplane the sample lays and assigns a class corresponding to the location. When an ANN is used in fault identification, the network learns the optimal weights of its neurons during the back-propagation procedure to minimize the loss function and meet the target values given a

set of input attributes (i.e., feature set) corresponding to different faulty conditions. These days, the trend in AI applications have shifted toward the deep learning (DL) approach, which focuses on learning data representations to achieve the target goals. This shift is primarily enabled by the significant increase of computational capabilities of modern computer systems. The most popular DL-based solutions used for solving different problems in condition monitoring are convolutional neural networks [140] (fault diagnosis), autoencoders [133] (fault diagnosis, feature extraction, and data augmentation), generative adversarial networks [141] (data augmentation), and recurrent neural networks [142] (fault prediction). The principles of DL-based solutions are similar to those of the ANN; they adapt the weights of neurons and tune the hyperparameters to meet the requirements according to the task. However, unlike ANNs, the deep networks are characterized by a large number of hidden layers and nodes, which necessitate the application of huge datasets to achieve a good generalization by these networks. Also, the computational time of DL-based methods significantly increases in comparison with the conventional ML-based approaches. In this work, we employ an ML-based classification technique called a decision tree (DT) [143-145] to complete the proposed fault diagnosis methodology and implement the decision-making procedure for REB fault detection and identification. During training, the conventional DT [63] algorithm relatively fastly learns and derives the logical set of easily interpretable rules that can be used for decision-making regarding the REB faulty conditions, while providing insights into the quality of the fault estimation procedure performed by the advanced fuzzy SMO (AFSMO) in the previous step.

Figure 5.1 illustrates the complete block diagram of the proposed algorithm for FEDI of the bearing. This figure indicates that this algorithm has three main parts. In the first step, the system is modeled using the fuzzy ARX-Laguerre (FAL) technique. This part itself has three steps: (i) modeling the bearing based on the ARX method, (ii) modifying the performance of the ARX technique based on an orthonormal function and designing the ARX-Laguerre method, and (iii) improving the accuracy and performance of ARX-Laguerre bearing modeling based on the fuzzy ARX-Laguerre technique. In the second step, the AFSMO is designed for accurate fault estimation and improved performance of the decision component. The second step has three sub-blocks: (i) run the SMO, (ii) reduce the chattering and increase

the robustness, in which the SMO is improved based on the advanced technique and the designed ASMO, and (iii) increase the fault estimation accuracy using the fuzzy algorithm and apply it to the ASMO. Apart from the advantages of the ASMO regarding robustness and reliability, it suffers from a suboptimal fault estimation accuracy. To address this issue, a fuzzy algorithm is used in parallel with the advanced SMO for the bearings.

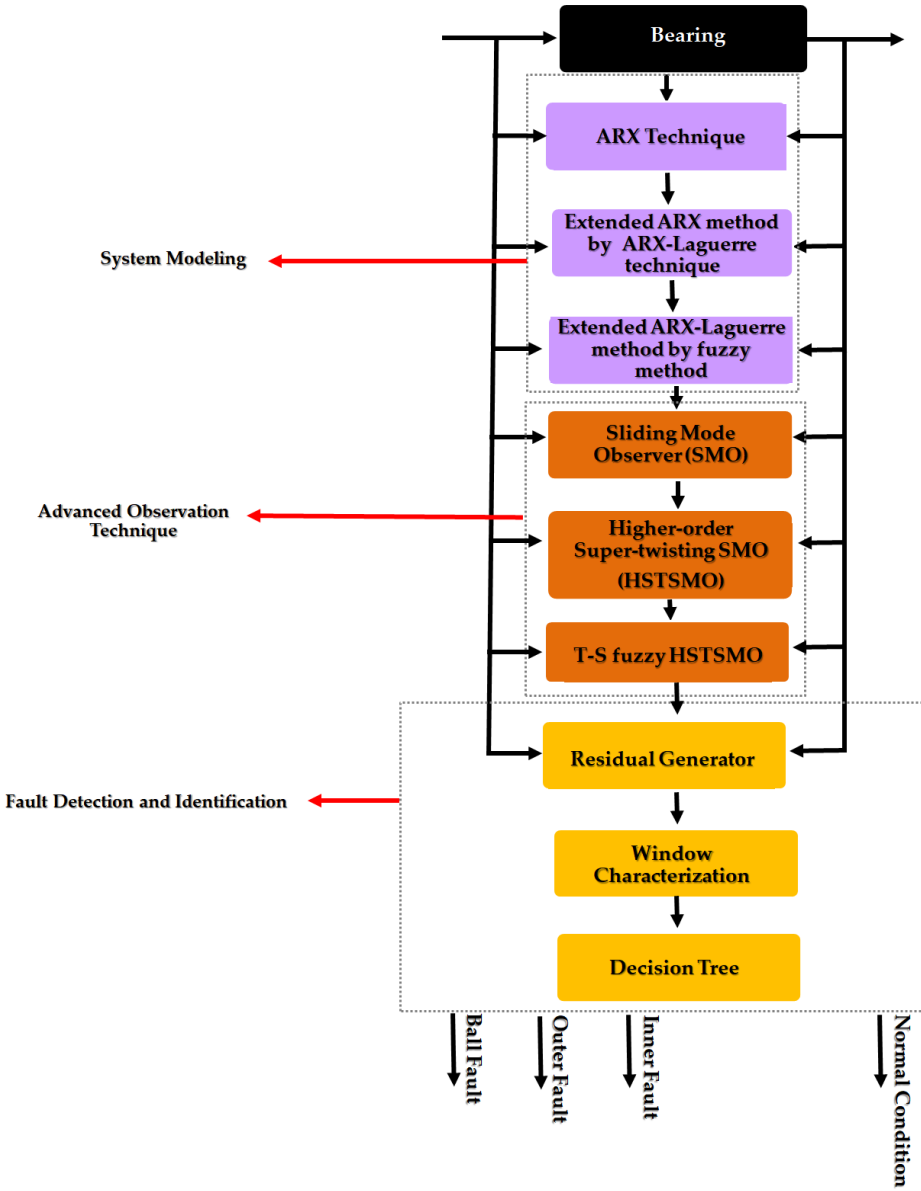

Figure 5.1. Proposed algorithm for FEDI (fault estimation, detection, and identification) in rolling-element bearing (REB).

In the third step, the faults are detected and identified based on the DT machine learning algorithm. The decision-making for fault detection and identification of REBs contain three parts applied in sequence. These parts are the (i) residual generator, (ii) window characterization, and (iii) deriving the logical decision rules for fault detection and identification using DTs. In the residual generator, the residual signals are calculated in various (normal and abnormal) conditions. Next, these residual signals are cut into windows of equal size and the amplitude-dependent feature parameter is extracted to quantitively characterize these obtained windows. Finally, the fault detection and identification are accomplished by the logical decision rules delivered by the DT technique. Specifically, the decision about the fault condition is accomplished by comparing the value of the extracted feature parameter from the window of the residual signal with the learned threshold provided by the DT classification algorithm. This chapter has the following contributions:

I. Robust technique for modeling the vibration signals in bearings based on the fuzzy ARX-Laguerre approach is proposed.

II. The estimation accuracy of the higher-order sliding mode observer for vibration signals has been improved by the T-S fuzzy algorithm.

III. The performance of fault detection and identification by the proposed hybrid observer is improved by the decision tree technique and hence, new machine learning-based hybrid observer is introduced in this chapter.

The rest of this chapter is organized as follows: Section 5.2 provides insights into the Case Western Reserve University (CWRU) benchmark and Smart HSE (SHSE) Lab datasets used in this chapter. In Section 5.3, the bearing is modeled based on the fuzzy ARX-Laguerre procedure. Section 5.4 includes two main steps. In the first step, the AFSMO is utilized for fault estimation. In the second step, the decision tree algorithm is used for the fault detection and identification. In Section 5.5, fault detection, estimation, and identification results for the bearing are analyzed. Finally, the conclusions are provided in the last section.

5.2 Dataset

In this chapter, two different datasets are used to evaluated the proposed algorithm. The Case Western Reserve University (CWRU) benchmark bearing dataset and the Smart HSE (SHSE) Lab bearing dataset are used to experimentally evaluate the effectiveness of machine learning-based AFSMO to test the single type and the multiple types of fault diagnosis, respectively.

5.2.1. Case Western Reverse University (CWRU) Bearing Data

To collect the vibration signals in normal and abnormal conditions, the vibration sensor (6205-2RS JEM SKF) is used. This sensor collects normal and single point faults that are seeded on the drive-end bearings at various bearing locations as the ball (Ball) fault, outer (OR) fault, and inner (IR) fault, respectively. The sampling rate of the record data is 12 kHz under four different motor torques loaded under different rotation velocities from 1730 rpm to 1790 rpm. Table 2.2 illustrates the data description of the CWRU benchmark bearing dataset. Four different datasets are defined in this table which are categorized by motor torque loaded from 0 to 3 hp. Moreover, the vibration signals in healthy and faulty (Ball, OR, IR) conditions have three different crack sizes (i.e., 0.007, 0.014, and 0.021 inches in diameter) [15, 77].

5.2.2. Smart HSE Lab Bearing Data

To transfer the torque to the no-drive-end shaft (NDES) through the gearbox, the three-phase induction motor is connected to the drive-end shaft [121]. Figure 4.6 shows the experimental data acquisition system to extract the normal and faulty signals. Faults with crack sizes of 3 mm and 6 mm in diameter are seeded on the drive-end bearings as the outer raceway fault (OR), inner raceway fault (IR), ball raceway fault (Ball), inner-outer raceway fault (IR-OR), inner-ball raceway fault (IR-Ball), outer-ball raceway fault (OR-Ball), and inner-outer-ball raceway fault (IR-OR-Ball). The data are recorded at 250 kHz sampling rate and the rotational speeds are 300, 400, 450, and 500 RPM. The details of the data are given in Table 4.1.

5.3 Rolling-Element-Bearing Modeling

In this chapter, the hybrid technique is proposed for FEDI. The model-based approach is the core of the proposed method. First, the Lagrangian formulation based on potential energy, kinetic energy, and generalized forces can be expressed as the following equation [74].

$$\frac{d}{dt}\left(\frac{\partial K}{\partial \dot{q}_i}\right) - \frac{\partial K}{\partial q_i} + \frac{\partial P}{\partial q_i} = Q_i, i = 1,2,3,4, \dots \quad (5.1)$$

Here, K, P, Q_i, and q_i are kinetic energy, potential energy, generalized force, and generalized coordinate, respectively. The energy equation can be obtained by the derivative of the Equation (5.1) and is expressed as follows [8, 74]:

$$F_{(q)} = (A + \Delta A)(q)[\ddot{q}] + (B + \Delta B)(q)[\dot{q}] + (C + \Delta C)(q)[q] + \varphi, \quad (5.2)$$

where $F_{(q)}, A(q), B(q), C(q), \varphi$, and $(\Delta A, \Delta B, \Delta C)$ are the force vector, mass vector, time-variant stiffness matrix, time-variant damping matrix, fault (IF, OF, BF) vectors, and unknown modeling parameters for mass, stiffness, and damping matrix, respectively. If $\Delta = \Delta A(q)[\ddot{q}] + \Delta B(q)[\dot{q}] + \Delta C(q)[q]$, the dynamic equation of the bearings can be represented as follows:

$$F_{(q)} = A(q)[\ddot{q}] + B(q)[\dot{q}] + C(q)[q] + \Delta + \varphi, \quad (5.3)$$

If $\omega(q, \dot{q}) = B(q)[\dot{q}] + C(q)[q]$ and $\psi(q, \dot{q}) = A^{-1}(q)(\Delta + \varphi)$ represent the uncertainties and faults, the bearing dynamic equation is rewritten as follows:

$$[\ddot{q}] = A(q)^{-1}\{F_{(q)} - \omega(q, \dot{q})\} - \psi(q, \dot{q}). \quad (5.4)$$

Apart from several advantages of mathematical-based system modeling, in most complicated systems, such as bearing systems, the precise mathematical formulation of energy and force in the bearing is nonlinear and complicated. In addition, mathematical modeling is not accurate in the presence of uncertainty. Moreover, the dynamic behavior of the bearing in theoretical and practical applications may be different, which causes challenges in system modeling for FEDI. Therefore, the fuzzy ARX-Laguerre (FAL) technique is represented for REB modeling. This system modeling technique has three main steps. In the first step, the

ARX system modeling is defined. To improve the robustness and reliability of the system modeling, the ARX-Laguerre technique is represented in the second step. In addition, to improve the system's modeling accuracy for the ARX-Laguerre technique, the fuzzy technique is represented. The mathematical formulation for an ARX system model is represented as [11, 12, 119]:

$$f_o(k) = \sum_{i=1}^{\delta_x} \varepsilon_x(i)\, f_o(k-i) + \sum_{i=1}^{\delta_y} \varepsilon_y(i)\, f_i(k-i), \tag{5.5}$$

where $f_o(k), \left(\varepsilon_x(i), \varepsilon_y(i)\right), f_i(k)$, and (δ_x, δ_y) are the output, model parameters, input, and order of the system, respectively. To represent the model parameters $(\varepsilon_x, \varepsilon_y)$, the following equation is presented.

$$\begin{cases} \varepsilon_x(i) = \sum_{n=0}^{\infty} \omega_{n,x}\, J_n^x\,(i, \gamma_x) \\ \varepsilon_y(i) = \sum_{n=0}^{\infty} \omega_{n,y}\, J_n^y\,(i, \gamma_y) \end{cases}, \tag{5.6}$$

Here, $(\omega_{n,x}, \omega_{n,y}), (\gamma_x, \gamma_y)$, and (J_n^x, J_n^y) are the coefficients of the Fourier decomposition, orthonormal basis, and orthonormal function, respectively. In the next step, ARX-Laguerre system modeling is used to obtain robust system modeling. The input and output orthonormal functions are represented in Equation (5.7).

$$\begin{cases} O_{n,f_o}(k, \gamma_x) = \sum_{i=1}^{\infty} J_n^x\,(i, \gamma_x) f_o(k-i) \\ O_{n,f_i}(k, \gamma_y) = \sum_{i=1}^{\infty} J_n^y\,(i, \gamma_y) f_i(k-i) \end{cases}, \tag{5.7}$$

Here, O_{n,f_o} and O_{n,f_i} are the filtered orthonormal functions for the output and input, respectively. The ARX orthonormal function is represented as the following equation.

$$f_o(k) = \sum_{n=0}^{\delta_x - 1} \omega_{n,x}\; O_{n,f_o}(k, \gamma_x) + \sum_{n=0}^{\delta_y - 1} \omega_{n,y}\; O_{n,f_i}(k, \gamma_y), \tag{5.8}$$

In addition, the Laguerre technique is defined as Equation (5.9).

$$\begin{cases} L_n^x = \frac{\sqrt{1-{\gamma_x}^2}}{Z-\gamma_x} \left(\frac{1-\gamma_x Z}{Z-\gamma_x}\right)^n \\ L_n^y = \frac{\sqrt{1-{\gamma_y}^2}}{Z-\gamma_y} \left(\frac{1-\gamma_y Z}{Z-\gamma_y}\right)^n \end{cases}, \tag{5.9}$$

Here, L_n^x and L_n^y are the input and output Laguerre functions, respectively. Based on Equations (5.7) and (5.9), the input and output orthonormal functions are modified to be the following equation.

$$\begin{cases} \bar{O}_{n,f_o}(k,\gamma_x) = \sum_{j=1}^{\infty} L_n^x(k) * f_o(k) \\ \bar{O}_{n,f_i}(k,\gamma_y) = \sum_{j=1}^{\infty} L_n^y(k) * f_i(k) \end{cases}, \tag{5.10}$$

Here, $\bar{O}_{n,f_o}$ and $\bar{O}_{n,f_i}$ are the input and output modified orthonormal functions, respectively. Thus, the ARX-Laguerre system modeling and estimation is represented as the following [119].

$$\begin{gathered} f_o(k) = \sum_{n=0}^{i_x-1} \omega_{n,x}\ \bar{O}_{n,f_o}(k,\gamma_x)W(k) + \sum_{n=0}^{i_y-1} \omega_{n,y}\ \bar{O}_{n,f_i}(k,\gamma_y)I(k) \\ f_o(k) = \Psi(z^{-1})W(z) + \Lambda(z^{-1})I(z) \end{gathered} \tag{5.11}$$

Here, ($\Psi(z^{-1})$, $\Lambda(z^{-1})$) and ($W(k), I(k)$) are the polynomial variables and filtering signals, respectively and defined as the following equations.

$$\begin{aligned} \Psi(z^{-1}) &= \sum_0^{n_x-1} \omega_{n,x}\ \bar{O}_{n,f_o}(k) \\ \Lambda(z^{-1}) &= \sum_0^{n_y-1} \omega_{n,y}\ \bar{O}_{n,f_i}(k) \end{aligned}, \tag{5.12}$$

Therefore, the state-space ARX-Laguerre technique is represented as Equation (5.13).

$$\begin{cases} J_s(k+1) = [\sigma_s J_s(k) + \sigma_o J_o(k) + \sigma_i J_i(k)] + \varphi(k) \\ J_o(k+1) = (\lambda)^T J_s(k) \end{cases}, \tag{5.13}$$

Here, $J_s(k), (\sigma_s, \sigma_o, \sigma_i), J_o(k), J_i(k), \varphi(k)$, and $(\lambda)^T$ are the system's state, modeling coefficients, measured output, input, uncertainties and fault, and Fourier coefficients, respectively. Here, the state system modeling coefficient σ_s is represented by the following equation:

$$\sigma_s = \begin{bmatrix} \sigma_{so} & O_{N_x,N_y} \\ O_{N_y,N_x} & \sigma_{si} \end{bmatrix}, \tag{5.14}$$

where O_{N_x,N_y} and O_{N_y,N_x} are null matrices and σ_{so} and σ_{si} are represented in Equations (5.15) and (5.16), respectively.

$$\sigma_{s_o} = \begin{bmatrix} \gamma_x & \cdots & 0 \\ \vdots & \ddots & \vdots \\ (-\gamma_x)^{N_x-1}(1-{\gamma_x}^2) & \cdots & \gamma_x \end{bmatrix}, \tag{5.15}$$

$$\sigma_{s_i} = \begin{bmatrix} \gamma_y & \cdots & 0 \\ \vdots & \ddots & \vdots \\ (-\gamma_y)^{N_y-1}\left(1-{\gamma_y}^2\right) & \cdots & \gamma_y \end{bmatrix}, \tag{5.16}$$

The output system modeling coefficient σ_o is represented in Equation (5.17).

$$\sigma_o = \sqrt{1-{\gamma_x}^2}\begin{bmatrix} 1 \\ -\gamma_x \\ -{\gamma_x}^2 \\ \vdots \\ (-\gamma_x)^{N_x-1} \end{bmatrix}, \tag{5.17}$$

In addition, the input system modeling coefficient σ_i can be represented in Equation (5.18).

$$\sigma_i = \sqrt{1-{\gamma_y}^2}\begin{bmatrix} 1 \\ -\gamma_y \\ -{\gamma_y}^2 \\ \vdots \\ (-\gamma_y)^{N_y-1} \end{bmatrix}, \tag{5.18}$$

To improve the ARX-Laguerre system modeling accuracy, the fuzzy technique is recommended in this research. The fuzzy ARX-Laguerre (FAL) system modeling is defined as follows.

$$\begin{cases} J_s(k+1) = \left[\sigma_s J_s(k) + \sigma_o J_o(k) + \sigma_i J_i(k) + \sigma_f J_f(k)\right] + \varphi(k) \\ J_o(k+1) = (\lambda)^T J_s(k) \end{cases}, \tag{5.19}$$

Here, σ_f and J_f are the fuzzy coefficient and fuzzy function for system estimation, respectively. The fuzzy if-then rule in this research is defined by the following rule.

$$\begin{gathered} If < first\ input > \ is < lingistic\ variable\ for\ first\ input > \ and \\ < second\ input > \ is \\ < linguistic\ variable\ for\ second\ input > \ then < output > \ is < \\ linguistic\ variable\ for\ output > \end{gathered} \tag{5.20}$$

The membership functions of a fuzzy set for the system estimation of error (e) in the interval of $[-0.3,\ \ 0.3]$ are the Gaussian and the linguistic variables, which are defined by negative high (NH), negative medium (NM), negative low (NL), zero (Z), positive low (PL), positive medium (PM), and positive high (PH). The fuzzy membership functions for the system estimation of the change of error ($\dot{e}$) in the interval of $[-0.1,\ \ 0.1]$ are the Gaussian and the linguistic variables, which are defined by NH, NM, NL, Z, PL, PM, and PH. In addition, the fuzzy linguistic variables for J_f in the interval of $[-0.08,\ \ 0.08]$ are the Gaussian and the fuzzy sets, which are defined by NH, NM, NL, Z, PL, PM, and PH. Table 5.1 illustrates the fuzzy rule table for the FAL system estimation technique. According to this table, the error has seven linguistic variables, the change of error has seven linguistic variables and the fuzzy system estimation has seven linguistic variables. Therefore, the fuzzy technique to improve system modeling has 49 rule-bases. Based on these 49 rule-bases, the fuzzy technique has improved the accuracy of system modeling to achieve the minimum estimation error.

Table 5.1. The fuzzy rule table for system modeling based on the fuzzy ARX-Laguerre (FAL) technique.

		Change of Error ($\dot{e}$)						
		NH	**NM**	**NL**	**Z**	**PL**	**PM**	**PH**
Error (e)	**NH**	PH	PH	PH	PH	PM	PL	Z
	NM	PH	PH	PH	PM	PL	Z	NL
	NL	PH	PH	PM	PL	Z	PL	PM
	Z	PH	PM	PL	Z	NL	NM	NH
	PL	PM	PL	Z	NL	NM	NH	NH
	PM	PL	Z	NL	NM	NH	NH	NH
	PH	Z	NL	NM	NH	NH	NH	NH

Figures 5.2 and 5.3 show the estimation accuracy and errors of REB modeling for the normal and faulty conditions based on the proposed FAL technique, ARX-Laguerre system modeling technique, and ARX system estimation method. Based on these figures, the system modeling accuracy in the proposed fuzzy ARX-Laguerre system modeling is higher than the ARX-Laguerre technique and ARX system modeling techniques. Regarding Figure 5.2, the error rate in the proposed fuzzy ARX-Laguerre technique is close to zero.

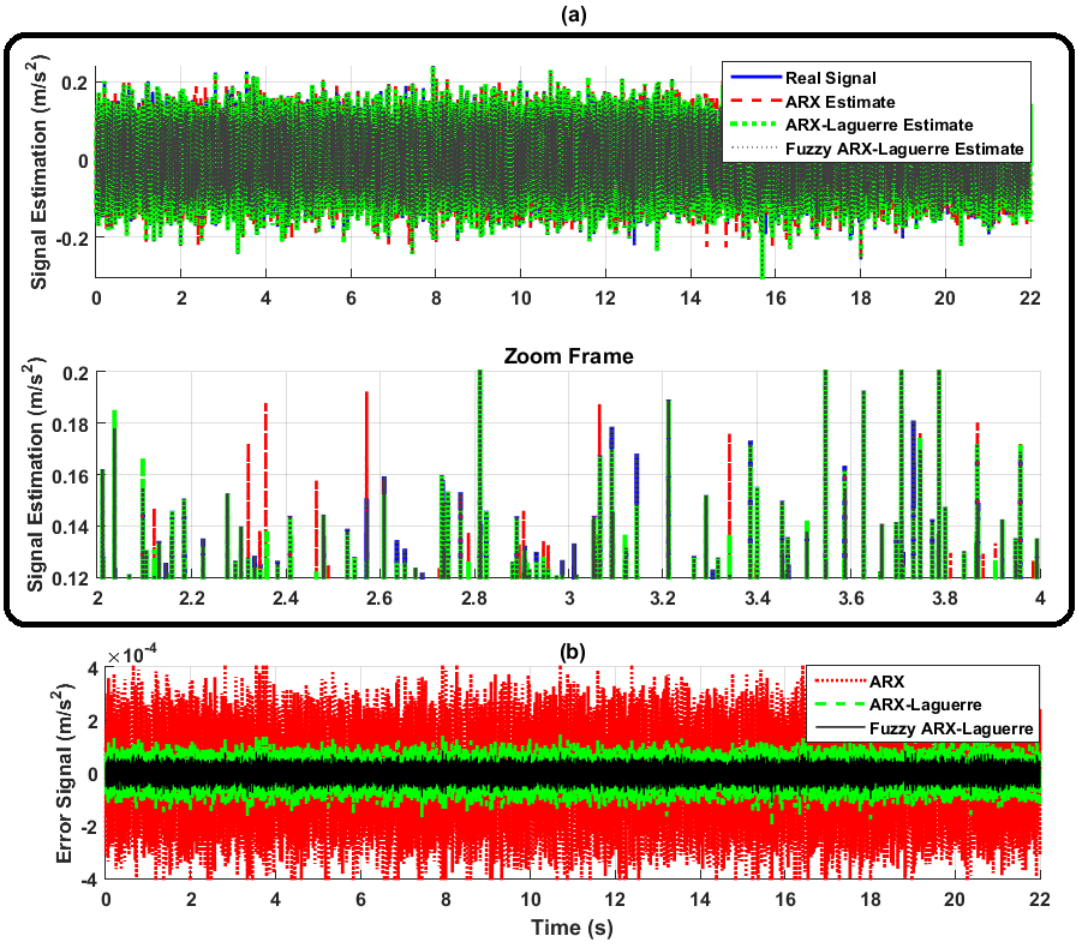

Figure 5.2. The estimation accuracies in the normal condition: (a) the real and estimated signal, and (b) the estimation signal's error.

5.4 Proposed Algorithm for Fault Diagnosis in Rolling-Element Bearing

According to Figure 5.1, the fuzzy ARX-Laguerre method was used to model the bearing in normal and abnormal conditions. The next step focuses on the designed advanced fuzzy sliding mode observation technique that comprises three main blocks: (a) apply SMO for fault estimation, (b) improve the robustness and chattering attenuation based on the high-order super-twisting (advance) SMO (ASMO), and (c) improve the accuracy of the fault estimation technique, i.e., the T-S fuzzy algorithm applied to the ASMO.

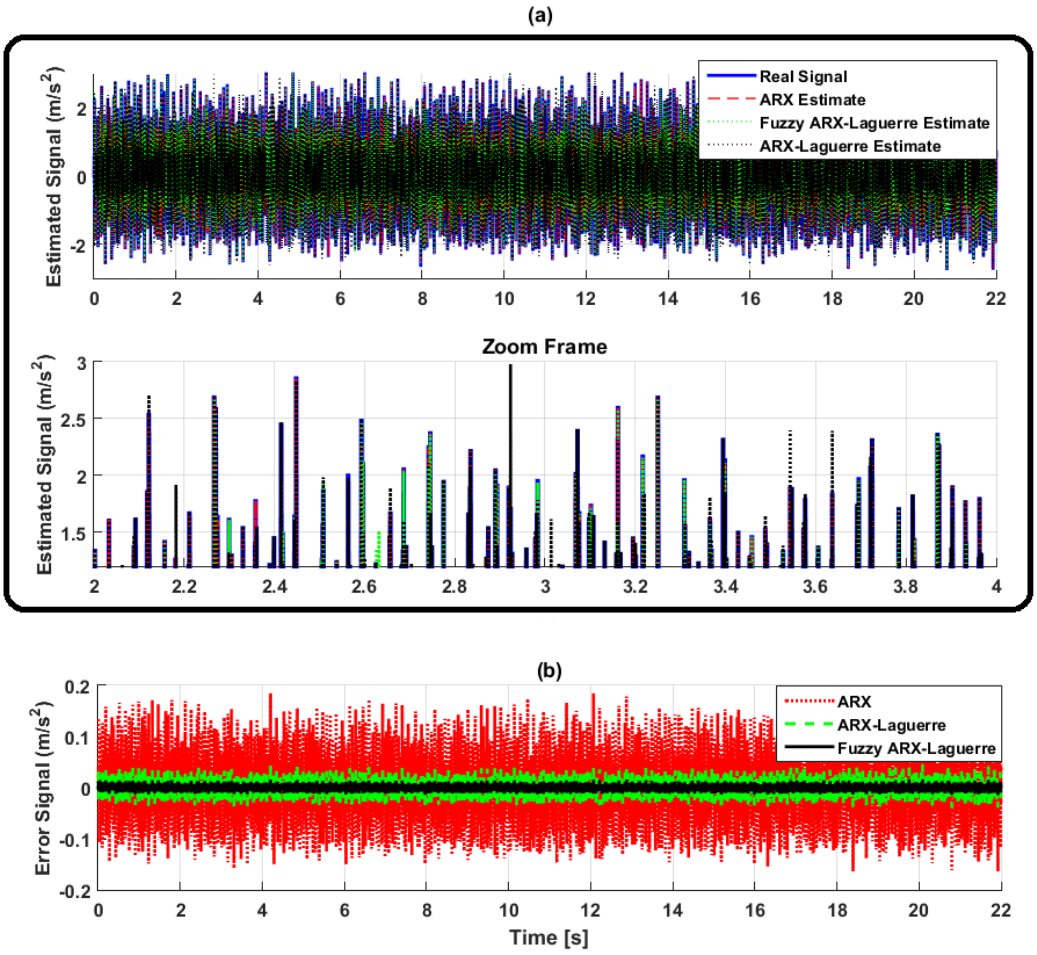

Figure 5.3. The estimation accuracies in the abnormal condition. (a) Real and estimated signals by three techniques, and (b) the estimation signal's error by three techniques.

5.4.1. Advance Sliding Mode Observer for Fault Estimation

Based on Equation (5.19) for FAL modeling of the REB, the SMO is proposed based on Equation (5.21).

$$\begin{cases} \hat{J}_{s-SMO}(k+1) = \left[\sigma_s \hat{J}_{s-SMO}(k) + \sigma_o \hat{J}_{o-SMO}(k) + \sigma_i J_i(k) + \sigma_f J_f(k)\right] + \hat{\varphi}_{SMO}(k) + \\ \sigma_p (J_o(k) - \hat{J}_{o-SMO}(k)) + \sigma_{sM}.sgn(J_o(k) - \hat{J}_{o-SMO}(k)) \\ \hat{J}_{o-SMC}(k+1) = (\lambda)^T \hat{J}_{s-SMO}(k) \end{cases}, \quad (5.21)$$

In addition, the equation to define fault estimation based on the SMO is:

$$\hat{\varphi}_{SMO}(k+1) = \hat{\varphi}_{SMO}(k) + \sigma_p \left(J_o(k) - \hat{J}_{o-SMO}(k)\right) + \sigma_{sM}.sgn(J_o(k) - \hat{J}_{o-SMO}(k)). \quad (5.22)$$

where $\hat{J}_{s-SMO}(k), \hat{J}_{o-SMO}(k), \hat{\varphi}_{SMO}(k)$, and $(\sigma_s, \sigma_o, \sigma_i, \sigma_p, \sigma_{SM})$ are the sliding mode system state estimation, sliding mode output estimation, sliding mode fault estimation, and coefficients, respectively. The SMO is a robust and stable technique for fault diagnosis in bearings, however, this technique suffers from the chattering phenomenon. To reduce the effect of the chattering, the following function is introduced:

$$Z = \sigma_x \left\| J_o(k) - \hat{J}_{o-SMO}(k) \right\|^{0.5} sgn\left(J_o(k) - \hat{J}_{o-SMO}(k)\right), \tag{5.23}$$

where Z and σ_x are new the observation definition and coefficient, respectively. If the unknown conditions are estimated $(\Delta + \varphi)$, the SMO error goes to zero in a finite time.

$$\begin{cases} \sigma_x \left\| J_o(k) - \hat{J}_{o-SMO}(k) \right\|^{0.5} sgn\left(J_o(k) - \hat{J}_{o-SMO}(k)\right) - \hat{\delta} \\ \dot{\hat{\delta}} = \sigma_{x_0} \times sgn\left(J_o(k) - \hat{J}_o(k)\right) \end{cases}, \tag{5.24}$$

Here, σ_{x_0} and $\dot{\hat{\delta}}$ are the respective coefficient and the variable for the super-twisting variable. Therefore, based on Equation (5.23), this technique can improve the performance of fault estimation in the unknown condition. Therefore, to reduce the chattering phenomenon, the ASMO state-space and the fault estimation equation can be represented in Equations (5.25) and (5.26).

$$\begin{cases} \hat{J}_{s-HSMO}(k+1) = \left[\sigma_s \hat{J}_{s-HSMO}(k) + \sigma_o \hat{J}_{o-HSMO}(k) + \sigma_i J_i(k) + \sigma_f J_f(k)\right] + \\ \hat{\varphi}_{HSMO}(k) + \sigma_p (J_o(k) - \hat{J}_{o-HSMO}(k)) + \sigma_{HsM}.sgn\left|(J_o(k) - \hat{J}_{o-HSMO}(k))\right|^{\frac{2}{3}}, \\ \hat{J}_{o-HSMC}(k+1) = (\lambda)^T \hat{J}_{s-HSMO}(k) \end{cases} \tag{5.25}$$

$$\begin{cases} \hat{\varphi}_{HSMO}(k+1) = \hat{\varphi}_{HSMO}(k) + \sigma_p \left(J_o(k) - \hat{J}_{o-HSMO}(k)\right) + \sigma_{HsM} \times sgn \\ (J_o(k) - \hat{J}_{o-HSMO}(k)) + \sigma_x \left\| J_o(k) - \hat{J}_{o-HSMO}(k) \right\|^{0.5} sgn\left(J_o(k) - \hat{J}_{o-HSMO}(k)\right) - \hat{\delta}. \\ \dot{\hat{\delta}} = \sigma_{x_0} \times sgn\left(J_o(k) - \hat{J}_o(k)\right) \end{cases} \tag{5.26}$$

Here, $\hat{J}_{s-HSMO}(k), \hat{J}_{o-HSMO}(k), \hat{\varphi}_{HSMO}(k)$, and (σ_x, σ_{HSM}) are the advanced sliding mode system state estimation, advanced sliding mode output estimation, advanced sliding mode fault estimation, and coefficients, respectively. To find the sliding gain, the estimation error is calculated based on the following equation.

$$\begin{cases} \tilde{J}_{s-HSMO}(k+1) = [\sigma_s \tilde{J}_{s-HSMO}(k) + \sigma_o \tilde{J}_{o-HSMO}(k)] + \tilde{\varphi}_{HSMO}(k) + \\ \sigma_p \left(J_o(k) - \tilde{J}_{o-HSMO}(k)\right) + \sigma_{HsM}.sgn\left|\left(J_o(k) - \tilde{J}_{o-HSMO}(k)\right)\right|^{\frac{2}{3}} \\ \tilde{J}_{o-HSMO}(k+1) = (\lambda)^T \tilde{J}_{s-HSMO}(k) \\ \tilde{J}_{s-HSMO}(k) = J_s(k) - \hat{J}_{s-HSMO}(k) \\ \tilde{J}_{o-HSMO}(k) = J_o(k) - \hat{J}_{o-HSMO}(k) \end{cases}. \quad (5.27)$$

Here, $\tilde{J}_{s-HSMO}(k), \tilde{J}_{o-HSMO}(k)$, and $\tilde{\varphi}_{HSMO}(k)$ are the state-estimation error, measured output estimation error, and fault estimation error based on the advanced SMO, respectively. Therefore, to guarantee the stability and robustness, the sliding surface slope coefficients are represented by the following equations [8].

$$\begin{cases} \sigma_{x_0} = 1.1 \times \Gamma \\ \sigma_{HSM} = 1.9 \times \sqrt[3]{\Gamma}. \\ \sigma_x = 1.5 \times \sqrt{\Gamma} \end{cases} \quad (5.28)$$

Here, Γ is an estimation error bounded and based on Equation (5.26), it can be determined by the nonlinear part of the estimation error performance. Though there is an improvement in the robustness and the attenuation of the chattering based on the ASMO for FEDI, this fails to improve the fault estimation accuracy. Therefore, the T-S fuzzy algorithm is used to improve the ASMO. The T-S fuzzy technique is represented based on the following equation [146].

$$\alpha_f(k) = \begin{cases} if\ r_x(k)\ is\ TH_n\ then\ \alpha_f(k+1) = \alpha_f(k) + \varsigma_n(J_o(k) - \hat{J}_{o-fHSMO}(k)) \\ if\ r_x(k)\ is\ TH_f\ then\ \alpha_f(k+1) = \alpha_f(k) + \varsigma_f(J_o(k) - \hat{J}_{o-fHSMO}(k)) \end{cases}. \quad (5.29)$$

Here, $r_x(k), \alpha_f, TH_n, TH_f$, and $(\varsigma_n, \varsigma_f)$ are the residual signal, fuzzy estimation function, threshold value for the normal condition, threshold value for the faulty condition, and normal and abnormal coefficients for the T-S fuzzy observer, respectively. Therefore, the proposed advanced fuzzy SMO and the fault estimation are represented in Equations (5.30) and (5.31).

$$\begin{cases} \hat{J}_{s-fHSMO}(k+1) = \left[\sigma_s \hat{J}_{s-fHSMO}(k) + \sigma_o \hat{J}_{o-fHSMO}(k) + \sigma_i J_i(k)\right] + \hat{\varphi}_{fHSMO}(k) + \\ \sigma_p \left(J_o(k) - \hat{J}_{o-fHSMO}(k)\right) + \sigma_{fHsM}.sgn\left|\left(J_o(k) - \hat{J}_{o-fHSMO}(k)\right)\right|^{\frac{2}{3}} + \alpha_f(k) \\ \hat{J}_{o-fHSMC}(k+1) = (\lambda)^T \hat{J}_{s-fHSMO}(k) \end{cases}, \quad (5.30)$$

$$\begin{cases} \hat{\varphi}_{fHSMO}(k+1) = \hat{\varphi}_{fHSMO}(k) + \sigma_p \left(J_o(k) - \hat{J}_{o-fHSMO}(k)\right) + \sigma_{fHsM} \times sgn \\ (J_o(k) - \hat{J}_{o-fHSMO}(k)) + \sigma_x \left\|J_o(k) - \hat{J}_{o-fHSMO}(k)\right\|^{0.5} sgn\left(J_o(k) - \hat{J}_{o-fHSMO}(k)\right) - \hat{\delta}. \\ \dot{\hat{\delta}} = \sigma_{x_0} \times sgn\left(J_o(k) - \hat{J}_{o-fHSMO}(k)\right) \end{cases} \quad (5.31)$$

Here, $\hat{J}_{s-fHSMO}$,$\hat{J}_{o-fHSMO}$,$\hat{\varphi}_{fHSMO}$, and σ_{fHsM} are the advanced fuzzy sliding mode system state estimation, advanced fuzzy sliding mode output estimation, advanced fuzzy sliding mode fault estimation, and coefficients, respectively. After estimating the output based on the proposed AFSMO, the residual signal can be calculated as follows:

$$r_x(k) = J_o(k) - \hat{J}_{o-fHSMO}(k). \quad (5.32)$$

Figures 5.4–5.6 illustrate the residual signal in normal and abnormal conditions based on the SMO, ASMO, and AFSMO (the proposed method).

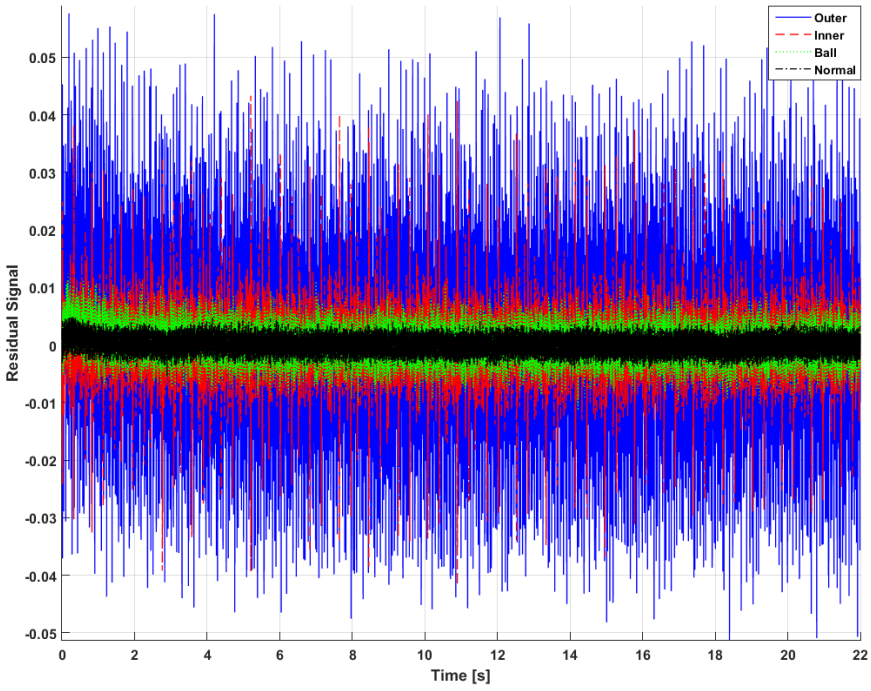

Figure 5.4. Residual signal based on sliding mode observer (SMO).

Based on these figures, the difference between various states of signals in the AFSMO is more clear than those of the ASMO and SMO. In the next part, the procedure of fault detection and identification is performed and described using the decision tree machine learning technique.

5.4.2. Fault Detection and Fault Identification Based on Decision Tree Technique

5.4.2.1 Residual Signal Characterization

Once the residual signal is obtained based on Equation (5.32), this signal can be successfully used to perform the fault detection and diagnosis process. To apply the DT approach for the problem of fault diagnosis, the specific numerical feature parameter sensitive to the changing signal conditions is essential. Because of the fact that the residual signal itself represents an error between the original signal and that estimated by the proposed observer, this signal cannot be quantified by most of the conventional feature parameters that are used in fault diagnosis. However, the parameters that are sensitive to the amplitude can be applied to characterize the residual (i.e., the error) signal.

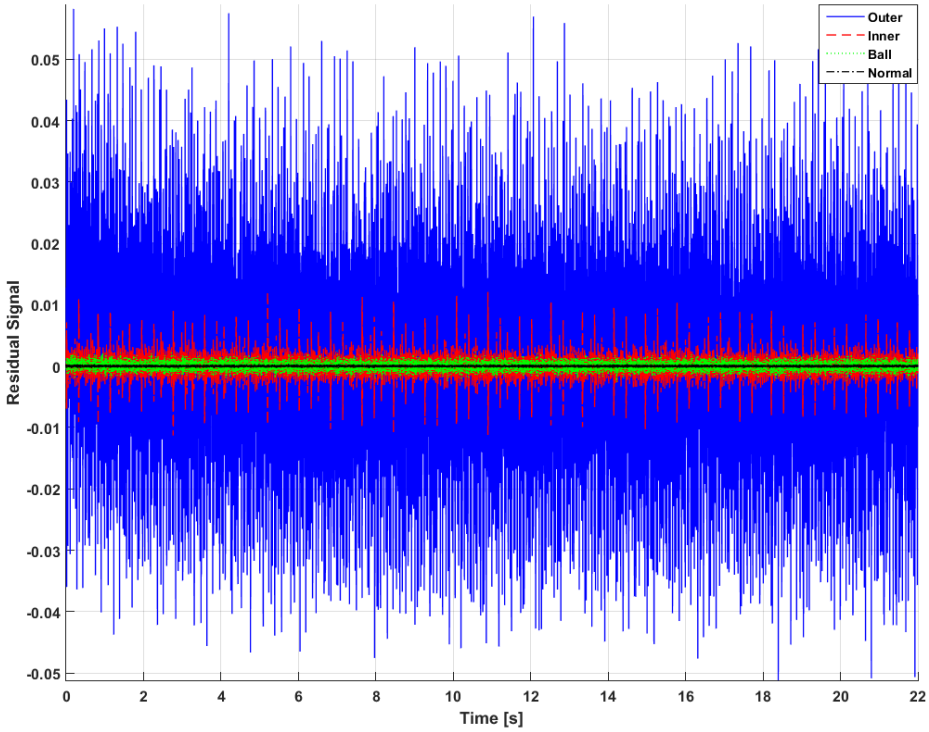

Figure 5.5. Residual signal based on advanced SMO (ASMO).

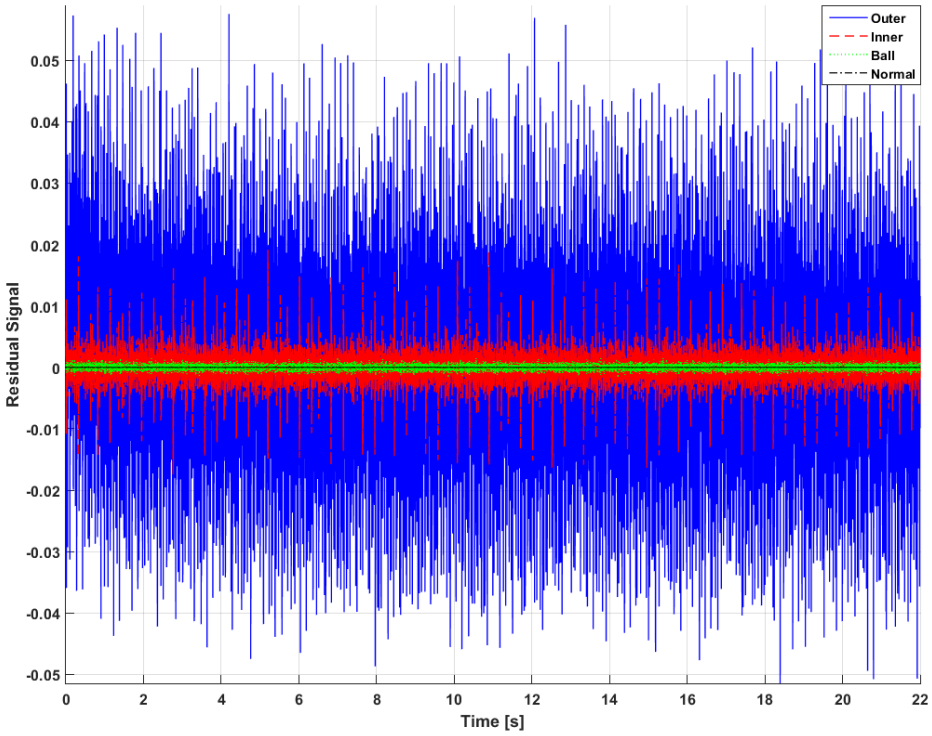

Figure 5.6. Residual signal based on advanced fuzzy SMO (AFSMO).

To characterize the residual signal by a numerical parameter, first, we split the time sequence into windows. Then, the feature parameter called the energy of the signal is extracted from these windows to deliver a numerical value that can be used to characterize "the amount of error" in the particular window. The formulation of the energy feature parameter is provided below:

$$E = \sum_{i=1}^{N} {r_{x_i}}^2. \tag{5.33}$$

Here, r_{x_i} is the i^{th} sample of the residual signal and N is the total number of samples. When the different types of mechanical faults appear in REBs, the amplitudes of the vibration signals change drastically. This signal behavior strongly affects the residues as well. Thus, the use of the energy as a numerical feature for characterizing the windows of the residual signals is a reasonable choice because the value of the energy is closely related to the amplitude of the sequence being investigated. Moreover, since the residue represents the error between the two signals, the values of its samples can be both positive and negative. The application of the energy feature allows us to consider the error values located on both sides from zero because of the squared term presented in Equation (5.33). Figure 5.7 shows the residual signal

characterization based on the energy for normal and faulty conditions. As can be seen from this figure, the extracted feature parameters corresponding to different system's conditions are well separable in one Dimensional (1D) feature space which means that the proposed methodology can be efficiently applied for purposes of REB fault diagnosis.

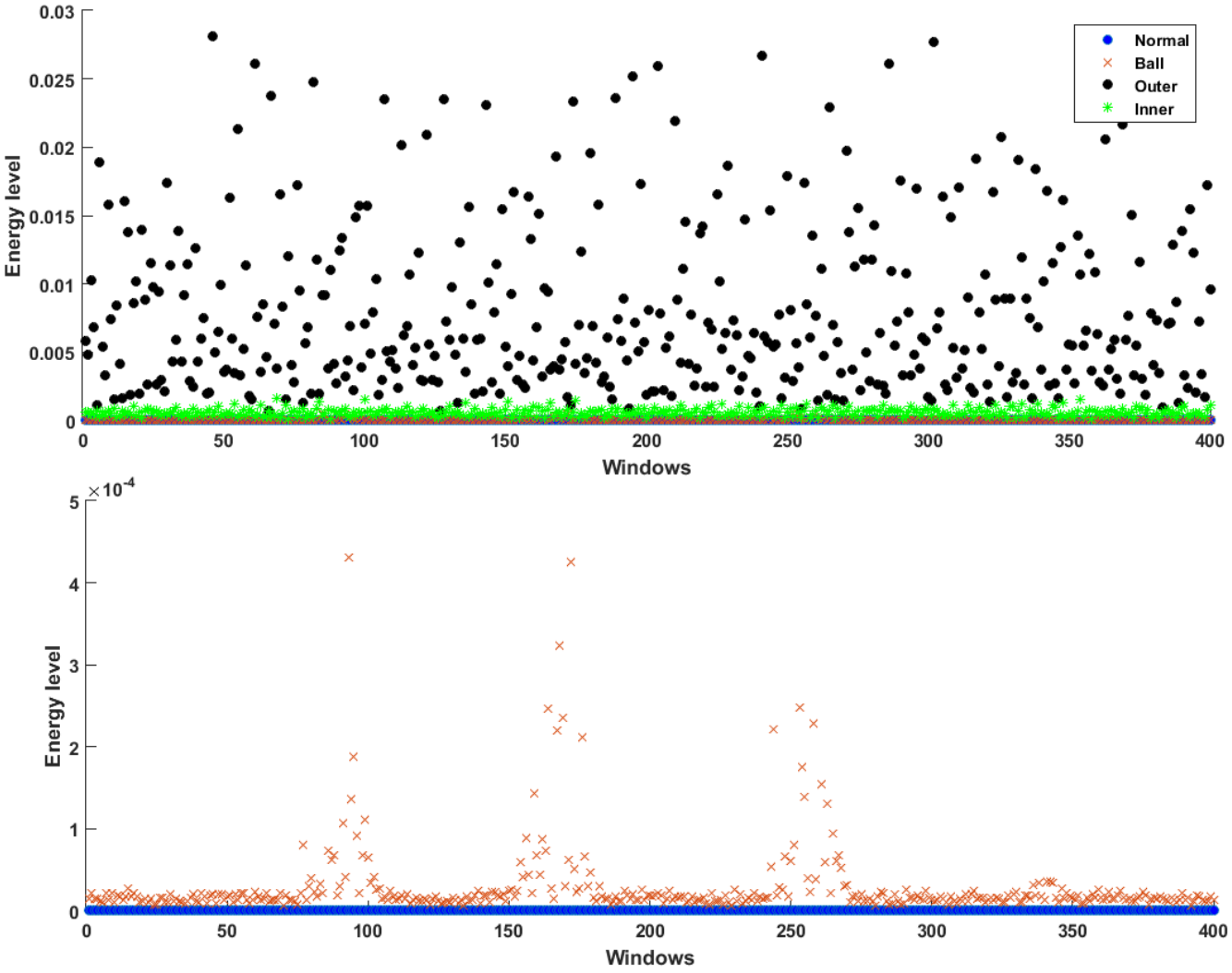

Figure 5.7. The energy of the residual signal based on the AFSMO: (a) original, (b) zoom frame.

5.4.2.2 Decision Tree-Based Fault Diagnosis

Once the windows of residual signals have been characterized using the energy feature parameter, these feature parameters are fed into the classifier, which is made using the DT. DT [63], as well as random forests (i.e., the ensemble of DTs) [64, 147], is a type of machine

learning technique that can perform both the classification and regression tasks while their decisions are fairly intuitive and easy to interpret. Because of their properties, decision trees are considered as white-box models; they automatically derive general classification rules that work well for the data given in the training set based on the specific attributes (i.e., feature parameters). Moreover, these obtained decision rules can be efficiently used manually for classifying different samples if necessary.

During training of the DT to perform fault detection and identification, the heuristic criteria that is based on the error and is called the Gini Diversity Index (GDI) [148], also known in the literature as the Gini Impurity, is applied in this chapter. The main advantage of employing the GDI criterion is that the DTs trained with this metric tends to isolate the most frequent data class in its branch of the tree which is useful for evaluating the quality of features in training set and their separability. The GDI is defined as follows:

$$GDI_i = 1 - \sum_{k=1}^{n} P_{i,k}{}^2. \tag{5.34}$$

where GDI_i is the Gini score for the i^{th} leaf of the DT, n is the total number of classes (i.e., bearing faults) presented in data, and $p_{i,k}$ is the ratio of the instances belonging to class k among all instances in the i^{th} leaf.

The training procedure of the DT can be summarized as follows. Given a specific feature parameter and GDI criterion, the training goal is to find a split for the features that induces a binary partition of the set of data samples with a minimum GDI criterion, where the weights of this criterion are given by the number of data samples that lie in each of the two branches [149]. The leaf node is said to be "pure" when all training samples it applies to belong to the same class. Finally, after the training of the DT with the energy values extracted from the windows of residual signals is completed, we obtain a set of rules for differentiating various bearing conditions. This set of rules is based on the threshold values automatically learned by the DT to minimize the weighted sum of Gini scores of the DT leaves. After completing the training process, the new data sample can be simply classified by tracing out a route from the root to one of the leaves of the tree while comparing the energy value with the learned threshold values for each of the leaves. In this chapter, the number of assigned

leaves is similar to the number of signal classes presented in the dataset, which is equal to four. Equations (5.35) and (5.36) are used to formulate the respective fault detection and fault diagnosis based on the DT algorithm.

$$\begin{cases} if\ E < \zeta_n \rightarrow Normal \\ if\ E \geq \zeta_n \rightarrow Faulty \end{cases} \tag{5.35}$$

$$\begin{cases} if\ E \geq \zeta_n \& E < \zeta_b \ \& E < \zeta_i \rightarrow Ball\ Fault \\ if\ E \geq \zeta_n \& E \geq \zeta_b \ \& E < \zeta_i \rightarrow Inner\ Fault \\ if\ E \geq \zeta_n \& E \geq \zeta_b \ \& E \geq \zeta_i \rightarrow Outer\ Fault \end{cases} \tag{5.36}$$

Here, ζ_n, ζ_b, and ζ_i are the normal condition threshold, ball fault condition threshold, and inner fault condition threshold, respectively. The proposed DT-based AFSMO for bearing FEDI is summarized in Algorithm 5.1, and an example of the DT trained using the energy values extracted from the residual signal windows for 0.021 inches crack size condition under 3 hp torque load is presented in Figure 5.8.

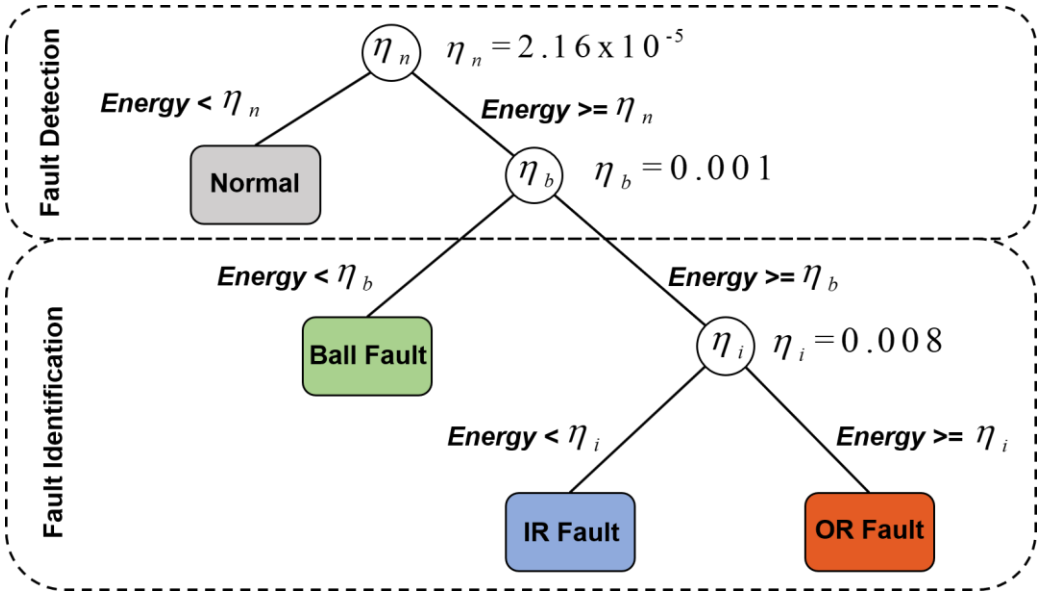

Figure 5.8. The decision tree trained for detecting and diagnosing various bearing faults using the energy values of the residual signal windows for 0.021 inches crack size condition under 3 hp torque load.

Algorithm 5.1. Decision trees-based fuzzy ARX-Laguerre fuzzy high-order super-twisting sliding mode (hybrid) observer for fault diagnosis of the bearing.

1: Perform system modeling based on the fuzzy ARX-Laguerre technique (5.19)
2: Run the SMO (5.21, 5.22)
3: Run the ASMO to reduce the chattering phenomenon (5.25, 5.26)
4: Run the AFSMO to increase the fault estimation (5.30, 5.31)
5: Run the residual generator (5.32)
6: Run the residual signal characterization by energy (5.33)
7: Run the learning process of decision trees (5.34)
8: Apply the classification rules delivered by decision trees for fault detection and identification (5.35, 5.36)

5.5 Experimental Results

In this section, the fault diagnosis capabilities of the proposed technique are validated against two state-of-the-art approaches that have reported results for the same publicly available datasets (e.g., CWRU dataset and SHSE Lab dataset). Specifically, the first employed method is the ASMO and the second approach used for the comparison is the SMO. The final fault diagnosis performance is expressed in terms of the average classification accuracy (ACA) as follows:

$$ACA = \frac{\sum_{m=1}^{4} TP_m}{N_{samples}} \times 100\% \quad (5.37)$$

where T_p is the number of true positive predictions (i.e., the number of data samples of the specific class m correctly identified as ones belonging to the class m), and $N_{samples}$ is the total number of samples available in the particular dataset. To provide a comprehensive performance evaluation, the two different conditions for each of case-studies are considered in this result sections: evaluating fault diagnosis accuracies on crack-variant datasets and the created custom load-variant datasets provided by CWRU and SHSE Lab.

5.5.1. Single Type Fault Detection and Identification Provided by CWRU Dataset

In this subsection, we investigate the fault identification capabilities of the proposed methodology on four crack-variant datasets, where the torque load remained fixed. In other words, each of the four datasets corresponding to the particular load levels contains three subsets, where each of the subsets is formed using the data instances collected under the

specific crack size. In this experiment, each subset comprises of $N_f \times N_w$ data samples, where N_f is the number of faulty conditions available in the CWRU benchmark dataset and N_w is the number of windows (equal to 400, Section 5.4.2) cut from the residual signals delivered by the AFSMO in the previous step. The fault diagnosis results obtained for the REB datasets with various crack diameters under fixed load conditions are tabulated in Tables 5.2–5.5.

Table 5.2. The accuracy of the single faults FEDI when the torque load is 0 hp.

Algorithms	**AFSMO (Proposed Method)**			**ASMO**			**SMO**		
Crack Diameters (in)	0.007	0.014	0.021	0.007	0.014	0.021	0.007	0.014	0.021
Normal	100%	100%	100%	100%	100%	100%	100%	100%	100%
BF	100%	100%	100%	93%	94%	94%	89%	91%	92%
OF	84%	100%	99%	81%	92%	92%	80%	88%	90%
IF	96%	100%	99%	94%	90%	96%	88%	91%	94%
ACA	95%	100%	99.5%	91.25%	94%	95.5%	89.25%	92.5%	94%

Table 5.3. The accuracy of the single faults FEDI when the torque load is 1 hp.

Algorithms	**AFSMO (Proposed Method)**			**ASMO**			**SMO**		
Crack Diameters (in)	0.007	0.014	0.021	0.007	0.014	0.021	0.007	0.014	0.021
Normal	100%	100%	100%	100%	100%	100%	98%	98%	98%
BF	100%	99%	100%	96%	90%	98%	90%	88%	92%
OF	100%	100%	100%	94%	94%	95%	90%	90%	90%
IF	100%	92%	100%	95%	98%	98%	88%	90%	89%
ACA	100%	97.75%	100%	96.25%	95.5%	97.75%	91.5%	91.5%	92.25%

Table 5.4. The accuracy of the single faults FEDI when the torque load is 2 hp.

Algorithms	**AFSMO (Proposed Method)**			**ASMO**			**SMO**		
Crack Diameters (in)	0.007	0.014	0.021	0.007	0.014	0.021	0.007	0.014	0.021
Normal	100%	100%	100%	100%	100%	100%	100%	100%	100%
BF	100%	95%	100%	91%	90%	88%	88%	90%	87%
OF	100%	100%	99%	90%	84%	85%	88%	84%	82%
IF	100%	100%	100%	98%	100%	100%	89%	90%	90%
ACA	100%	98.75%	99.75%	94.75%	93.5%	93.25%	91.25%	91%	89.75%

Table 5.5. The accuracy of the single faults FEDI when the torque load is 3 hp.

Algorithms	**AFSMO (Proposed Method)**			**ASMO**			**SMO**		
Crack Diameters (in)	0.007	0.014	0.021	0.007	0.014	0.021	0.007	0.014	0.021
Normal	100%	100%	100%	100%	100%	100%	100%	100%	100%
BF	100%	100%	100%	92%	86%	88%	85%	85%	85%
OF	100%	100%	100%	86%	87%	90%	80%	87%	89%
IF	100%	100%	100%	94%	96%	96%	87%	93%	90%
ACA	100%	100%	100%	93%	92.25%	93.5%	88%	91.25%	91%

The experimental results demonstrated in Tables 5.2–5.5 show that the proposed methodology based on the AFSMO, and DT for fault identification of the REBs clearly outperforms the state-of-the-art techniques used for comparison in this chapter for all the available fault types with various fault severity degrees (i.e., crack sizes). Despite the advantages of the proposed methodology, the significant drop in classification accuracy can be observed for OR Fault under a 0 hp load with a crack of size 0.007 inches—around 84% (Table 5.2). This performance drop can be explained as follows. During the analysis of this behavior, it was discovered that the CWRU signals acquired under the conditions mentioned above for the OR Fault and IR Fault overlap significantly. Since the proposed and referenced methodologies create the model of the system being investigated based on the actual data collected from the testbed, they tend to transfer some of the uncertainty conditions presented in the original data into the created model. Because of this overlapping behavior appearing in the originally collected data, the residual signals provided by the proposed methodology and energy values extracted to characterize the windows of these residuals also overlap each other. However, the proposed technique allowed for the improvement of fault identification for the ball and IR faults compared to the counterparts used in this paper. Thus, even with the significant accuracy decrease for the OR faulty condition, it is clear that the proposed methodology demonstrates better classification performance in terms of the ACA.

In addition, based on Table 2.2 we re-configured the available CWRU dataset and created three custom load-variant datasets to validate the robustness of the proposed fault identification technique under changing load conditions. In more detail, each of the three new datasets corresponded to three different sizes of the crack (i.e., 0.007, 0.014, and 0.021 inches in diameter), which contains $N_f \times N_{load} \times N_w$ data instances, where N_f is the number of fault conditions presented in the available CWRU dataset, N_{load} is the number of load levels, and N_w is the number of windows cut from the residual signals delivered by the AFSMO. The results obtained during this experiment are presented in Table 5.6.

The results presented in this table allow us to conclude that the proposed method is highly robust to the changing experimental conditions, such as torque loads and rotating speeds. The proposed approach outperformed its counterparts with the lowest average

classification accuracy of 93.8%, achieved for the crack with a diameter of 0.007 inches under different load level conditions in this case study.

Table 5.6. The accuracy of the single faults FEDI for the custom load-variant datasets.

Algorithms	AFSMO (Proposed Method)			ASMO			SMO		
Crack Diameters (in)	0.007	0.014	0.021	0.007	0.014	0.021	0.007	0.014	0.021
Normal	100%	100%	100%	100%	100%	100%	99%	99%	100%
BF	100%	99%	100%	95%	95%	95%	89%	88%	91%
OF	75%	99%	95%	81%	90%	92%	75%	79%	84%
IF	100%	99%	93%	93%	96%	91%	90%	91%	94%
ACA	93.8%	99.1%	97%	92.3%	95.25%	94.5%	88.3%	89.3%	92.3%

5.5.2. Multiple Type Fault Detection and Identification Provided by SHSE Lab Dataset

To validate the efficacy of the proposed method (AFSMO), ASMO, and SMO approaches for multiple types fault diagnosis, we test it with benchmark Smart HSE Lab (SHSE) bearing datasets as described in Section 4.4.2. Tables 5.7–5.10 illustrate the accuracy of fault diagnosis using the proposed technique (AFSMO) ASMO, and SMO approaches for the normal condition, faulty ball (Ball) state, inner (IR) fault, outer (OR) fault, inner-outer (IR-OR) fault, inner-ball (IR-Ball) fault, outer-ball (OR-Ball) fault, and inner-outer-ball (IR-OR-Ball) fault. The diagnostic accuracy is reported as a percentage of correct fault identification in all data.

Table 5.7. The accuracy of the multiple types FEDI to test the crack-variant dataset when the torque speed is 300 RPM

Algorithms	AFSMO (Proposed Method)		ASMO		SMO	
Crack Diameters (mm)	3	6	3	6	3	6
Normal Stat	100%	100%	100%	100%	88%	90%
IR Fault	100%	100%	94%	94%	80%	80%
OR Fault	100%	98%	95%	96%	74%	75%
Ball Fault	98%	99%	94%	94%	78%	79%
IR-Ball Fault	98%	98%	95%	96%	79%	80%
OR-Ball Fault	98%	98%	96%	96%	80%	83%
IR-OR Fault	99%	98%	94%	95%	80%	83%
IR-OR-Ball Fault	98%	98%	96%	96%	82%	82%
ACA%	98.88	98.63	95.5	95.88	80.13	81.5

Regarding theses tables, the average rate of fault identification is 99.12% for the proposed method (AFSMO), 96.44% for the ASMO, and 81.9% for the SMO. The proposed method fault diagnosis outperforms the ASMO, yielding an average performance

improvement of 3.63%, and 2.47% for 3 mm and 6 mm cracks, respectively. In addition, the proposed method fault diagnosis outperforms the SMO, yielding an average performance improvement of 17.69%, and 16.75% for 3 mm and 6 mm cracks, respectively. Overall, the proposed method fault diagnosis efficiently identifies single and composite faults in the bearing.

Table 5.8. The accuracy of the multiple types FEDI to test the crack-variant dataset when the torque speed is 400 RPM

Algorithms	**AFSMO (Proposed Method)**		**ASMO**		**SMO**	
Crack Diameters (mm)	3	6	3	6	3	6
Normal Stat	100%	100%	100%	100%	90%	90%
IR Fault	100%	100%	95%	94%	82%	82%
OR Fault	100%	99%	95%	97%	78%	79%
Ball Fault	98%	98%	95%	95%	78%	79%
IR-Ball Fault	100%	100%	97%	96%	78%	81%
OR-Ball Fault	98%	99%	95%	96%	81%	82%
IR-OR Fault	99%	99%	96%	97%	81%	84%
IR-OR-Ball Fault	97%	98%	96%	97%	82%	83%
ACA%	99	99.13	96.13	96.5	81.25	82.5

Table 5.9. The accuracy of the multiple types FEDI to test the crack-variant dataset when the torque speed is 450 RPM

Algorithms	**AFSMO (Proposed Method)**		**ASMO**		**SMO**	
Crack Diameters (mm)	3	6	3	6	3	6
Normal Stat	100%	100%	100%	100%	90%	90%
IR Fault	100%	100%	95%	96%	83%	83%
OR Fault	98%	100%	96%	97%	79%	80%
Ball Fault	100%	99%	95%	96%	78%	79%
IR-Ball Fault	100%	100%	98%	97%	77%	80%
OR-Ball Fault	97%	99%	96%	96%	82%	82%
IR-OR Fault	99%	99%	95%	97%	83%	84%
IR-OR-Ball Fault	99%	99%	96%	97%	81%	82%
ACA%	99.13	99.5	96.38	97	81.63	82.5

Table 5.10. The accuracy of the multiple types FEDI to test the crack-variant dataset when the torque speed is 500 RPM

Algorithms	**AFSMO (Proposed Method)**		**ASMO**		**SMO**	
Crack Diameters (mm)	3	6	3	6	3	6
Normal Stat	100%	100%	100%	100%	90%	90%
IR Fault	100%	100%	95%	96%	82%	83%
OR Fault	99%	100%	95%	97%	82%	80%
Ball Fault	98%	99%	97%	97%	79%	81%
IR-Ball Fault	100%	100%	98%	97%	79%	80%
OR-Ball Fault	99%	99%	97%	96%	83%	83%
IR-OR Fault	99%	98%	96%	98%	83%	84%
IR-OR-Ball Fault	99%	99%	96%	98%	82%	84%
ACA%	99.25	99.38	96.75	97.38	82.5	83.13

In addition, the bearing data are collected under four different motor speeds, as shown in Table 4.1. The proposed method (AFSMO) is robust even if the motor speed changes. Table 5.11 presents the fault diagnosis accuracy for variable motor speeds (e.g., 300 RPM, 400 RPM, 450 RPM, and 500 RPM) in two types of crack sizes (e.g., 3 mm and 6 mm), various conditions (normal, ball fault, inner fault, outer fault, inner-outer fault, inner-ball fault, outer-ball fault, and inner-outer-ball fault) of the proposed method, ASMO, and SMO.

Table 5.11. The accuracy of the multiple types FEDI to test the motor speed-variant dataset.

Algorithms	**AFSMO (Proposed Method)**		**ASMO**		**SMO**	
Crack Diameters (mm)	3	6	3	6	3	6
Normal Stat	100%	100%	100%	100%	87%	87%
IR Fault	97%	97%	93%	93%	80%	83%
OR Fault	98%	99%	94%	95%	82%	83%
Ball Fault	95%	96%	96%	97%	78%	81%
3IR-Ball Fault	100%	100%	96%	97%	76%	80%
OR-Ball Fault	98%	98%	96%	97%	80%	81%
IR-OR Fault	98%	98%	92%	92%	80%	81%
IR-OR-Ball Fault	97%	97%	91%	90%	83%	84%
ACA%	97.88	98.13	94.75	95.13	80.75	82.5

Regarding Table 5.11, the proposed method (AFSMO) in the presence of the motor speed-variant dataset outperforms the ASMO technique yielding performance improvements of 3.13% and 3% for two fault severity levels characterized by crack sizes of 3 and 6 mm, respectively. Moreover, the proposed method in the presence of the motor speed-variant dataset outperforms the SMO technique yielding performance improvements of 17.13% and 15.63% for two fault severity levels characterized by crack sizes of 3 and 6 mm, respectively.

5.6 Conclusions

This chapter proposed a hybrid technique using decision tree-based advanced fuzzy sliding mode observer to perform reliable fault diagnosis in a rotating machine. Rolling element bearing (REB) presents a nonlinear system that can now be analyzed in uncertain conditions. To improve the system modeling accuracy, the fuzzy ARX-Laguerre technique is presented in the first step. In the second step, the sliding mode observer (SMO) is designed for the signal estimation. To reduce the chattering and increase the estimation accuracy of the sliding mode observer, in the third step, the advanced fuzzy sliding mode observer (AFSMO) is considered. To increase the fault estimation accuracy, the T-S fuzzy algorithm is applied to

the AFSMO in the fourth step. To perform fault detection and identification in the presence of uncertainties, decision trees govern the AFSMO to find the exact solution for fault diagnosis under various crack types and motor speed conditions. The effectiveness of the proposed algorithm is validated using two available vibration datasets: CWRU vibration dataset for single fault diagnosis and SHSE Lab vibration dataset for multiple fault diagnosis. The proposed decision tree-based AFSMO outperformed the ASMO and SMO in terms of classification accuracy. As a result, in a single fault diagnosis, the proposed method improved the average fault identification performance by about 4.5%, 5.3%, and 4.8% compared with the ASMO for the crack sizes of 0.007, 0.014, and 0.021 inches, respectively. In addition, the AFSMO improved the average performance of fault identification by about 8.8%, 7.6%, and 8.1% compared with the SMO for the crack sizes of 0.007, 0.014, and 0.021 inches, respectively. Moreover, the average rate of fault identification is 99.12% for the proposed method (AFSMO), 90.07% for the ASMO, and 81.9% for the SMO for multiple types fault diagnosis. The proposed technique demonstrated its robustness while performing the tasks of REB fault detection and identification under changing operating conditions, such as variable load levels and variable rotating speeds. Based on the results we can conclude that the proposed methodology is highly efficient in diagnosing bearing faults. However, to ensure the robustness and efficacy in the industrial environment, it is crucial to reduce the error of the system modeling. To address this issue, we will focus on developing an adaptive algorithm in our future work. Moreover, we will focus on exploring and evaluating the capabilities of applying the proposed methodology in conjunction with various vibration health indicators for a task of REB fault prognosis on run-to-failure experimental data.

Part III

Summary and Future Work

Chapter 6

Summary of Contributions and Future Work

6.1 Introduction

The main contributions of this dissertation and future aspects of the current work are given in this chapter. Section 6.2 highlights the main contributions of this thesis whereas future research direction is given in section 6.3.

6.2 Summary of Contributions

The dissertation has focused on the hybrid fault diagnosis of rotating machinery. It covers the fault diagnosis of bearing based on two different algorithms, i.e., extended-state observation fault diagnosis of bearing, and fuzzy extended-state observation fault diagnosis of bearing. Chapters 2 to 4 are about the schemes and investigations into extended-state observers for fault diagnosis of bearings while chapter 5 focuses on fault diagnosis of bearing based on fuzzy extended-state sliding mode observer, respectively. The contributions of this dissertation to fault diagnosis of bearings are given below:

Robust and reliable fault diagnosis of rotary machine bearing based on hybrid approach using SVM-based higher-order super-twisting (extended-state) sliding mode observation technique was presented in Chapter 2. In the first step, the rotary machine bearing was modeled based on five degrees of freedom mathematical vibration system modeling. Next, the sliding mode observation technique was designed for signal estimation. The sliding mode observer is reliable and robust, but is prone to high-frequency oscillations (chattering) and accuracy, especially in faulty and uncertain conditions. A high-order sliding mode observer was developed to reduce the chattering phenomenon. Besides, to increase the fault estimation accuracy, a high-order super-twisting (extended-state) sliding mode observer was proposed. Once the residual signal is obtained based on the difference between the original signal and estimated signal, this signal can be successfully used to perform the decision making. In addition, the support vector machine (SVM) is used for fault detection and diagnosis. The effectiveness of the proposed technique is evaluated using a vibration dataset

provided by Case Western Reserve University, which consists of vibration acceleration signals recorded for rotary machine bearing with the inner, outer, ball, and no faults, i.e., normal. Experimental results indicate that the average of fault diagnosis accuracy for the proposed technique to test the crack-variant dataset is, yielding 96.2%, 94.9%, and 96.5% for three levels of crack severity of 0.007, 0.014, and 0.021 inches, respectively. Moreover, the average of fault diagnosis accuracy for the proposed technique to validate the robustness based on the torque/speed-variant dataset are, yielding 94.5%, 94.5%, and 94.75% for three levels of crack severity of 0.007, 0.014, and 0.021 inches, respectively.

To eliminate the effect of chattering phenomenon especially in faulty and uncertain conditions the next hybrid technique using an SVM-based extended variable structure (extended-state) feedback linearization observer for fault diagnosis of rotary machine bearing was presented in Chapter 3. After modeling the rotary machine bearing based on five degrees of freedom mathematical vibration system modeling, a reliable technique based on the feedback linearization observer was developed for signal estimation. The feedback linearization observer is stable and chattering-free; however, this technique suffers from a lack of robustness. The proposed variable structure technique was used to improve the robustness of the fault estimation while reducing the effect of uncertainties in the feedback linearization observer. After improving the accuracy and robustness of bearing signal estimation based on the variable structure (extended-state) feedback linearization observer, the residual signal is obtained based on the difference between the original signal and estimated signal. Once the residual signal is obtained, the support vector machine (SVM) technique is used for fault detection and diagnosis. The effectiveness of the proposed extended variable structure feedback linearization observer procedure for the identification of the outer, inner, and ball faults was tested using the Case Western University vibration dataset. Experimental results show that the average of fault diagnosis accuracy for the proposed extended variable structure feedback linearization observer to validate the crack-variant dataset are, yielding 96%, 95.7%, and 96.7% for three levels of crack severity of 0.007, 0.014, and 0.021 inches, respectively. In addition, the average of fault diagnosis accuracy for the recommended procedure to validate the robustness based on the torque/speed-variant dataset are, yielding 93.25%, 93.75%, and 94.75% for three levels of crack severity of 0.007, 0.014, and 0.021 inches, respectively.

Apart from the reliability and accuracy of mathematical-based system modeling, this technique has drawbacks in uncertain and unknown conditions. The main limitation in Chapters 2 and 3 was mathematical-based bearing modeling. To address this issue, in Chapter 4, the system identification techniques based on Auto-Regressive with eXogenous input (ARX)-Laguerre technique was implemented. After modeling the rotary machine bearing based on the ARX-Laguerre technique, a reliable technique based on the ARX-Laguerre Proportional-Integral (PI) observer was developed for signal estimation. To increase the robustness and accuracy of signal estimation for fault diagnosis of bearing, the sliding mode (extended-state) ARX-Laguerre PI observer was developed. Once the residual signal is obtained based on the difference between the original signal and estimated signal obtained by the sliding mode (extended-state) ARX-Laguerre PI observer, this signal can be successfully used to perform the decision making. In addition, the support vector machine (SVM) is used for fault detection and diagnosis. The effectiveness of the hybrid approach using SVM-based sliding mode (extended-state) ARX-Laguerre PI observer was evaluated using two different datasets: a) the Case Western Reverse University (CWRU) bearing dataset and b) the Smart HSE (SHSE) Lab bearing dataset to validate the single and multiple-types of fault diagnosis, respectively. Experimental results for CWRU bearing dataset show that the average of fault diagnosis accuracy for the proposed sliding mode extended-state ARX-Laguerre PI observer to validate the crack-variant dataset is, yielding 93.7%, 94%, and 95.2% for three fault severity levels characterized by crack sizes of 0.007, 0.014, and 0.021 inches, respectively. Besides, the average of fault diagnosis accuracy for the proposed method to validate the robustness based on the torque/speed-variant dataset are, yielding 92%, 93%, and 93.25% for three levels of crack severity of 0.007, 0.014, and 0.021 inches, respectively. Moreover, results for the second scenario (SHSE Lab bearing dataset) illustrate that the average fault diagnosis accuracy for the proposed technique to validate the crack-variant dataset is, yielding 95.3% and 95.7% for two fault severity levels characterized by crack sizes of 3 and 6 millimeters, respectively. In addition, to validate the robustness based on the torque/speed-variant dataset the average of fault diagnosis accuracy for the proposed method are, yielding 94.8% and 95.3% for two fault severity levels characterized by crack sizes of 3 and 6 millimeters, respectively.

The second part of the dissertation contributes to the literature on fuzzy extended-state observation fault diagnosis of rotary machine bearing as below:

To reduce/eliminate the effect of the chattering phenomenon, improve the signal estimation accuracy, and increase the system modeling accuracy especially in the uncertain and unknown conditions the last hybrid technique using machine learning-based fuzzy ARX-Laguerre fuzzy higher-order super-twisting sliding mode observer for fault diagnosis of rotary machine bearing was presented in Chapter 5. The complexity of the system's dynamic behavior and uncertainty result in substantial challenges for fault estimation, detection, and identification in rotating machines. First, an ARX-Laguerre algorithm is presented to model the bearing in the presence of uncertainty. In addition, a fuzzy algorithm is applied to the ARX-Laguerre technique to increase the system's modeling accuracy. Next, the conventional sliding mode observer is applied to resolve the problems of signal estimation in a complex system with a high degree of uncertainty, such as rotating machinery. To address the problem of the chattering phenomenon that is inherent in the conventional sliding mode observer, the higher-order super-twisting (extended-state) technique is introduced in this chapter. In addition, the fuzzy method is applied to the higher-order super-twisting (extended-state) sliding mode observer to improve the accuracy of fault estimation in uncertain conditions. As a result, the higher-order super-twisting (extended-state) fuzzy sliding mode observer adaptively improves the reliability, robustness, and estimation accuracy of rolling-element bearing signal estimation. Then, the residual signal delivered by the proposed methodology is split in the windows and each window is characterized by a numerical parameter. Finally, a machine learning technique, called a decision tree, adaptively derives the threshold values that are used for problems of fault detection and fault identification in this chapter. The effectiveness of the machine-learning-based advanced fuzzy sliding mode observer was evaluated using two diverse datasets: a) the Case Western Reverse University (CWRU) bearing dataset and b) the Smart HSE (SHSE) Lab bearing dataset to validate the single and multiple-types of fault diagnosis, respectively. Experimental results for CWRU bearing dataset show that the average of fault diagnosis accuracy for the machine-learning-based advanced fuzzy sliding mode observer to validate the crack-variant dataset are, yielding 98.8%, 99.1%, and 99.8% for three fault severity levels characterized by crack sizes of 0.007,

0.014, and 0.021 inches, respectively. Besides, the average of fault diagnosis accuracy for the machine-learning-based advanced fuzzy sliding mode observer to validate the robustness based on the torque/speed-variant dataset are, yielding 93.8%, 99.1%, and 97% for three levels of crack severity of 0.007, 0.014, and 0.021 inches, respectively. Moreover, results for the next scenario (SHSE Lab bearing dataset) illustrate that the average of fault diagnosis accuracy for the proposed technique to validate the crack-variant dataset are, yielding 99.1% and 99.2% for two fault severity levels characterized by crack sizes of 3 and 6 millimeters, respectively. In addition, to validate the robustness based on the torque/speed-variant dataset the average of fault diagnosis accuracy for the proposed method are, yielding 97.9% and 98.1% for two fault severity levels characterized by crack sizes of 3 and 6 millimeters, respectively. Therefore, the machine learning-based advanced fuzzy sliding mode observation methodology significantly improves the reliability and accuracy of the fault estimation, detection, and identification of rolling element bearing faults under variable crack sizes and load conditions.

6.3 Future Work

As explained in the previous section the primary focus of this dissertation is the fault diagnosis of rotating machinery. Chapters 2 to 5 elaborated on the contributions and the investigations carried out on the topics. Though the research on these areas was a detailed one there are other topics and techniques which are needed to be investigated for exhaustive details. These topics can be classified into three main divisions: fault diagnosis, fault-tolerant control, and fault prognosis. Some of these future topics are presented below:

Fault diagnosis: In fact, the real system's faults are complex, non-stationary, and nonlinear which occurs in various components. Extracting features for diagnosing these faults at their early stages requires complex and computationally expensive signal processing approaches that are not always suitable for industrial applications. Therefore, hybrid approaches that use a combination of deep learning/machine learning and modern control algorithms (e.g., linear observers and nonlinear observers) will be introduced for diagnosing the system's faults of various intensities. In future work, I would like to verify the applicability

of these techniques to solve the issues of fault diagnosis in different systems, such as bearing, gearbox, and pipeline.

Fault prognostics: Prognosis is the process of remaining useful life (RUL) estimation. The RUL estimation has several challenges, such as the machine health degradation model and abnormal conditions threshold to define end-of-life. Various techniques can be used for degradation modeling that can be divided into model-based techniques and data-driven approaches. The fusion of these techniques could be the ultimate vision of fault prognostics capabilities that could able to utilize the advantages of both techniques to design a hybrid approach for the mission-critical solution. So, hybrid approaches that use a combination of data-driven and observation algorithms will be introduced for RUL estimation of various intensities. In future work, I would like to verify the applicability of these techniques to solve the issues of fault prognostics in various systems.

Fault-tolerant control: Numerous procedures have been introduced for fault-tolerant control. These strategies are classified into two groups: a) active fault-tolerant control and b) passive fault-tolerant control. The active fault-tolerant control includes two steps. First, the fault is detected and identified then, the effect of the fault is reduced based on various control algorithms. In passive fault-tolerant control, the impact of the fault is decreased directly based on control techniques. In the future investigation, active fault-tolerant control will be adopted for fault-tolerant control in various industrial applications such as motors, gearboxes, and robots. The active fault-tolerant control is classified into two main groups: a) linear and b) nonlinear. Linear procedures lead to unsatisfactory fault-tolerant control due to nonlinear parameters, and uncertain conditions. To address these issues, the use of a nonlinear fault-tolerant controller will be suggested. Various nonlinear active fault-tolerant controllers have been presented in the literature, including model-based, artificial intelligence-based and hybrid. The model-based active fault-tolerant controllers have numerous advantages, such as stability, robustness, and reliability, but its performance under unknown conditions is the main argument against its use. To address this weakness, artificial intelligence-based and hybrid controllers can be used. However, artificial intelligent active fault-tolerant controllers procedures have many issues concerning robustness and reliability. To address the faults in model-based and artificial intelligence, a hybrid fault-tolerant controller based on the

combination of data-driven techniques, observation algorithms, and control methods will be developed in the future.

Publications

International Journal Papers

1. **Farzin Piltan**; Kim, J.-M. Nonlinear Extended-state ARX-Laguerre PI Observer Fault Diagnosis of Bearings. *Applied Sciences.* **2020**, *10*, 3587.

2. **Farzin Piltan**; Prosvirin, A.E.; Sohaib, M.; Saldivar, B.; Kim, J.-M. An SVM-Based Neural Adaptive Variable Structure Observer for Fault Diagnosis and Fault-Tolerant Control of a Robot Manipulator. *Applied Sciences.* **2020**, *10*, 1344.

3. **Farzin Piltan;** Jong-Myon Kim. Advanced Fuzzy-Based Leak Detection and Size Estimation for Pipelines. *Journal of Intelligent and Fuzzy Systems.* **2020,** 38, 947-961**.**

4. **Farzin Piltan,** Prosvirin, A. E; Jeong, I; Im, K; and Kim, J. M. Rolling Element Bearing Fault Diagnosis Using Advanced Machine Learning-Based Observer. *Applied Sciences.* **2019**, 9(24), 5404.

5. **Farzin Piltan**; Kim, C.-H.; Kim, J.-M. Adaptive Fuzzy-Based Fault-Tolerant Control of a Continuum Robotic System for Maxillary Sinus Surgery. *Applied Sciences.* **2019**, *9 (12)*, 2490.

6. **Farzin Piltan,** Shahnaz TayebiHaghighi, Amirzubir Sahamijoo, Hossein Rashidi Bod, Somayeh Jowkar, Jong-Myon Kim. Adaptive Finite Time Convergence Fuzzy ARX-Laguerre System Estimation. *International Journal of Intelligent Systems and Applications*. **2019,** 11(5), 27-35.

7. **Farzin Piltan**; Kim, C.-H.; Kim, J.-M. Advanced Adaptive Fault Diagnosis and Tolerant Control for Robot Manipulators. *Energies.* **2019**, *12*, 1281.

8. **Farzin Piltan,** Shahnaz TayebiHaghighi, Somayeh Jowkar, Hossein Rashidi Bod, Amirzubir Sahamijoo, Jeong-Seok Heo. A Novel Intelligent ARX-Laguerre Distillation Column Estimation Technique. *International Journal of Intelligent Systems and Applications*. **2019,** 11(4), 52-60.

9. **Farzin Piltan**, and Jong-Myon Kim. Nonlinear Extended-state ARX-Laguerre PI Observer Fault Diagnosis of Bearings. *Applied Sciences.* **2019,** 9(5), 888.

10. **Farzin Piltan**, and Jong-Myon Kim. Bearing Fault Diagnosis Using an Extended

Variable Structure Feedback Linearization Observer. *Sensors.* **2018,** 18(12), 4359.

11. **Farzin Piltan**, Jong-Myon Kim. Bearing fault Diagnosis by a Robust Higher-order Super-Twisting Sliding Mode Observer. *Sensors.* **2018**, 18(4), 1128.

12. Niloofar Mirzavand, **Farzin Piltan**, Jong-Myon Kim. Intelligent Control of an Uncertain Distillation Column Using a Multivariable Filter Decoupling-based PID Like Fuzzy Controller. *International Journal of Control and Automation*. **2018,** 11(1), 99-112.

13. Shahnaz Tayebihaghighi, **Farzin Piltan**, Jong-Myon Kim. Control of Uncertain Robot Manipulator Using an Observation Based Modified Fuzzy Sliding Mode Controller. *International Journal of Intelligent Systems and Applications***. 2018**, 10(3), 41-49**.**

14. Shahnaz Tayebihaghighi, **Farzin Piltan**, Jong-Myon Kim. Robust Composite High-Order Super-Twisting Sliding Mode Control of Robot Manipulators. *Robotics.* **2018**, 7(13).

15. **Farzin Piltan**, Jong-Myon Kim. FPGA-Based ARX-Laguerre PIO Fault Diagnosis in Robot Manipulator. *Advances in Robotics Research*. **2018,** 2(1), 99-112.

Journal Papers Under-review

1. Prosvirin, A.E.; **Farzin Piltan**; Kim, J.-M. Hybrid Rub-impact Fault Diagnosis Using a Deep Learning-based Observation Technique. (*IEEE Transactions on Neural Networks and Learning Systems*).

2. **Farzin Piltan;** Prosvirin, A.E.; Jong-Myon Kim. Robot Manipulator Active Fault-Tolerant Control Using Machine Learning-based Automated Robust Hybrid Observer. (*Journal of Intelligent and Fuzzy Systems*)**.**

3. **Farzin Piltan;** Jong-Myon Kim. Adaptive Fuzzy Orthonormal Regressive Fuzzy-Robust PI Observer. (*Applied Sciences*)**.**

Book Chapters

1. **Farzin Piltan**, and Jong-Myon Kim. "Machine Learning-Based Robust Feedback Observer for Fault Diagnosis in Bearings." Springer, **2021**.

2. **Farzin Piltan**, and Jong-Myon Kim. "SVM-Based Hybrid Robust PIO Fault Diagnosis for Bearings." Springer, **2021**.

3. **Farzin Piltan**, and Jong-Myon Kim. "Pipeline Leak Detection and Estimation Using Fuzzy-Based PI Observer." Springer, **2020,** pp. 1122-1129. **(Best Research Award).**

4. **Farzin Piltan,** and Jong-Myon Kim. "Advanced Fuzzy Observer-Based Fault Identification for Robot Manipulators." Springer, **2020,** pp. 141-148. **(Best research award).**

5. **Farzin Piltan**, Manjurul Islam, and Jong-Myon Kim. "Input-Output Fault Diagnosis in Robot Manipulator Using Fuzzy LMI-Tuned PI Feedback Linearization Observer Based on Nonlinear Intelligent ARX Model." Springer, **2019,** pp. 305-315.

6. **Farzin Piltan**, and Jong-Myon Kim. "Fault Diagnosis of a Wireless Sensor Network Using a Hybrid Method." Springer, **2019,** pp. 133-142.

7. **Farzin Piltan**, Muhammad Sohaib, and Jong-Myon Kim. "Fault Diagnosis of a Robot Manipulator Based on an ARX-Laguerre Fuzzy PID Observer." Springer, **2019,** pp. 393-407.

International Conferences

1. **Farzin Piltan**, and Jong-Myon Kim. "Machine Learning-Based Robust Feedback Observer for Fault Diagnosis in Bearings." *International Conference on Intelligent and Fuzzy Systems*, Izmir, Turkey, **2020**.

2. **Farzin Piltan**, and Jong-Myon Kim. "SVM-Based Hybrid Robust PIO Fault Diagnosis for Bearings." *International Conference on Intelligent and Fuzzy Systems*, Izmir, Turkey, **2020**.

3. **Farzin Piltan**, and Jong-Myon Kim. "Pipeline Leak Detection and Estimation Using Fuzzy-Based PI Observer." *International Conference on Intelligent and Fuzzy Systems*, Istanbul, Turkey, **2019**. **(Best Research Award).**

4. **Farzin Piltan,** and Jong-Myon Kim. "Advanced Fuzzy Observer-Based Fault Identification for Robot Manipulators." *International Conference on Intelligent and Fuzzy Systems*, Istanbul, Turkey, **2019. (Best research award).**

5. **Farzin Piltan**, and Jong-Myon Kim. "Fault Diagnosis of a Wireless Sensor Network Using a Hybrid Method." *International Conference on Parallel and Distributed Computing: Applications and Technologies*, Jeju, South Korea, **2018**.

6. **Farzin Piltan**, Manjurul Islam, and Jong-Myon Kim. "Input-Output Fault Diagnosis in Robot Manipulator Using Fuzzy LMI-Tuned PI Feedback Linearization Observer Based on Nonlinear Intelligent ARX Model." *International Conference on Computer Communication and Computational Sciences*, Phuket, Thailand, **2017**.

7. **Farzin Piltan**, Muhammad Sohaib, and Jong-Myon Kim. "Fault Diagnosis of a Robot Manipulator Based on an ARX-Laguerre Fuzzy PID Observer." *International Conference on Robot Intelligence Technology and Applications*, Daejeon, South Korea, **2017**.

Domestic Conferences

1. **Farzin Piltan,** Jong-Myon Kim**.** "Prevent the Risk of Cancer Progression Based on Air Pollution Control." *The Engineering and Art Society in Korea*, University of Ulsan, South Korea, **2019**.

2. **Farzin Piltan,** Jong-Myon Kim**.** " PI Fuzzy-Based Fault Estimation Design Approach for Leak Detection in Pipeline." *The Engineering and Art Society in Korea*, University of Ulsan, South Korea, **2018**. **(Best paper award)**

3. **Farzin Piltan,** Kichang Im, and Jong-Myon Kim**.** " An ARX-ANFIS Sliding Mode Control Based Industrial Motor Fault Tolerant." *The Engineering and Art Society in Korea*, University of Ulsan, South Korea, **2017**. **(Best paper award)**

References

[1] M. Höök and X. Tang, "Depletion of fossil fuels and anthropogenic climate change—A review," *Energy policy*, vol. 52, pp. 797-809, 2013.

[2] N. Abas, A. Kalair, and N. Khan, "Review of fossil fuels and future energy technologies," *Futures*, vol. 69, pp. 31-49, 2015.

[3] M. Asif and T. Muneer, "Energy supply, its demand and security issues for developed and emerging economies," *Renewable and Sustainable Energy Reviews*, vol. 11, no. 7, pp. 1388-1413, 2007.

[4] F. Duan, "Induction motor parameters estimation and faults diagnosis using optimisation algorithms," 2015.

[5] Z. Gao, C. Cecati, and S. X. Ding, "A survey of fault diagnosis and fault-tolerant techniques—Part I: Fault diagnosis with model-based and signal-based approaches," *IEEE Transactions on Industrial Electronics*, vol. 62, no. 6, pp. 3757-3767, 2015.

[6] C. Cecati, "A survey of fault diagnosis and fault-tolerant techniques—Part II: Fault diagnosis with knowledge-based and hybrid/active approaches," 2015.

[7] M. R. Mehrjou, N. Mariun, M. H. Marhaban, and N. Misron, "Rotor fault condition monitoring techniques for squirrel-cage induction machine—A review," *Mechanical Systems and Signal Processing*, vol. 25, no. 8, pp. 2827-2848, 2011.

[8] F. Piltan and J.-M. Kim, "Bearing fault diagnosis by a robust higher-order super-twisting sliding mode observer," *Sensors*, vol. 18, no. 4, p. 1128, 2018.

[9] F. Piltan and J.-M. Kim, "Bearing fault diagnosis using an extended variable structure feedback linearization observer," *Sensors*, vol. 18, no. 12, p. 4359, 2018.

[10] F. Piltan, A. E. Prosvirin, I. Jeong, K. Im, and J.-M. Kim, "Rolling-Element Bearing Fault Diagnosis Using Advanced Machine Learning-Based Observer," *Applied Sciences*, vol. 9, no. 24, p. 5404, 2019.

[11] F. Piltan and J.-M. Kim, "Nonlinear Extended-state ARX-Laguerre PI Observer Fault Diagnosis of Bearings," *Applied Sciences*, vol. 9, no. 5, p. 888, 2019.

[12] T. Najeh, C. B. Njima, T. Garna, and J. Ragot, "Input fault detection and estimation using PI observer based on the ARX-Laguerre model," *The International Journal of Advanced Manufacturing Technology*, vol. 90, no. 5-8, pp. 1317-1336, 2017.

[13] F. Piltan, J.-M. J. J. o. I. Kim, and F. Systems, "Advanced fuzzy-based leak detection and size estimation for pipelines," vol. 38, no. 1, pp. 947-961, 2020.

[14] F. Piltan, A. E. Prosvirin, M. Sohaib, B. Saldivar, and J.-M. Kim, "An SVM-Based Neural Adaptive Variable Structure Observer for Fault Diagnosis and Fault-Tolerant Control of a Robot Manipulator," *Applied Sciences*, vol. 10, no. 4, p. 1344, 2020.

[15] M. L. Adams, "Analysis of rolling element bearing faults in rotating machinery: experiments, modeling, fault detection and diagnosis," Case Western Reserve University, 2001.

[16] S. Agrawal, S. R. Mohanty, and V. Agarwal, "Bearing fault detection using Hilbert and high frequency resolution techniques," *IETE Journal of Research*, vol. 61, no. 2, pp. 99-108, 2015.

[17] X. Gong and W. Qiao, "Bearing fault diagnosis for direct-drive wind turbines via current-demodulated signals," *IEEE Transactions on Industrial Electronics*, vol. 60, no. 8, pp. 3419-3428, 2013.

[18] H. Chen and S. Lu, "Fault diagnosis digital method for power transistors in power converters of switched reluctance motors," *IEEE Transactions on Industrial Electronics*, vol. 60, no. 2, pp. 749-763, 2012.

[19] V. Climente-Alarcon, J. A. Antonino-Daviu, M. Riera-Guasp, and M. Vlcek, "Induction motor diagnosis by advanced notch FIR filters and the Wigner–Ville distribution," *IEEE Transactions on Industrial Electronics*, vol. 61, no. 8, pp. 4217-4227, 2013.

[20] N. M. Freire, J. O. Estima, and A. J. M. Cardoso, "Open-circuit fault diagnosis in PMSG drives for wind turbine applications," *IEEE Transactions on Industrial electronics*, vol. 60, no. 9, pp. 3957-3967, 2012.

[21] L. Xiang and X. Yan, "A self-adaptive time-frequency analysis method based on local mean decomposition and its application in defect diagnosis," *Journal of Vibration and Control*, vol. 22, no. 4, pp. 1049-1061, 2016.

[22] G. M. Joksimović, J. Riger, T. M. Wolbank, N. Perić, and M. Vašak, "Stator-current spectrum signature of healthy cage rotor induction machines," *IEEE Transactions on Industrial Electronics*, vol. 60, no. 9, pp. 4025-4033, 2012.

[23] H. Badihi, Y. Zhang, and H. Hong, "Fault-tolerant cooperative control in an offshore wind farm using model-free and model-based fault detection and diagnosis approaches," *Applied Energy,* vol. 201, pp. 284-307, 2017.

[24] F. Lafont, J.-F. Balmat, N. Pessel, and M. Fliess, "A model-free control strategy for an experimental greenhouse with an application to fault accommodation," *Computers and Electronics in Agriculture,* vol. 110, pp. 139-149, 2015.

[25] F. R. López-Estrada, J.-C. Ponsart, D. Theilliol, Y. Zhang, and C.-M. Astorga-Zaragoza, "LPV model-based tracking control and robust sensor fault diagnosis for a quadrotor UAV," *Journal of Intelligent & Robotic Systems,* vol. 84, no. 1-4, pp. 163-177, 2016.

[26] D. Stavrou, D. G. Eliades, C. G. Panayiotou, and M. M. Polycarpou, "Fault detection for service mobile robots using model-based method," *Autonomous Robots,* vol. 40, no. 2, pp. 383-394, 2016.

[27] M. Van, P. Franciosa, and D. Ceglarek, "Fault diagnosis and fault-tolerant control of uncertain robot manipulators using high-order sliding mode," *Mathematical Problems in Engineering,* vol. 2016, 2016.

[28] B. M. Ebrahimi, M. J. Roshtkhari, J. Faiz, and S. V. Khatami, "Advanced eccentricity fault recognition in permanent magnet synchronous motors using stator current signature analysis," *IEEE Transactions on Industrial Electronics,* vol. 61, no. 4, pp. 2041-2052, 2013.

[29] E. Khalastchi, M. Kalech, and L. Rokach, "A hybrid approach for improving unsupervised fault detection for robotic systems," *Expert Systems with Applications,* vol. 81, pp. 372-383, 2017.

[30] H.-T. Yau, S.-Y. Wu, C.-L. Chen, and Y.-C. Li, "Fractional-order chaotic self-synchronization-based tracking faults diagnosis of ball bearing systems," *IEEE Transactions on Industrial Electronics,* vol. 63, no. 6, pp. 3824-3833, 2016.

[31] X. Dai, Z. Gao, T. Breikin, and H. Wang, "Disturbance attenuation in fault detection of gas turbine engines: A discrete robust observer design," *IEEE Transactions on Systems, Man, and Cybernetics, Part C (Applications and Reviews),* vol. 39, no. 2, pp. 234-239, 2009.

[32] A. Forrai, "System identification and fault diagnosis of an electromagnetic actuator," *IEEE Transactions on Control Systems Technology,* vol. 25, no. 3, pp. 1028-1035, 2016.

[33] Z. Gao, T. Breikin, and H. Wang, "Discrete-time proportional and integral observer and observer-based controller for systems with both unknown input and output disturbances," *Optimal Control Applications and Methods,* vol. 29, no. 3, pp. 171-189, 2008.

[34] K. Zhang, B. Jiang, V. Cocquempot, and H. Zhang, "A framework of robust fault estimation observer design for continuous-time/discrete-time systems," *Optimal control applications and methods,* vol. 34, no. 4, pp. 442-457, 2013.

[35] Z. Gao and D. W. Ho, "Proportional multiple-integral observer design for descriptor systems with measurement output disturbances," *IEE Proceedings-Control Theory and Applications,* vol. 151, no. 3, pp. 279-288, 2004.

[36] D. Koenig, "Unknown input proportional multiple-integral observer design for linear descriptor systems: application to state and fault estimation," *IEEE Transactions on Automatic control,* vol. 50, no. 2, pp. 212-217, 2005.

[37] Z. Gao, S. X. Ding, and Y. Ma, "Robust fault estimation approach and its application in vehicle lateral dynamic systems," *Optimal Control Applications and Methods,* vol. 28, no. 3, pp. 143-156, 2007.

[38] Z. Gao and H. Wang, "Descriptor observer approaches for multivariable systems with measurement noises and application in fault detection and diagnosis," *Systems & Control Letters,* vol. 55, no. 4, pp. 304-313, 2006.

[39] Z. Gao, X. Shi, and S. X. Ding, "Fuzzy state/disturbance observer design for T–S fuzzy systems with application to sensor fault estimation," *IEEE Transactions on Systems, Man, and Cybernetics, Part B (Cybernetics),* vol. 38, no. 3, pp. 875-880, 2008.

[40] K. Zhang, B. Jiang, and V. Cocquempot, "Adaptive observer-based fast fault estimation," *International Journal of Control, Automation, and Systems,* vol. 6, no. 3, pp. 320-326, 2008.

[41] Q. Zhang and G. Besancon, "An adaptive observer for sensor fault estimation in a class of uniformly observable non-linear systems," *International Journal of Modelling, Identification and Control,* vol. 4, no. 1, pp. 37-43, 2008.

[42] M. Gholizadeh and F. R. Salmasi, "Estimation of state of charge, unknown nonlinearities, and state of health of a lithium-ion battery based on a comprehensive unobservable model," *IEEE Transactions on Industrial Electronics*, vol. 61, no. 3, pp. 1335-1344, 2013.

[43] E. Cruz-Zavala, J. A. Moreno, and L. Fridman, "Uniform second-order sliding mode observer for mechanical systems," in *2010 11th international workshop on variable structure systems (vss)*, 2010, pp. 14-19: IEEE.

[44] M. Van, H.-J. Kang, and Y.-S. Suh, "A novel neural second-order sliding mode observer for robust fault diagnosis in robot manipulators," *International Journal of Precision Engineering and Manufacturing*, vol. 14, no. 3, pp. 397-406, 2013.

[45] H. Alwi and C. Edwards, "Robust fault reconstruction for linear parameter varying systems using sliding mode observers," *International Journal of Robust and Nonlinear Control*, vol. 24, no. 14, pp. 1947-1968, 2014.

[46] X. Han, E. Fridman, and S. K. Spurgeon, "Sampled-data sliding mode observer for robust fault reconstruction: A time-delay approach," *Journal of the Franklin Institute*, vol. 351, no. 4, pp. 2125-2142, 2014.

[47] L. Fridman, A. Levant, and J. Davila, "Observation of linear systems with unknown inputs via high-order sliding-modes," *International Journal of systems science*, vol. 38, no. 10, pp. 773-791, 2007.

[48] M. Van, H.-J. Kang, Y.-S. Suh, and K.-S. Shin, "Output feedback tracking control of uncertain robot manipulators via higher-order sliding-mode observer and fuzzy compensator," *Journal of Mechanical Science and Technology*, vol. 27, no. 8, pp. 2487-2496, 2013.

[49] L. F. Cuesta, L. Fridman, and V. V. Alexandrov, "Position stabilization of a Stewart platform: High-order sliding mode observers based approach," in *2011 50th IEEE Conference on Decision and Control and European Control Conference*, 2011, pp. 5971-5976: IEEE.

[50] Y. Shtessel, C. Edwards, L. Fridman, and A. Levant, *Sliding mode control and observation*. Springer, 2014.

[51] J. Davila, L. Fridman, A. Pisano, and E. Usai, "Finite-time state observation for nonlinear systems with application to compressor surge detection: A high order

sliding-mode approach," in *2008 International Workshop on Variable Structure Systems*, 2008, pp. 197-202: IEEE.

[52] L. Fridman, Y. Shtessel, C. Edwards, and X. G. Yan, "Higher-order sliding-mode observer for state estimation and input reconstruction in nonlinear systems," *International Journal of Robust and Nonlinear Control: IFAC-Affiliated Journal,* vol. 18, no. 4-5, pp. 399-412, 2008.

[53] A. Ferreira, F. J. Bejarano, and L. M. Fridman, "Robust control with exact uncertainties compensation: With or without chattering?," *IEEE Transactions on Control Systems Technology*, vol. 19, no. 5, pp. 969-975, 2010.

[54] Y. B. Shtessel, S. Baev, C. Edwards, and S. Spurgeon, "HOSM observer for a class of non-minimum phase causal nonlinear MIMO systems," *IEEE Transactions on Automatic Control*, vol. 55, no. 2, pp. 543-548, 2010.

[55] L. Fridman, J. Davila, and A. Levant, "High-order sliding-mode observation for linear systems with unknown inputs," *Nonlinear Analysis: Hybrid Systems*, vol. 5, no. 2, pp. 189-205, 2011.

[56] J. Dávila, H. Ríos, and L. Fridman, "State observation for nonlinear switched systems using nonhomogeneous high-order sliding mode observers," *Asian Journal of Control*, vol. 14, no. 4, pp. 911-923, 2012.

[57] A. Ferrara and M. Rubagotti, "A sub-optimal second order sliding mode controller for systems with saturating actuators," *IEEE Transactions on Automatic Control*, vol. 54, no. 5, pp. 1082-1087, 2009.

[58] M. Van, H.-J. Kang, and K.-S. Shin, "Backstepping quasi-continuous high-order sliding mode control for a Takagi–Sugeno fuzzy system with an application for a two-link robot control," *Proceedings of the Institution of Mechanical Engineers, Part C: Journal of Mechanical Engineering Science*, vol. 228, no. 9, pp. 1488-1500, 2014.

[59] G. Bartolini, A. Pisano, E. Punta, and E. Usai, "A survey of applications of second-order sliding mode control to mechanical systems," *International Journal of control*, vol. 76, no. 9-10, pp. 875-892, 2003.

[60] L. M. Capisani, A. Ferrara, A. F. De Loza, and L. M. Fridman, "Manipulator fault diagnosis via higher order sliding-mode observers," *IEEE Transactions on Industrial Electronics*, vol. 59, no. 10, pp. 3979-3986, 2012.

[61] M. Van, H.-J. Kang, and Y.-S. Suh, "A novel fuzzy second-order sliding mode observer-controller for a TS fuzzy system with an application for robot control," *International Journal of Precision Engineering and Manufacturing,* vol. 14, no. 10, pp. 1703-1711, 2013.

[62] M. J. Hasan and J.-M. Kim, "Fault detection of a spherical tank using a genetic algorithm-based hybrid feature pool and k-nearest neighbor algorithm," *Energies,* vol. 12, no. 6, p. 991, 2019.

[63] J. R. Quinlan, "Decision trees and decision-making," *IEEE Transactions on Systems, Man, and Cybernetics,* vol. 20, no. 2, pp. 339-346, 1990.

[64] G. Iannace, G. Ciaburro, and A. Trematerra, "Wind Turbine Noise Prediction Using Random Forest Regression," *Machines,* vol. 7, no. 4, p. 69, 2019.

[65] I. Eski, S. Erkaya, S. Savas, and S. Yildirim, "Fault detection on robot manipulators using artificial neural networks," *Robotics and Computer-Integrated Manufacturing,* vol. 27, no. 1, pp. 115-123, 2011.

[66] G. Iannace, G. Ciaburro, and A. Trematerra, "Fault Diagnosis for UAV Blades Using Artificial Neural Network," *Robotics,* vol. 8, no. 3, p. 59, 2019.

[67] W. Ahmad, S. A. Khan, and J.-M. Kim, "A hybrid prognostics technique for rolling element bearings using adaptive predictive models," *IEEE Transactions on Industrial Electronics,* vol. 65, no. 2, pp. 1577-1584, 2017.

[68] V. N. Vapnik, "An overview of statistical learning theory," *IEEE transactions on neural networks,* vol. 10, no. 5, pp. 988-999, 1999.

[69] X. Wu *et al.*, "Top 10 algorithms in data mining," *Knowledge and information systems,* vol. 14, no. 1, pp. 1-37, 2008.

[70] K. Elangovan, Y. Krishnasamy Tamilselvam, R. E. Mohan, M. Iwase, N. Takuma, and K. L. Wood, "Fault Diagnosis of a Reconfigurable Crawling–Rolling Robot Based on Support Vector Machines," *Applied Sciences,* vol. 7, no. 10, p. 1025, 2017.

[71] A. Prosvirin, J. Kim, and J.-M. Kim, "Efficient rub-impact fault diagnosis scheme based on hybrid feature extraction and SVM," in *Advances in Computer Communication and Computational Sciences*: Springer, 2019, pp. 405-415.

[72] L. M. Manevitz and M. Yousef, "One-class SVMs for document classification," *Journal of machine Learning research,* vol. 2, no. Dec, pp. 139-154, 2001.

[73] R. Debnath, N. Takahide, and H. Takahashi, "A decision based one-against-one method for multi-class support vector machine," *Pattern Analysis and Applications,* vol. 7, no. 2, pp. 164-175, 2004.

[74] C. Mishra, A. Samantaray, and G. Chakraborty, "Ball bearing defect models: A study of simulated and experimental fault signatures," *Journal of Sound and Vibration,* vol. 400, pp. 86-112, 2017.

[75] T. A. Harris and M. N. Kotzalas, *Essential concepts of bearing technology*. CRC press, 2006.

[76] N. Sawalhi and R. Randall, "Simulating gear and bearing interactions in the presence of faults: Part I. The combined gear bearing dynamic model and the simulation of localised bearing faults," *Mechanical Systems and Signal Processing,* vol. 22, no. 8, pp. 1924-1951, 2008.

[77] B. D. Center, "Case Western Reserve University Seeded Fault Test Data," ed.

[78] S. Simatrang, "Fault Detection for Rolling Element Bearings Using Model-Based Technique," Case Western Reserve University, 2015.

[79] A. Boudiaf, A. Moussaoui, A. Dahane, and I. Atoui, "A comparative study of various methods of bearing faults diagnosis using the case Western Reserve University data," *Journal of Failure Analysis and Prevention,* vol. 16, no. 2, pp. 271-284, 2016.

[80] N. Afshari and K. A. Loparo, "A model-based technique for the fault detection of rolling element bearings using detection filter design and sliding mode technique," in *Proceedings of the 37th IEEE Conference on Decision and Control (Cat. No. 98CH36171)*, 1998, vol. 3, pp. 2593-2598: IEEE.

[81] M. Kang, J. Kim, J.-M. Kim, A. C. Tan, E. Y. Kim, and B.-K. Choi, "Reliable fault diagnosis for low-speed bearings using individually trained support vector machines with kernel discriminative feature analysis," *IEEE Transactions on Power Electronics,* vol. 30, no. 5, pp. 2786-2797, 2014.

[82] A. Glowacz, "Acoustic-based fault diagnosis of commutator motor," *Electronics,* vol. 7, no. 11, p. 299, 2018.

[83] A. Glowacz, "Fault diagnosis of single-phase induction motor based on acoustic signals," *Mechanical Systems and Signal Processing*, vol. 117, pp. 65-80, 2019.

[84] Z. Li, Y. Jiang, Q. Guo, C. Hu, and Z. Peng, "Multi-dimensional variational mode decomposition for bearing-crack detection in wind turbines with large driving-speed variations," *Renewable Energy*, vol. 116, pp. 55-73, 2018.

[85] C. Zhang, Z. Li, S. Chen, J. Wang, and X. Zhang, "Optimised ensemble empirical mode decomposition with optimised noise parameters and its application to rolling element bearing fault diagnosis," *Insight-Non-Destructive Testing and Condition Monitoring*, vol. 58, no. 9, pp. 494-501, 2016.

[86] W. Caesarendra and T. Tjahjowidodo, "A review of feature extraction methods in vibration-based condition monitoring and its application for degradation trend estimation of low-speed slew bearing," *Machines*, vol. 5, no. 4, p. 21, 2017.

[87] C.-s. Wang, C.-y. Sha, M. Su, and Y.-k. Hu, "An algorithm to remove noise from locomotive bearing vibration signal based on self-adaptive EEMD filter," *Journal of Central South University*, vol. 24, no. 2, pp. 478-488, 2017.

[88] M. M. Tahir, A. Q. Khan, N. Iqbal, A. Hussain, and S. Badshah, "Enhancing fault classification accuracy of ball bearing using central tendency based time domain features," *IEEE Access*, vol. 5, pp. 72-83, 2016.

[89] Z. Wang, Z. Huang, C. Song, and H. Zhang, "Multiscale adaptive fault diagnosis based on signal symmetry reconstitution preprocessing for microgrid inverter under changing load condition," *IEEE Transactions on Smart Grid*, vol. 9, no. 2, pp. 797-806, 2016.

[90] Z. Liu, T. Liu, J. Han, S. Bu, X. Tang, and M. Pecht, "Signal model-based fault coding for diagnostics and prognostics of analog electronic circuits," *IEEE Transactions on Industrial Electronics*, vol. 64, no. 1, pp. 605-614, 2016.

[91] H. Wang and X. Jing, "Vibration signal–based fault diagnosis in complex structures: A beam-like structure approach," *Structural Health Monitoring*, vol. 17, no. 3, pp. 472-493, 2018.

[92] B. Cai *et al.*, "Application of Bayesian networks in reliability evaluation," *IEEE Transactions on Industrial Informatics*, vol. 15, no. 4, pp. 2146-2157, 2018.

[93] R. Liu, B. Yang, E. Zio, and X. Chen, "Artificial intelligence for fault diagnosis of rotating machinery: A review," *Mechanical Systems and Signal Processing*, vol. 108, pp. 33-47, 2018.

[94] B. Cai, L. Huang, and M. Xie, "Bayesian networks in fault diagnosis," *IEEE Transactions on Industrial Informatics,* vol. 13, no. 5, pp. 2227-2240, 2017.

[95] B. Cai, Y. Zhao, H. Liu, and M. Xie, "A data-driven fault diagnosis methodology in three-phase inverters for PMSM drive systems," *IEEE Transactions on Power Electronics,* vol. 32, no. 7, pp. 5590-5600, 2016.

[96] B. Cai *et al.*, "Multi-source information fusion based fault diagnosis of ground-source heat pump using Bayesian network," *Applied energy,* vol. 114, pp. 1-9, 2014.

[97] M. Sohaib and J.-M. Kim, "Reliable fault diagnosis of rotary machine bearings using a stacked sparse autoencoder-based deep neural network," *Shock and Vibration,* vol. 2018, 2018.

[98] X. Xue and J. Zhou, "A hybrid fault diagnosis approach based on mixed-domain state features for rotating machinery," *ISA transactions,* vol. 66, pp. 284-295, 2017.

[99] M. M. Islam, J. Kim, S. A. Khan, and J.-M. Kim, "Reliable bearing fault diagnosis using Bayesian inference-based multi-class support vector machines," *The Journal of the Acoustical Society of America,* vol. 141, no. 2, pp. EL89-EL95, 2017.

[100] L. D. Avendaño-Valencia and S. D. Fassois, "Damage/fault diagnosis in an operating wind turbine under uncertainty via a vibration response Gaussian mixture random coefficient model based framework," *Mechanical Systems and Signal Processing,* vol. 91, pp. 326-353, 2017.

[101] I. N. Doye, K. N. Salama, and T.-M. Laleg-Kirati, "Robust fractional-order proportional-integral observer for synchronization of chaotic fractional-order systems," *IEEE/CAA Journal of Automatica Sinica,* vol. 6, no. 1, pp. 268-277, 2018.

[102] P. Kühne, F. Pöschke, and H. Schulte, "Fault estimation and fault-tolerant control of the FAST NREL 5-MW reference wind turbine using a proportional multi-integral observer," *International Journal of Adaptive Control and Signal Processing,* vol. 32, no. 4, pp. 568-585, 2018.

[103] L. Ouhib, "State and unknown inputs estimation for Takagi–Sugeno systems with immeasurable premise variables: Proportional Multiple Integral observer design," *Mathematics and Computers in Simulation,* vol. 167, pp. 372-380, 2020.

[104] D. Du, "Fault detection for discrete-time linear systems based on descriptor observer approach," *Applied Mathematics and Computation,* vol. 293, pp. 575-585, 2017.

[105] H. K. Alaei and A. Yazdizadeh, "Robust output disturbance, actuator and sensor faults reconstruction using H∞ sliding mode descriptor observer for uncertain nonlinear boiler system," *International Journal of Control, Automation and Systems,* vol. 16, no. 3, pp. 1271-1281, 2018.

[106] F. Wang *et al.*, "Finite control set model predictive torque control of induction machine with a robust adaptive observer," *IEEE Transactions on Industrial Electronics,* vol. 64, no. 4, pp. 2631-2641, 2016.

[107] A. Abbaspour, P. Aboutalebi, K. K. Yen, and A. Sargolzaei, "Neural adaptive observer-based sensor and actuator fault detection in nonlinear systems: Application in UAV," *ISA transactions,* vol. 67, pp. 317-329, 2017.

[108] J. Liu, S. Vazquez, L. Wu, A. Marquez, H. Gao, and L. G. Franquelo, "Extended state observer-based sliding-mode control for three-phase power converters," *IEEE Transactions on Industrial Electronics,* vol. 64, no. 1, pp. 22-31, 2016.

[109] B. Xiao, S. Yin, and H. Gao, "Reconfigurable tolerant control of uncertain mechanical systems with actuator faults: A sliding mode observer-based approach," *IEEE Transactions on Control Systems Technology,* vol. 26, no. 4, pp. 1249-1258, 2017.

[110] S. S. Seyedalipour, M. S. Hosseini, and G. B. Gharehpetian, "Grid interconnection of distributed generation units at distribution level using feedback linearization technique," in *2016 21st Conference on Electrical Power Distribution Networks Conference (EPDC)*, 2016, pp. 239-244: IEEE.

[111] F. Alonge, M. Cirrincione, M. Pucci, and A. Sferlazza, "Input–output feedback linearization control with on-line MRAS-based inductor resistance estimation of linear induction motors including the dynamic end effects," *IEEE Transactions on Industry Applications,* vol. 52, no. 1, pp. 254-266, 2015.

[112] F. Piltan, M. Sohaib, and J.-M. Kim, "Fault diagnosis of a robot manipulator based on an ARX-Laguerre fuzzy PID observer," in *International Conference on Robot Intelligence Technology and Applications*, 2017, pp. 393-407: Springer.

[113] W. A. Smith and R. B. Randall, "Rolling element bearing diagnostics using the Case Western Reserve University data: A benchmark study," *Mechanical Systems and Signal Processing,* vol. 64, pp. 100-131, 2015.

[114] J. A. Moreno and M. Osorio, "A Lyapunov approach to second-order sliding mode controllers and observers," in *2008 47th IEEE conference on decision and control*, 2008, pp. 2856-2861: IEEE.

[115] A. Glowacz, W. Glowacz, Z. Glowacz, and J. Kozik, "Early fault diagnosis of bearing and stator faults of the single-phase induction motor using acoustic signals," *Measurement,* vol. 113, pp. 1-9, 2018.

[116] H. Shao, H. Jiang, H. Zhang, and T. Liang, "Electric locomotive bearing fault diagnosis using a novel convolutional deep belief network," *IEEE Transactions on Industrial Electronics,* vol. 65, no. 3, pp. 2727-2736, 2017.

[117] X. Liu, Y. Yang, and J. Zhang, "Resultant vibration signal model based fault diagnosis of a single stage planetary gear train with an incipient tooth crack on the sun gear," *Renewable Energy*, vol. 122, pp. 65-79, 2018.

[118] H. Yang, Y. Jiang, and S. Yin, "Fault-Tolerant Control of Time-Delay Markov Jump Systems With $ It\hat {o} $ Stochastic Process and Output Disturbance Based on Sliding Mode Observer," *IEEE Transactions on Industrial Informatics,* vol. 14, no. 12, pp. 5299-5307, 2018.

[119] K. Bouzrara, T. Garna, J. Ragot, and H. Messaoud, "Decomposition of an ARX model on Laguerre orthonormal bases," *ISA transactions,* vol. 51, no. 6, pp. 848-860, 2012.

[120] S. Tayebi-Haghighi, F. Piltan, and J.-M. Kim, "Robust composite high-order super-twisting sliding mode control of robot manipulators," *Robotics,* vol. 7, no. 1, p. 13, 2018.

[121] D. K. Appana, A. Prosvirin, and J.-M. Kim, "Reliable fault diagnosis of bearings with varying rotational speeds using envelope spectrum and convolution neural networks," *Soft Computing,* vol. 22, no. 20, pp. 6719-6729, 2018.

[122] F. Piltan, C.-H. Kim, and J.-M. Kim, "Adaptive Fuzzy-Based Fault-Tolerant Control of a Continuum Robotic System for Maxillary Sinus Surgery," *Applied Sciences,* vol. 9, no. 12, p. 2490, 2019.

[123] X. Lou and K. A. Loparo, "Bearing fault diagnosis based on wavelet transform and fuzzy inference," *Mechanical systems and signal processing*, vol. 18, no. 5, pp. 1077-1095, 2004.

[124] J. Antoni, "Fast computation of the kurtogram for the detection of transient faults," *Mechanical Systems and Signal Processing,* vol. 21, no. 1, pp. 108-124, 2007.

[125] Y. Lei and M. J. Zuo, "Fault diagnosis of rotating machinery using an improved HHT based on EEMD and sensitive IMFs," *Measurement Science and Technology,* vol. 20, no. 12, p. 125701, 2009.

[126] X. Guo, L. Chen, and C. Shen, "Hierarchical adaptive deep convolution neural network and its application to bearing fault diagnosis," *Measurement,* vol. 93, pp. 490-502, 2016.

[127] L. Bai, Z. Han, Y. Li, and S. Ning, "A hybrid de-noising algorithm for the gear transmission system based on CEEMDAN-PE-TFPF," *Entropy,* vol. 20, no. 5, p. 361, 2018.

[128] J. Cheng, D. Yu, J. Tang, and Y. Yang, "Local rub-impact fault diagnosis of the rotor systems based on EMD," *Mechanism and Machine Theory,* vol. 44, no. 4, pp. 784-791, 2009.

[129] P. H. Nguyen and J.-M. Kim, "Multifault diagnosis of rolling element bearings using a wavelet kurtogram and vector median-based feature analysis," *Shock and Vibration,* vol. 2015, 2015.

[130] A. E. Prosvirin, M. Islam, J. Kim, and J.-M. Kim, "Rub-impact fault diagnosis using an effective IMF selection technique in ensemble empirical mode decomposition and hybrid feature models," *Sensors,* vol. 18, no. 7, p. 2040, 2018.

[131] D. Wang, "Some further thoughts about spectral kurtosis, spectral L2/L1 norm, spectral smoothness index and spectral Gini index for characterizing repetitive transients," *Mechanical Systems and Signal Processing,* vol. 108, pp. 360-368, 2018.

[132] D. Wang, "Spectral L2/L1 norm: A new perspective for spectral kurtosis for characterizing non-stationary signals," *Mechanical Systems and Signal Processing,* vol. 104, pp. 290-293, 2018.

[133] C. Lu, Z.-Y. Wang, W.-L. Qin, and J. Ma, "Fault diagnosis of rotary machinery components using a stacked denoising autoencoder-based health state identification," *Signal Processing,* vol. 130, pp. 377-388, 2017.

[134] Z. Chu, F. Meng, D. Zhu, and C. Luo, "Fault reconstruction using a terminal sliding mode observer for a class of second-order MIMO uncertain nonlinear systems," *ISA transactions,* vol. 97, pp. 67-75, 2020.

[135] H. Yang and S. Yin, "Reduced-Order Sliding-Mode-Observer-Based Fault Estimation for Markov Jump Systems," *IEEE Transactions on Automatic Control,* vol. 64, no. 11, pp. 4733-4740, 2019.

[136] A. Guezmil, H. Berriri, R. Pusca, A. Sakly, R. Romary, and M. F. Mimouni, "High order sliding mode observer-based backstepping fault-tolerant control for induction motor," *Asian Journal of Control,* vol. 21, no. 1, pp. 33-42, 2019.

[137] Y. Adhikari, "Inference and Decision Making Methods in Fault Diagnosis System of Industrial Processes," *IFAC Proceedings Volumes,* vol. 37, no. 16, pp. 193-198, 2004.

[138] Z. Huo, Y. Zhang, L. Shu, and M. Gallimore, "A new bearing fault diagnosis method based on fine-to-coarse multiscale permutation entropy, laplacian score and SVM," *IEEE Access,* vol. 7, pp. 17050-17066, 2019.

[139] H. A. Darwish, A.-M. Taalab, and T. A. Kawady, "Development and implementation of an ANN-based fault diagnosis scheme for generator winding protection," *IEEE Transactions on Power Delivery,* vol. 16, no. 2, pp. 208-214, 2001.

[140] A. Prosvirin, J. Kim, and J.-M. Kim, "Bearing fault diagnosis based on convolutional neural networks with kurtogram representation of acoustic emission signals," in *Advances in Computer Science and Ubiquitous Computing*: Springer, 2017, pp. 21-26.

[141] W. Mao, Y. Liu, L. Ding, and Y. Li, "Imbalanced fault diagnosis of rolling bearing based on generative adversarial network: A comparative study," *IEEE Access,* vol. 7, pp. 9515-9530, 2019.

[142] T. De Bruin, K. Verbert, and R. Babuška, "Railway track circuit fault diagnosis using recurrent neural networks," *IEEE transactions on neural networks and learning systems,* vol. 28, no. 3, pp. 523-533, 2016.

[143] T. G. Dietterich, "An experimental comparison of three methods for constructing ensembles of decision trees: Bagging, boosting, and randomization," *Machine learning,* vol. 40, no. 2, pp. 139-157, 2000.

[144] M. A. Al-Barrak and M. Al-Razgan, "Predicting students final GPA using decision trees: a case study," *International Journal of Information and Education Technology,* vol. 6, no. 7, p. 528, 2016.

[145] Q. Zhang, Y. Yang, H. Ma, and Y. N. Wu, "Interpreting cnns via decision trees," in *Proceedings of the IEEE Conference on Computer Vision and Pattern Recognition*, 2019, pp. 6261-6270.

[146] L. Li, S. X. Ding, J. Qiu, Y. Yang, and D. Xu, "Fuzzy observer-based fault detection design approach for nonlinear processes," *IEEE Transactions on Systems, Man, and Cybernetics: Systems,* vol. 47, no. 8, pp. 1941-1952, 2016.

[147] G. Iannace, G. Ciaburro, and A. Trematerra, "Heating, Ventilation, and Air Conditioning (HVAC) Noise Detection in Open-Plan Offices Using Recursive Partitioning," *Buildings,* vol. 8, no. 12, p. 169, 2018.

[148] P. K. Sen, "Gini diversity index, hamming distance and curse of dimensionality," *Metron-International Journal of Statistics,* vol. 63, no. 3, pp. 329-349, 2005.

[149] E. Laber, M. Molinaro, and F. M. Pereira, "Binary partitions with approximate minimum impurity," in *International Conference on Machine Learning*, 2018, pp. 2854-2862.